Multilane transport systems : application to pedestrian traffic

Julien Cividini

Université Paris-Sud

Ecole Doctorale de Physique de la Région Parisienne - ED 107
Laboratoire de Physique Théorique d'Orsay

Discipline : Physique

Thèse de doctorat

Soutenue le 27 juin 2014 (14h) par

Julien Cividini

Systèmes de transport multivoies : application au trafic piétonnier

Directrice de thèse :	Mme. Cécile Appert-Rolland	Directeur de recherche CNRS (LPT, Orsay)
Composition du jury :		
Rapporteurs :	M. Éric Bertin	Chargé de recherche CNRS (LIPhy, Grenoble)
	M. Martin R. Evans	Professeur (ICMCS, Université d'Edimbourg)
Examinateurs :	Mme. Estelle Pitard	Chargé de recherche CNRS (LCC, Montpellier)
	M. Emmanuel Trizac	Professeur (LPTMS, Université Paris-Sud)
	M. Frédéric van Wijland	Professeur (MSC, Université Paris Diderot)

II

Paris-Sud university

Doctoral school 'Physique de la Région Parisienne' - ED 107
Laboratory of Theoretical Physics of Orsay

Discipline : Physics

PhD thesis

Presented on 27th June 2014 (2pm) by

Julien Cividini

Multilane transport systems: application to pedestrian traffic

Supervisor :	Mrs. Cécile Appert-Rolland	CNRS research director (LPT, Orsay)
Composition of the jury :		
Reviewers :	Mr. Éric Bertin	CNRS research fellow (LIPhy, Grenoble)
	Mr. Martin R. Evans	Professor (ICMCS, Edinburgh university)
Examiners :	Mrs. Estelle Pitard	CNRS research fellow (LCC, Montpellier)
	Mr. Emmanuel Trizac	Professor (LPTMS, Paris-Sud university)
	Mr. Frédéric van Wijland	Professor (MSC, Paris Diderot university)

Contents

Acknowledgements

Here I simply thank all the people who have helped at the fulfilment of this thesis from a professional point of view.

First of all I thank my supervisor Cécile Appert-Rolland who accepted to take me as a student and introduced me to the interdisciplinary problems that will be presented here, opening the doors of a field in which I could of course meet physicists, but also mathematicians, computer scientists, engineers and so on. Secondly I thank Henk Hilhorst, a less official supervisor with whom I had the opportunity to work from the beginning of my master internship at the LPT until the very end of my PhD and whose knowledge of statistical mechanics and rigour were always useful to our work. I add here that I am grateful to Chloé Barré and Yann Chiffaudel, two interns that were both under the direction of Henk in 2012 and 2013, respectively. They have both explored problems related to my work, which I partly present in this thesis.

During the second half of my thesis I was a regular member of the 'tea group' held in the IPhT. Here I want to express my gratitude to its members. Special thanks are addressed to Kirone Mallick and Tridib Sadhu for useful advice, and to Chikashi Arita for his work in our current collaboration. Of course all the permanent or temporary members of the tea group are warmly thanked for sharing their work with the rest of the group, including myself.

In a more collective way, I thank the LPT as a whole for the logistic and the financial support and the ENS for providing me with a fellowship. It goes without saying that the administrative staff of the LPT has always made things easy for me, whether I simply had to go to a conference or in more complicated cases. I certainly have to thank all the people that managed to teach me something during the last 25 years, starting with my family and other people that contributed to my education, followed by some of my math, physics, or even chemistry teachers I met during my teenage years all the way to the people that taught me basic, advanced statistical mechanics or other interesting aspects of physics. I also have to thank all the speakers to whom I had the opportunity to listen at seminars, conferences, summer schools, on the Internet and so on. At this rate I should even thank the whole theoretical physics community for deciding to make it a common practice to put papers on the arXiv.

Finally, I thank Eric Bertin, Martin R. Evans, Estelle Pitard, Emmanuel Trizac and Frédéric van Wijland for having accepted to be either examiners or

reviewers of this thesis.

Introduction

A statistical physicist usually has to deal with systems having a huge number of degrees of freedom that interact, sometimes in a complex fashion. Methods have then been developed to handle these complex systems using approximations, numerical simulations or exactly solvable toy models. Often these methods from statistical physics can however be applied to other problems from various fields such as social sciences [1], economy [2], evolutionary processes [3], management of firms [4] or transport phenomena [5]. In all these problems a 'macroscopic' variable is determined by the interactions of a large number of agents while a stochastic 'noise' in the determination of this variable comes from the variability in the individual behaviour of agents from one realization to another, making it similar in spirit to textbook models of statistical physics, *e.g.* a gas of interacting particles or the Ising model.

In this thesis I will concentrate on the particular case of pedestrian dynamics. The motion of pedestrian crowds is of interest for several reasons. The design of new buildings, for example, should be adapted to the people that will have to evolve in them. If we wanted to design a station, this procedure would include optimizing the geometry to avoid bottlenecks and to facilitate a possible evacuation if needed, but also trying to have as much daylight as possible penetrate the building or making sure that most people have access to important information, *e.g.* have a clock and the departure board in their line of sight. In more extreme events people are injured or killed because of collective stampedes that may occur during mass events such as religious pilgrimages or all sorts of festivals [6, 7]. Many examples of these problems and proposed solutions can be found for instance in the proceedings of the PED (Pedestrian and Evacuation Dynamics) or TGF (Traffic and Granular Flow) conferences, see Refs. [8] and [9] for the most recent ones. It is therefore clearly of interest both to engineers and scientists to understand these collective modes.

Many methods have been used to study collective pedestrian behaviour. Experiments have been and are now regularly performed in various typical situations such as one-dimensional corridors with pedestrians flowing in a single or both directions [10, 11, 12, 13, 14, 15], perpendicularly intersecting flows [10] or directed flow through a bottleneck [16, 17, 18, 19]. Numerous numerical studies have been performed as well, that either aim at realism and use rather complicated models [20, 21, 22, 23, 24, 25, 15, 26, 27, 28] or seek to isolate the main ingredients that compose pedestrian motion while keeping things

simple [20, 29, 30, 31]. On some models analytical progress can be made as well, such as models of ordinary [20] or partial [20, 32, 33] differential equations, and the behaviour of certain cellular automata can be studied as well [34, 29, 35].

From a statistical mechanics point of view the presence of a stationary current implies that the system is intrinsically out-of-equilibrium. In particular, there is no quantity similar to the partition function from which one can derive all the quantities of interest. All the models studied in this thesis are out of equilibrium simply because the pedestrians want to go from one place to another, *i.e* they are self-propelled. Even though we lack a general theory of out-of-equilibrium systems, some understanding can be achieved by studying simple particular cases of systems. The Totally Asymmetric Simple Exclusion Process, or TASEP, is the cornerstone of all the models studied in this thesis and ranks among these simple models. A quick-and-dirty definition of the TASEP could be the following: take a one-dimensional lattice, put 0 or 1 particle on each site, and let the particles hop stochastically from left to right while imposing simple exclusion.

This definition in terms of occupied and empty sites of a lattice may remind the reader of the *cellular automata* first defined and studied in mathematics and computer science, see Ref. [36] for example. In statistical physics lattice-gas systems that consist of particles with hard-core exclusion are referred to as 'cellular automata', among them the TASEP and all the models will study in this manuscript. In our case we will in fact study probabilistic cellular automata in which the evolution rules are allowed to be stochastic, *e.g.* the particles hopping with some probability $p \leq 1$. We also allow the particles to have an internal state that can be specified in terms of discrete or continuous variables, even though the second case does not strictly fit into the definition of a cellular automaton. However, and as often in statistical mechanics, our primary interest will always be ensemble-averaged quantities, in which we will trace out the internal degrees of freedom. These ensemble averages are of course expected to follow smooth deterministic laws thanks to the law of large numbers.

When studying out-of-equilibrium problems new ambiguities arise that have to do with the dynamics of the system studied. For the case of the TASEP one has to choose an update scheme, that determines in which order the particles are allowed to hop. In theoretical studies this element of modelization is sometimes overlooked due to the fact that the so-called 'continuous time' update is considered the most convenient for analytical calculations. Here we however want to model pedestrians, and some of their expected properties seem incompatible with continuous time update. In part I we therefore study some of the properties of systems that are well suited to the modelization of pedestrian traffic. In particular, instead of picking one of the already existing update schemes we propose a new one, believed to be adapted to pedestrians. This new 'frozen shuffle update' will be studied in detail to confirm that it is

adapted to pedestrians and to get an intuition of the behaviour of the particles following this new rule. Note that different communities may have different names for a given procedure or use the same name for two different procedures. To avoid confusion, all the update schemes relevant for this thesis are defined in subsection 1.1.3 for one-dimensional systems and in subsection 4.2.2 for two-dimensional ones.

One of the important qualitative features of the TASEP is its jamming transition: for certain parameter values blockings between particles become very common and the flux is reduced. Although the static properties of this transition is understood for many updates, the dynamics have been studied almost only for continuous time update thanks to the approximate 'domain wall' theory. Domain wall theory supposes that the system is divided in macroscopic homogeneous domains separated by a wall, and seeks to write an equation for this wall. In chapter 3 we partly extend this theory to updates relevant to traffic (deterministic parallel update), this time in an exact microscopic way. Although only the stationary density profile is considered, the work presented in chapter 3 can be used to derive more complicated nonstationary quantities.

After understanding its properties in simple cases, the natural continuation is to use frozen shuffle update to simulate a situation relevant for pedestrians, namely the intersection of perpendicular flows. The system is of course still out-of-equilibrium and constitutes a natural bidimensional extension of the TASEP. In pedestrian experiments and sophisticated numerical simulations, the observations are mostly made by eye and rarely reach the quantitative level when it comes to bidimensional behaviour. In the case of intersecting flows going, say, from west to east and from south to north, it has been known for a long time [37, 38] that pedestrians tend to self-organize into alternating stripes of pedestrians going in the same direction, these stripes going from northwest to southeast.

One of our tasks is then to show that with our simple model the pattern formation can be reproduced, which will be done in part II. The generality of this prediction will then be tested by considering an other update scheme, alternating parallel update, and a system of mean-field-like equations that all reproduce the same behaviour. Once such a validation will be provided we will try to make predictions. At the quantitative level it will be shown that under certain conditions the stripes are expected to get slightly inclined with respect to their original northwest-to-southeast direction. Though being small, this 'chevron' effect is present in the particle models as well as in the equations, which proves its generality.

From a wider perspective, in the particle model this effect can be understood to arise because of nontrivial effective interactions that appear between particles going in the same direction. To take a fluid mechanics analogy, a particle will tend to attract particles going in the same direction as it, towards a set of sites that we will call its 'wake'. The interaction is entirely mediated by the particles going in a perpendicular direction, which offers an interesting analogy with *e.g.* colloids in a solution. The conclusion of this study will be a quantitative prediction of the pattern, in terms of the deviation between the

angle of the stripes and the northwest-southeast direction.

The effect being small, it is not clear that it should be observed in pedestrian experiments. The model being an idealized version of pedestrian experiments, we test the effect of numerous natural extensions of the intersection model studied so far, and try to explain the principal changes that occur. Most importantly, the pattern could be destroyed by noise. We will show that it is the case in the particle model, but we will also argue that the parameters of a real pedestrian intersection are such that the effect could still be observed. Indeed, pedestrian crossings being much denser than the intersection in our model, not only the pattern is less sensitive to noise, but its magnitude is also larger.

This thesis contains contributions to both pedestrian dynamics and statistical mechanics. Firstly, it has been stressed that we want to address problems relevant for pedestrian applications, even though the models presented here are very theoretical. Here we will explain a well-known phenomenon characteristic of intersecting pedestrian flows, namely diagonal pattern formation. We will also observe and predict a new effect in our models, that might be observed in experiments. Secondly, all our objects of study are deeply connected to out-of-equilibrium statistical mechanics. Several original out-of-equilibrium models will be exhibited, and in many of them exact results will be obtained. The fact that the particle models and the mean-field equations are minimal, *i.e.* the simplest possible exhibiting a given phenomenon, is also a strong methodological requirement shaping the whole thesis.

Part I is dedicated to the one-dimensional cases for updates relevant to pedestrians, for which we can often obtain exact results. In chapter 1 the TASEP is introduced and some of its basic properties are reviewed. The focus of chapter 2 is then on the computation of the average quantities of interest for variants of the TASEP with frozen shuffle update, namely the current-density relation in 1D and the phase diagrams. Chapter 3 deals with the domain wall theory and its application to TASEP, and presents a case where the equation for the wall can be written exactly and disagrees with the usual approximations made.

Part II deals with pattern formation in the wider intersection. Chapter 4 presents literature about some simulations or experiments with intersecting flows in wide areas, with a focus on pedestrian experiments and simulations on the one hand and on the celebrated BML model for car traffic [39] on the other hand. The simple intersection model that will be at the core of part II is then defined. Pattern formation in this latter model is studied in chapter 5. This effect is then explained analytically in terms of effective interactions in chapter 6. Finally we lift some of the restrictions that we put on the parameters when we defined the model in chapter 7.

Part I and part II are largely independent and can almost be read separately, as the techniques and the goals of both parts are to a large extent disjoint.

Someone who reads part II may want to check some basic definitions about the TASEP or frozen shuffle update in sections 1.1 or 2.1 for instance. In this thesis there is however a logical progression from the simplest cases to the most complex ones, which suggests reading it from the beginning to the end.

Inside part I, chapter 1 is introductory and may be skipped by the reader familiar to the TASEP. The two following chapters 2 and 3 are independent and can be read separately. Part II begins with chapter 4, in which subsections 4.2.1 and 4.2.2 are very important, as they define the model that will be studied in the rest of part II. Chapter 5 offers a complete phenomenological picture of the intersection model, but lacks some elements of explanation and is therefore tightly bound with chapter 6. The final chapter 7 presents extensions to the discoveries made in both chapter 5 and 6.

Part I

TASEP for traffic applications

In this first part of the thesis we address fundamental questions and theoretical models of statistical physics that are triggered by pedestrian applications. Indeed, we start with introducing the Totally Asymmetric Simple Exclusion Process (TASEP), a simple model of out-of-equilibrium statistical mechanics. In the whole thesis we will study many models, all based on the TASEP, while we will allow ourselves to modify the geometry or the dynamical rules usually considered in theoretical physics. The TASEP being out-of-equilibrium, nonzero currents flow through it in the stationary state. It is therefore quite natural that it serves as a simplified model for many real systems involving flows. Some exact theoretical results are presented to help the reader get familiar with the basic properties of the TASEP.

We however keep in mind that we intend to design a model for pedestrian flows. This will draw the focus on a particular element of modelization of these flows, namely the update scheme. The TASEP is a model of particles hopping on a lattice, and the update scheme tells us exactly in which order these particles are allowed to move. In theoretical physics this issue is often overlooked, simply because the widely used 'continuous time' update has been used historically and is both quite physical and convenient from an analytic standpoint. It is however not adapted to car or pedestrian traffic applications, as the expectedly predictable and regular behaviour of the agents is in conflict with the rather high noise that continuous time evolution implies. Alternatives exist, but in chapter 2 we choose to design our own update scheme for pedestrians, called frozen shuffle update.

We then focus on understanding the characteristics of this update in simple geometries. In particular we derive the 'fundamental diagram', *e.g.* the density-current relation. We also show that organized structures called 'platoons' appear, that can be seen as groups of pedestrians with synchronized steps. Finally, we make a step towards what will be the focus of part II, namely a large intersection of pedestrian flows. Indeed, we consider the intersection of two one-dimensional lanes on a single site.

It has been said that most of the analytical results are derived for the continuous time version of the TASEP. In particular, this statement is true for the 'domain wall' theory that was applied in chapter 2 to approximate the density profile of the TASEP with frozen shuffle update. Whereas the theory has an impressive success when using continuous time, small discrepancies are observed for other choices of updating schemes, including ours. We start chapter 3 with a proper introduction of the domain wall theory. We then direct our interest towards an extension of the domain wall theory to an update useful to traffic, the deterministic parallel update. An exact set of equations for the dynamics of the model is then written. Here we focus on the stationary state, where the exact density profile is derived for arbitrary system size. In principle, the dynamical equations can however be solved and give an exact dynamical solution of the system. This will conclude part I of the thesis.

To summarize, in this part we propose some modifications of the dynamics of the TASEP adapted to traffic, while always keeping the one-dimensional geometry. The motivation comes from pedestrian dynamics but the models for-

mulated here can as well be considered as instances of simple out-of-equilibrium models. Many quantities of interest can be computed analytically in these cases, which also makes them of interest for the statistical mechanics community.

Chapter 1

The TASEP

This introductory chapter deals with a paradigmatic model of out-of-equilibrium statistical physics, the Totally Asymmetric Exclusion Process (TASEP). This model was first introduced by MacDonald *et al.* to study the synthesis of proteins by ribosoms moving on a mRNA strand [40]. It was studied in the mathematical literature shortly after by Spitzer [41] and has now become an important member of the wide class of interacting particle systems, for which it is possible to derive rigorous results [42, 43]. In the landscape of theoretical physics the study of the TASEP is motivated by the fact that it constitutes a toy model for transport processes.

The study of the TASEP can be used as a basis for many generalizations. Fields of application outside physics include cell biology, road and pedestrian traffic and some specific instances of animal behavior such as ants. Such applications are described in subsection 1.2.4 and references therein. In statistical physics, the TASEP belongs to the large class of lattice gas models, of which it constitutes a one-dimensional infinite-field limiting case. Lattice gas models have been used to study transport in condensed matter or in soft matter since advances in computer science made it possible [44, 45]. Besides being useful for describing energy or mass transport, the TASEP is known to be equivalent to many other models of theoretical statistical mechanics. The TASEP can be exactly turned into to the XXZ spin chain with fixed magnetization and dynamical constraints simply by writing the occupation variables as spins. There is also an exact mapping between the very simple Zero-Range Process (ZRP) [46] and the TASEP. The TASEP on an infinite line can also be shown to be equivalent to a simple growth model. The evolution of the height of the growing medium, which corresponds to the current of particles in the TASEP, is described by the celebrated KPZ equation [47], which implies that the TASEP could be a representative of the KPZ universality class of out-of-equilibrium systems [48]. Finally, the (time- and space-) continuous limit of the density profile in a TASEP is described to the deterministic order by the well-studied Burgers' equation. Many properties of the TASEP can be computed exactly and even proved rigorously, *e.g.* such as the density profile or the large devia-

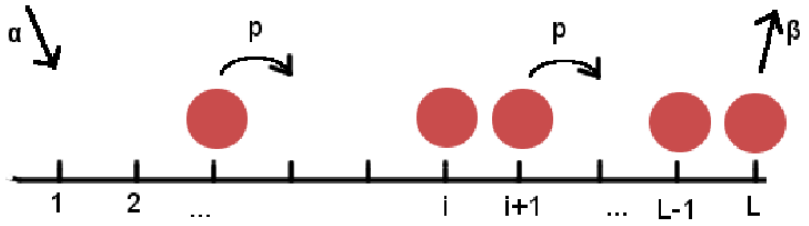

Figure 1.1: TASEP of sites $1, 2, \ldots, L$. Red disks represent particles and arrows represent transition probabilities for the particles. Besides the size of the system there are 3 parameters in the system: the entrance probability per time step α, the hopping probability p and the exit probability per time step β.

tion functional [49].

The TASEP is precisely defined in section 1.1 and some properties from previous literature are given in the following section 1.2.

1.1 Definitions

1.1.1 Main ingredients

In this section we recall the classical definition of the Totally Asymmetric Simple Exclusion Process (TASEP). Consider a one-dimensional discrete lattice, whose boundary conditions we do not specify at the moment. The sites are labeled by integers from left to right ranging from 1 to an integer L if the number of sites is finite, from $-\infty$ to $+\infty$ otherwise. Links between sites of the system will be denoted with half-integers such that link $i + 1/2$ links sites i and $i + 1$.

Particles with no internal structure are dropped on the lattice so that the *exclusion rule* is respected, *i.e.* there cannot be more than one particle on each site. A site which is not occupied by a particle is called a *hole*, and a sequence of particles occupying consecutive sites is called a *cluster*. The number of particles in the system will be denoted by the letter N in the case it is finite and the mean density by $\overline{\rho}$, which of course takes the value N/L in a finite system. Under time evolution, particles are allowed to hop stochastically from site i to site $i + 1$ with the restriction provided by the exclusion rule. A scheme of the system is drawn in Fig. 1.1.

The precise order in which particles hop is specified by an *updating scheme*, to be made precise in subsection 1.1.3. Once a particle is chosen for update the hopping attempt wil be successful with probability $p \leq 1$. Time will be denoted by the letter t and we define a *time step* as an interval of time in which

each particle is updated on average once.

We can define the occupation of site i, τ_i as being 0 if there is no particle on site i and 1 if there is. A *configuration* can then be denoted by the set containing the occupation of all sites $\tau \equiv \{\tau_1, \tau_2, \ldots, \tau_L\}$ with obvious modifications if the system is infinite. If there are N particles in the system, another way to specify the configuration of the system is to keep track of the positions of the particles in an other set $\mathbf{x} = (x_1, x_2, \ldots, x_N)$, where $x_1 > x_2 > \ldots > x_N$ are the labels of the sites occupied by particle 1,2,...,N. Note that particles cannot overtake each other because of the exclusion principle.

For many updates, the time evolution of the TASEP is also symmetric under exchange between particles and holes, which must be combined with an inversion of right and left, *i.e.* replacing site i by site $L - i + 1$. Indeed, a particle hopping from left to right is equivalent to a hole hopping from right to left.

The TASEP is arguably the simplest out of equilibrium statistical system, as a steady-state current will flow from left to right. Detailed balance is strongly violated as individual particles are allowed to hop only from left to right. Despite its simplicity this model shows an interesting phenomenology. Nonequilibrium phase transitions of first and second order may be observed. In certain parts of the phase diagram long-range correlations are also observed, which would be impossible for a one-dimensional statistical system at equilibrium with nearest-neighbour interactions. Since exact stationary states have been found, approximate theories may conveniently be tested on the TASEP because of its simplicity, describing it in terms of domain walls or hydrodynamic equations. Moreover, these theories may also give access to dynamical quantities whose exact computation is out of reach.

1.1.2 Geometry

We now specify the geometries in which the TASEP has mainly been studied.

One of the simplest is the ring, *i.e.* an unidimensional chain with periodic boundary conditions. Using this geometry, site $L + 1$ (which would be to the right of site L) is identified with site 1. As there is neither any exit nor any entrance the number of particles is conserved as well as their relative order, and N becomes an input parameter. We will see in section 1.2.3 that the stationary state is very simple in this case.

An infinite TASEP can also be considered. The absence of boundaries makes this system easier to handle from a theoretical point of view, which makes it a preferred geometry for mathematicians [42, 43]. A particular importance is given to the initial condition in that case, so that the infinite line is well suited to study transient states. A widely studied example of these transient regimes is given by the relaxation of singular profiles such as shocks, a particular instance of shock being the *step* initial condition in which all the sites $i \leq 0$ are occupied and all others are empty at the initial time.

The TASEP can also be studied with open boundary conditions. In that case, particles can enter the system on site 1 with a probability $\alpha < 1$ per

unit of time and exit the system from site L with probability $\beta < 1$ per unit of time. For updates with particle-hole symmetry the system may be equivalently described in terms of holes entering on site L with probability β and exiting the system on site 1 with probability α. Also note that in the case of open boundaries, fictitious links $1/2$ and $L+1/2$ can be considered to link the TASEP with the particle reservoirs maintaining the flow. This geometry is then of great interest to statistical physicists, as it provides an example of boundary-driven out-of-equilibrium system.

1.1.3 Updating schemes

We have seen that making a TASEP evolve in time consists of performing a sequence of local operations (hops, entrance, exit) on the links of the lattice, to be called *link updates* from now on. However we said nothing about the order in which the link updates are performed or even about the continuous or discrete nature of time. Here we review some the update schemes that are the most relevant to this thesis, either because they are ubiquitous in statistical mechanics (continuous time, random sequential, parallel) or because they are related to the work presented in it (random shuffle, parallel). Of course this list is not exhaustive, omitting *e.g.* sublattice parallel update or ordered updates.

• **Continuous time :** In continuous time the links can be updated one after another in an uncorrelated fashion. Each link is then updated at a constant rate. This procedure is equivalent to defining an exponentially distributed variable on each link representing the time one needs to wait before the next update, often called 'exponential clocks'. This updating scheme is rather noisy, as a particle may attempt to hop several times or none in a given time interval. However, this scheme is the easiest to handle from a theoretical point of view [50, 51] due to this absence of correlations and the continuous nature of time and also has historical importance [52]. In particular, defining a hopping probability $p < 1$ simply amounts to rescaling time. An open TASEP with continuous time update and parameters α, β and p is rigorously equivalent to another one with parameters α/p, β/p and 1 if one rescales the time t as pt. This update can be obtained as the limit of many discrete update schemes. From a numerical point of view, fast simulations of continuous-time processes with constant rates can be obtained using Gillespie's algorithm [53].

• **Random sequential update :** *Random sequential update* is an algorithm that is often used in simulations because of the fact that it probably constitutes the most natural discretization of continuous time. A link is chosen at random and updated, this procedure being repeated over and over. For a system with n_{links} links, a time step is then simply defined as n_{links} link updates. Each link is then updated at a constant rate equal to 1, and continuous time is recovered in the limit where n_{links} is large. It may be preferable, to reduce the computation time, or necessary, on the infinite line, to choose a particle at random instead of a link, defining a time step as N updates of particles. Updating links or particles are expected to give the same results, keeping in mind that the second procedure is useful only when the number of particles is

conserved. Random sequential update finds applications in biology [5], where the motion of intracellular agents is expected to be triggered by stochastic processes, such as the absorption of an ATP molecule.

• **Random shuffle update :** *Random shuffle update* provides an alternative to random sequential update with less fluctuations. It consists of randomly defining a new order of the particles at each time step and updating them in this prescribed order. This procedure ensures that each particle attempts to hop exactly once per time step, thus lowering the fluctuations. It has originally be introduced to simulate pedestrians, for whom there were too many fluctuations with random sequential update [29]. In Ref. [29] this random shuffle update is however called 'random sequential update'. This name has stayed the same in the pedestrian community whereas physicists now call it 'random shuffle update'. This update has been analytically studied in Refs. [54] and [55].

• **Parallel update :** All the links can be updated in *parallel*. In that case, time is discrete and denoted by integers. At each time step, all the links are updated simultaneously. In the case of open boundaries, the entrance and the exit are updated at the same time as well. Using parallel update one notices that no two particles occupying consecutive sites can hop at the same time step, which introduces an incompressible time scale. This updating scheme has the advantage of limiting the noise, since every particle can hop only once per time step. This update is therefore believed to be convenient for simulating vehicular traffic [31, 39, 56, 57, 58, 59], the incompressible time scale being interpreted as a reaction time. It is also often used to simulate pedestrians, for example in evacuation problems [60, 61], mainly because it has relatively low noise. Also note that parallel update tends to continuous time when all the probabilities α, p and β go to zero, as events in which more than one successful update per time step occurs become negligible.

Even though some points may be obvious to the reader, some elements of terminology are made precise here. The updating schemes presented here may be divided according to the nature of time. Obviously in continuous time the time is continuous while for the three other schemes described here time is discrete. Among these discrete schemes, particles may be updated sequentially, *i.e.* one after the other, as in random sequential and random shuffle updates, or in parallel, as the name 'parallel update' indicates.

In the following we will define new update schemes, such as frozen shuffle update in section 2.1 and, for bidimensional cases, alternating parallel update in section 4.2. For now we concentrate on some properties of the TASEP.

1.2 Properties

In this section we summarize some already known properties of the TASEP, that are presented mostly from a statistical mechanics point of view. The last subsection 1.2.4 however deals with the applications of the TASEP to traffic modelization.

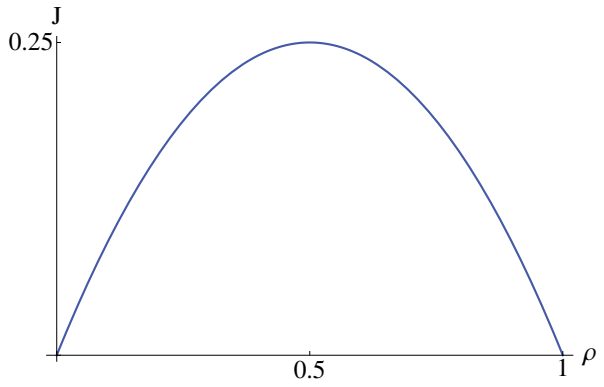

Figure 1.2: Fundamental diagram of the TASEP with continuous time update. For large systems with periodic boundary conditions the current-density relation is simply the mean-field expression $\mathcal{J} = \overline{\rho}(1-\overline{\rho})$, as shown in subsection 1.2.3. The current starts increasing linearly at low densities as the particles can hop forward unimpeded, admits a maximum $\mathcal{J} = \frac{1}{4}$ for a density $\overline{\rho} = \frac{1}{2}$ and then decreases to 0 as the system progressively gets blocked.

1.2.1 Fundamental diagram

We have already seen that on a ring, if one sends the system size to infinity, the behaviour of the system in the stationary state will depend only on its conserved density $\overline{\rho}$. The macroscopic quantity characterizing the fact that the system is out of equilibrium is the nonvanishing *particle current* $\mathcal{J}$. More precisely, $\mathcal{J}$ is equal to the number of particles crossing a given bond during one time step after averaging on the dynamics. The plot of $\mathcal{J}$ as a function of $\overline{\rho}$ in then called *fundamental diagram* in the traffic literature, whose name proves its importance.

In continuous time we will see in subsection 1.2.3 that the occupations of different sites are uncorrelated. This leads to the intuitive mean-field expression $\mathcal{J} = \overline{\rho}(1-\overline{\rho})$ for an infinite system. As a reference, the corresponding curve is shown in Fig. 1.2. It already illustrates some general properties of fundamental diagrams. The current obviously has to vanish for $\overline{\rho} = 0$, as there are no particles to be transported, and for $\overline{\rho} = 1$, as the flow is then fully congested. As a consequence, there exists a maximum flow, here occurring for $\overline{\rho} = 1/2$ as a consequence of the particle-hole symmetry. The corresponding value of the current is $1/4$.

1.2.2 Phase diagram

In open boundary conditions the control parameters are the injection probability α and the exit probability β. A bidimensional phase diagram can for example be drawn in the (α, β) plane for fixed p, as shown in Fig.1.3. It was

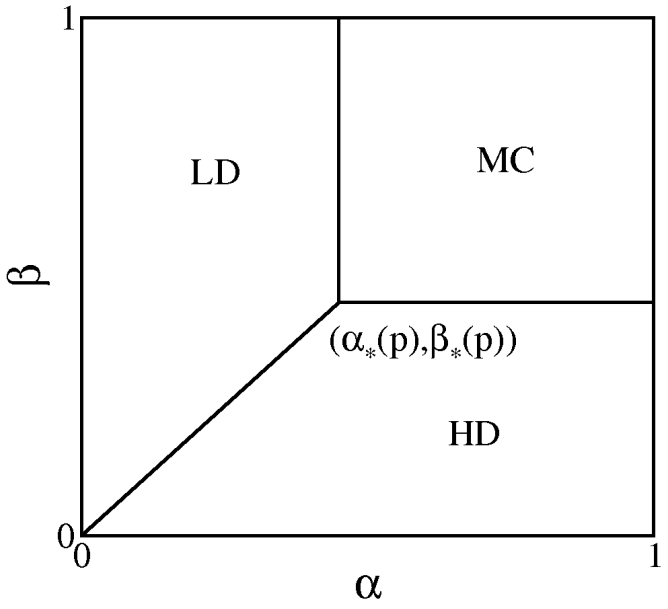

Figure 1.3: General form of the phase diagram of the TASEP for a wide class of updates. In discrete updates the input parameters α,β and p are probabilities and belong to $[0;1]$ whereas in continuous time they become rates possibly going from 0 to $+\infty$. In general three phases LD, HD and MC can be distinguished, that are discussed in more detail in the text.

derived in Ref. [62] by a mean-field method and confirmed by exact solutions in Refs. [63, 64, 65]. Here we give the qualitative picture, in the symmetric case for simplicity ($\alpha_*(p) = \beta_*(p)$, see Fig. 1.3). For α smaller than β and α smaller than a critical value $\alpha_*(p)$ that depends on the hopping rate and on the update scheme, the stationary current is limited by the entrance and the system is in the *low density* (LD) phase. When $\beta < \alpha$ and $\beta < \beta_*(p)$ a symmetrical phase exists in which the exit limits the maximal current, the system being in *high density* (HD) phase. For $\alpha > \alpha_*(p)$ and $\beta > \beta_*(p)$ there exists a third phase called *maximal current* phase (MC) in which the bulk dynamics is limiting. For random sequential update we have $\alpha_*(p) = \beta_*(p) = p/2$ and for parallel update $\alpha_*(p) = \beta_*(p) = 1 - \sqrt{1-p}$ [66].

In Table. 1.1 we report a table from Ref. [66] showing the expressions of densities and currents for some of the most common updates.

1.2.3 Some exact results

The simplest of the described systems is perhaps the periodic TASEP in continuous time. In that case it can be seen that the probability to enter any configuration is the same as the probability to exit it. We call $P(\mathbf{x}, t)$ the

	Continuous time	Parallel
Low density	$\overline{\rho} = \alpha$ $\mathcal{J} = p\alpha(1-\alpha)$	$\overline{\rho} = \frac{\alpha(1-\alpha)}{p-\alpha^2}$ $\mathcal{J} = \alpha\frac{p-\alpha}{p-\alpha^2}$
High density	$\overline{\rho} = 1-\beta$ $\mathcal{J} = p\beta(1-\beta)$	$\overline{\rho} = \frac{p-\beta}{p-\beta^2}$ $\mathcal{J} = \beta\frac{p-\beta}{p-\beta^2}$
Maximal current	$\overline{\rho} = \frac{1}{2}$ $\mathcal{J} = \frac{p}{4}$	$\overline{\rho} = \frac{1}{2}$ $\mathcal{J} = \frac{1-\sqrt{1-p}}{2}$
Critical rate	$\alpha_*(p) = \frac{p}{2}$	$\alpha_*(p) = 1-\sqrt{1-p}$

Table 1.1: Expressions of the currents and densities in the three phases for continuous time and parallel update. In both cases the phases diagram is symmetric $\alpha_*(p) = \beta_*(p)$. Adapted from Ref. [66].

probability to find the system in state $\mathbf{x} = (x_1, \ldots, x_N)$ at time t and define $\mathbf{x}_{i-} = (x_1, \ldots, x_i - 1, \ldots, x_N)$. In a given state we also denote by $\mathcal{N}_c(\mathbf{x})$ the number of clusters in a given state $\mathbf{x}$. The probability $P(\mathbf{x}, t)$ obeys the master equation

$$\frac{\mathrm{d}P}{\mathrm{d}t}(\mathbf{x}, t) = \left(\sum_{\text{clusters}} pP(\mathbf{x}_{i-}, t) \right) - \mathcal{N}_c(\mathbf{x}) pP(\mathbf{x}, t). \tag{1.1}$$

The first sum is taken on the existing clusters in configuration $\mathbf{x}$, particle i being the leftmost particle of the chosen cluster in each of the $\mathcal{N}_c(\mathbf{x})$ terms of the sum. Each term of this sum is associated to an event where, starting from configuration $\mathbf{x}_{i-}$, particle i hops, thus completing a cluster and giving configuration $\mathbf{x}$. The second term represents the loss associated with the rightmost particle of a cluster hopping, thus leaving configuration $\mathbf{x}$. The function $P(\mathbf{x}, t)$ defines a probability distribution in the domain $x_1 > x_2 > \ldots > x_N$. The boundary conditions of Eq. (1.1) simply read

$$P((x_1, \ldots, x_i, x_{i+1} = x_i, \ldots, x_N), t) = 0, \tag{1.2}$$

and sites 1 and $L+1$ are of course identified. From Eq. (1.1) it is clear that a probability independent of the configuration gives the stationary state. In the stationary state a site of the lattice is empty with probability $1-\overline{\rho}$ or occupied with probability $\overline{\rho}$, and the current is equal to p times the probability of having an occupied site followed by an empty site. We get [50]

$$\mathcal{J} = p\frac{N}{L}\left(1 - \frac{N-1}{L-1}\right), \tag{1.3}$$

which goes to $p\overline{\rho}(1-\overline{\rho})$ as $L \to \infty$ with $N/L = \overline{\rho}$. The expression of the current as a function of the density is plotted in Fig. 1.2 after rescaling time so that $p = 1$.

The dynamical properties of the periodic TASEP can be obtained exactly as well by using Bethe Ansatz techniques, see Ref. [5] for a 'crash-course'. Indeed,

Eqs. (1.1) and (1.2) are equivalent to another set of equations (for another function $\tilde{P}(\mathbf{x},t)$)

$$\frac{\mathrm{d}\tilde{P}}{\mathrm{d}t}(\mathbf{x},t)=\sum_{i=1}^{N}p\tilde{P}(\mathbf{x}_{i-},t)-Np\tilde{P}(\mathbf{x},t), \tag{1.4}$$

with boundary conditions

$$\begin{aligned}&\tilde{P}((x_1,\dots,x_i,x_{i+1}=x_i,\dots,x_N),t)\\ =\;&\tilde{P}((x_1,\dots,x_i,x_{i+1}=x_i+1,\dots,x_N),t),\end{aligned} \tag{1.5}$$

so that $\tilde{P}(\mathbf{x},t)=P(\mathbf{x},t)$ inside the domain $x_1>x_2>\ldots>x_N$. A superposition of plane waves can then be shown to solve Eq. (1.4) while Eq. (1.5) constrains the amplitudes of these waves and the periodicity of the lattice selects the wavevectors.

The exact propagator $G(\mathbf{x}|\mathbf{y};t)$ for an arbitrary number N of particles has been obtained in the case of an infinite system with no boundaries, still by applying Bethe Ansatz to Eqs. (1.4) and (1.5), this time without boundaries [67]. After rescaling time to absorb the factor p, one obtains the final result as an $N\times N$ determinant

$$G(\mathbf{x}|\mathbf{y};t)=\det\left[F_{l-j}(x_{N-l+1}-y_{N-j+1};t)\right]_{j,l=1,\dots,N}, \tag{1.6}$$

where $\mathbf{x}=(x_1,x_2,\dots,x_N)$, $\mathbf{y}=(y_1,y_2,\dots,y_N)$ and [68]

$$F_n(x;t)\equiv\frac{1}{2\pi\mathrm{i}}\oint_{\Gamma_{0,-1}}dw\frac{w^{-n}}{(1+w)^{x+1-n}}\mathrm{e}^{wt}. \tag{1.7}$$

In Eq. (1.7), $\Gamma_{0,-1}$ is an anticlockwise oriented contour circling around 0 and -1 in the complex w plane, and $\mathrm{i}^2=-1$. Many developments have been carried out in the case of a step initial condition. Indeed, a mapping between the infinite TASEP starting with an initial step and a first-passage percolation model has been found [69], and connections with random matrix theory have been unveiled [68].

Open boundary conditions make the system a bit harder to solve, however many observables of interest can still be derived analytically. For example, the stationary probabilities can be obtained in the form of a product of matrices [64, 70]. The average stationary density profile can also be deduced from this Matrix Product Ansatz [64]. Large deviation methods have also been successfully applied in the large system limit for the current [49] and the density [71, 72].

1.2.4 Application to transport models

The out-of-equilibrium character of the TASEP and the existence of a transition between free flow and jammed phase makes it the fundamental ingredient of many one-dimensional transport models and the basis of many generalizations. For review see Refs. [5] or [73].

Biological applications constitute a wide class of such generalizations. Being first introduced to study the motion of ribosomes on mRNA [40], a natural extension to the TASEP is to introduce attachment and detachment rates in the bulk ('Langmuir kinetics') [74, 75], thus modeling the arrival or the departure of particles from a surrounding solution. The update is almost always continuous time in these applications. The internal processes that characterize some biological entities may however be important, leading for example to the introduction of internal state for the particles that constrain the dynamics [76]. These extensions may thus lead to non-exponential waiting times between consecutive hops [77, 76].

Modified geometries may be considered as well. Transport on two parallel TASEP lanes [78] or equivalent systems [79] have been considered, and junctions between two lanes have been studied as well [80]. Finally entire networks have been studied [81, 82] to model microtubular networks.

Road traffic models also constitute an important part of these applications, for review one can for example see the very detailed Ref. [57]. The first model came from Nagel and Schreckenberg [56, 59] who enabled cars to have a velocity greater than 1, thereby adding rules for accelerating or braking. Some more complex geometries can be studied, incorporating for example the importance of traffic lights [57, 83]. Among these models one finds the BML model [39], to which extensive reference is made in part II. In these car traffic applications the preferred update is the parallel one. Indeed with this discrete-time update an incompressible time scale necessary to change a particle's state of motion naturally appears, which reproduces the important inertia of cars and the reaction time of drivers. Another advantage is that with parallel update fluctuations are bounded, which reproduces the expected regularity of car traffic.

Pedestrians have also been modeled using cellular automata, mostly in two-dimensional evacuation situations. In these models the preferred update is also parallel, again because it has low fluctuations. The will of pedestrians to evacuate the room is modeled through a 'floor field' [60, 34]. One part of this floor field is simply a static potential that attracts pedestrians towards the exit of the room, while the other part is dynamical and models the tendency people have to follow each other. These models have then become more sophisticated with the introduction of a 'friction' that models the supplementary difficulties pedestrians may encounter when moving in a very crowded area [84, 61] or with conflict resolution based on game theory [85, 35, 86]. It is interesting to note that such models also have a similarity with ant trail models, in which ants are attracted by a dynamical 'pheromone' field that other ants deposit when they occupy a site [30, 87].

It should however be noted that, even though similarities are observed between pedestrians and cars [88], in experiments pedestrians seem to exhibit a more complex behaviour than cars, exhibiting large individual variability [89] or noticeable quantitative differences between cultures [11]. Some experiments seem contradictory [16, 18] and are somewhat hard to interpret because of the greater adaptability of the human body compared to a car, which enables many more varied effects to occur. Moreover, while car motion on roads is

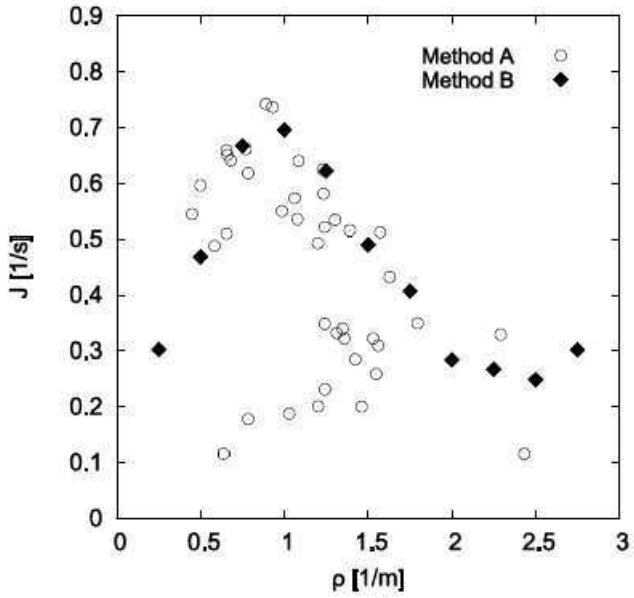

Figure 1.4: Experimental fundamental diagram for pedestrians in a single lane. The measurements are obtained either by time-averaging at a given space point (method A) or by space-averaging at a given moment of time (method B). Different measurement methods can lead to deviations. Taken from Ref. [89].

usually unidimensional, pedestrians generically evolve in two dimensions. Different pedestrians are therefore allowed to have different targets and various path optimization strategies are possible.

In Fig. 1.4 we represent an experimental fundamental diagram of pedestrians, in other words the relation between current and density. Fig. 1.4 shows that difficulties occur during such measurements, here the difference between time- and space-averaging when determining the velocities and the headways of pedestrians. In our simplified models these problems will never occur, so that we will be able to speak of the fundamental diagram unambiguously. Which one is the experimental fundamental diagram of interest and how it should be compared to simplified models are debatable points, which are clearly out of the scope of this thesis.

Experimental measurements on pedestrians have shown that the fundamental diagram can be divided into two parts [11, 89, 13]. On Fig. 1.4, preferably the points from method B, we see the following. For small densities $\rho \lesssim 1\,\mathrm{m}^{-1}$ the current is proportional to the density, interactions between pedestrians are small and each pedestrian moves as if he was alone in what may be called a free flow phase. In more crowded situations $\rho \gtrsim 1\,\mathrm{m}^{-1}$ the current begins to

decrease with increasing density, pedestrians block each other and the flow is jammed.

Chapter 2

Frozen shuffle update

The description of the TASEP in chapter 1 was general and oriented towards statistical physics. We now want to apply this model to pedestrian dynamics, thinking of the particles on the lattice as pedestrians in a street. While several geometries will be considered in the rest of the thesis, we have to select which update schemes can reasonably be applied to pedestrians. Among those we presented in subsection 1.1.3, some of them present clear drawbacks. It has already been argued that continuous time and random sequential updates are believed to have too much fluctuations to reproduce the regular behaviour of pedestrians. Random shuffle update performs a lot better than random sequential and has been used in some applications [29, 90], possibly with some modifications [54]. It however turns out that applications to pedestrians have been preferentially developed with the very regular parallel update, under which two consecutive updates of a pedestrian are separated by exactly one time step. Finally, the principal problem with parallel update is the possible appearance of conflicts in bidimensional situations, *i.e.* cases where two pedestrians target the same arrival site and in which we have to decide what happens. This issue will be taken care of in chapter 4. In this chapter we choose to introduce a new updating rule, the frozen shuffle update, which is designed to be very regular and to propose a natural mechanism for conflict resolution. As an introduction to more complicated problems, this new update scheme is then studied in the simplest geometries.

Frozen shuffle update is defined in section 2.1 and studied on a ring in section 2.2. It is then studied in other simple geometries: open boundary conditions in section 2.3 and in an intersection of two one-dimensional lanes in section 2.4. Note that this work was done almost exclusively during an internship I did at the LPT during my master, sections 2.2, 2.3 and 2.4 constituting summaries of Refs. [91], [92] and [93], respectively, while section 2.1 is the definition of frozen shuffle update common to all the papers. These findings have also been presented on a poster at the PED2012 conference [94].

2.1 Frozen shuffle update

We define frozen shuffle update in subsection 2.1.1, and we show that the free flow phase can be mapped on a time and space-continuous system in subsection 2.1.2.

2.1.1 A tentative update for pedestrians: definition

We want to define an updating scheme that reproduces the expected behaviour of pedestrians. Compared to cars, pedestrians have much less inertia and are expected to adapt their velocity much more easily. Compared to the paradigmatic Nagel-Schreckenberg model for cars [56], we therefore do not need to take the acceleration and deceleration phases into account when modeling pedestrians. For simplicity we neglect the individual variability of free speeds in pedestrians as well, so that all the particles of the model will hop at the same rate. Although this hypothesis seems very crude for real-life situations at low density, it can hopefully be closer to what happens in some experiments where participants are selected according to their age or gender, or in more dense streets where overtaking becomes hard. Pedestrians can flow at very high densities, so that jams will occur mainly if the flux is restricted downstream. In our models, this corresponds to reducing the size of the MC phase in the phase diagram. Another difference with cars is that the natural environment of pedestrians is usually bidimensional, so that when pedestrians target the same site an effective conflict resolution algorithm is required.

Among the most common updating schemes, few of them satisfy these conditions. Continuous time and random sequential update have very high stochasticity that does not suit rational agents like pedestrians. Even random shuffle update can be considered to have too strong fluctuations for our purpose, because of the fact that there is no memory from one time step to another. The bulk dynamics of parallel update is suitable in 1 dimension, however it should be supplemented with a procedure for conflict resolution in higher dimensions. In part II we will be using a variation of it, called alternating parallel update and defined in subsection 4.2.2.

For now we focus on the definition of our update procedure, the *frozen shuffle update*. When a particle P is created, we stochastically give it a real *phase* $\tau_P \in [0; 1)$. During each time step, the particles in the system are updated in the order of increasing phase. In an equivalent continuous-time picture a particle with phase τ_P can be considered to be updated at times $s + \tau_P$, where s is an integer. If the target site of the updated particle is found to be empty, the particle hops on this target site with probability $p \leq 1$ in the generic case. In this thesis we will however consider the case $p = 1$ unless otherwise stated. This updating scheme is low on fluctuations, as there is exactly one time unit between two updates of a given particle, so that the particles are always updated in the same order, and exactly once per time step.

The phases introduce frozen disorder in the particle system, with respect to which the system will tend to self-organize. Since no noise comes directly from

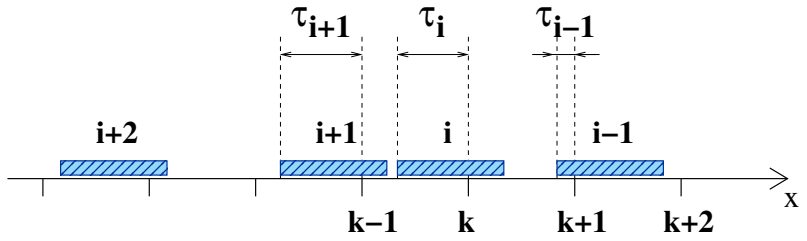

Figure 2.1: Mapping between the free flow phase of the deterministic TASEP with frozen shuffle update and a series of translating rods. The particles correspond to the rods and are denoted by $i-1$, i, ... and the sites are identified with the ticks on the x axis and are denoted by $k-1$, k, ...

the update procedure, when $p = 1$ and for low enough density the stationary state simply consists of uniformly translating the existing particles. The fact that the bulk dynamics is deterministic and organized will in particular lead to the fact that the usual maximal current phase described in subsection 1.2.2 is here reduced to a point (see section 2.3), in accordance with the ability of pedestrians to move at high density. The phase variables can arguably be interpreted in terms of walking cycle [14], even though it is not clear experimentally whether phenomena such as step synchronization are of primary importance or not.

The way the particles are created depends on geometry and will be made precise in the following sections 2.2 and 2.3. The bulk dynamics being deterministic, the initial phases and positions however constitute the only stochastic element of modelization. An ensemble average will therefore always be an average over the phases of the particles, the particles either being all present at initial time or being injected as the process evolves in time.

2.1.2 Interpretation of the phases and continuous mapping

In the free flow phase all the particles hop one site to the right at each time step. The system can then be mapped on a system of non-overlapping rods of length 1 translating with velocity 1 in continuous time and space, which is shown in Fig. 2.1. A particle is then identified with a rod. Each rod covers exactly one integer tick on the position axis, which corresponds to the site occupied by the particle. The phase of the particle is then identified with the distance between the end of the rod and the covered integer tick at integer time, *i.e.* the time the rod has to wait to change the tick it covers. This mapping will prove useful when defining the injection procedure at open boundaries (section 2.3).

Frozen shuffle update clearly is a sequential update scheme. It can be considered intermediate between discrete and continuous time. On the one hand the phases of the particles take continuous values and sometimes benefit from a continuous time picture, but on the other hand once the set of phases is

fixed only a discrete set of moments that is known once for all will contribute to the evolution of the system.

This being said, we now want to explore the properties of this updating scheme by studying it on the simplest possible geometry, *i.e.* the one-dimensional periodic TASEP.

2.2 Study on a ring

The ring is maybe the simplest geometry in which a new update can be studied. We will be forced to understand the basic dynamics of the system (see Fig. 2.2), thereby showing that the TASEP with frozen shuffle update is not ergodic when PBC are used, in the sense that not only the number of particles in the system but also the spatial order of the phases of the particles are conserved by the time evolution. For finite-size systems at a fixed density, some realizations will therefore be in free flow while others will be jammed. In the thermodynamic limit we will however show that, for a given density, either almost all the realizations are in free flow or almost all the realizations are in jammed flow. We will have access to the ensemble-averaged fundamental diagram of the model, an important quantity in the case of experiments with real pedestrians. As frozen shuffle is more regular than other updates, we will see that the jamming transition occurs later with frozen shuffle than with most update schemes, reproducing the better organization that pedestrians are supposed to have compared to *e.g.* ribosomes. This whole section constitutes a summary of Ref. [91].

We consider a one-dimensional lattice, with sites labeled from 1 to L. Periodic boundary conditions (PBC) are imposed, *i.e.* we identify sites 1 and $L+1$. At time $t=0$, N particles are dropped on random sites corresponding to an average density $\overline{\rho} = \frac{N}{L}$. The phases of these particles are independent and identically distributed (i.i.d.) random variables drawn from the flat distribution on $[0;1)$. The averages are then taken on the frozen disorder, *i.e.* the initial phases, as the initial positions do not affact the stationary current. We let the system evolve under frozen shuffle update. As already discussed in subsection 1.2.1, the physical variable of interest is the averaged particle current $\mathcal{J}$.

To understand the dynamics of the system, we first focus on the case of two particles A and B with phases τ_A and τ_B occupying sites i and $i+1$, respectively. If $\tau_A > \tau_B$, B will be updated first. Since site $i+2$ is supposed to be empty particle B will hop, thus freeing site $i+1$. Then A will be updated and hop towards site $i+1$. On the contrary, if $\tau_A < \tau_B$, particle A will be updated first and blocked by particle B which occupies $i+1$. Particle B will then hop towards $i+2$. In the first case the pair is said to be *well-ordered* whereas the second pair is *ill-ordered*. An illustration of such a situation is shown in Fig. 2.2

The first case shows that a sequence of particles occupying consecutive sites is stable if their phases increase with decreasing site number. We will call such

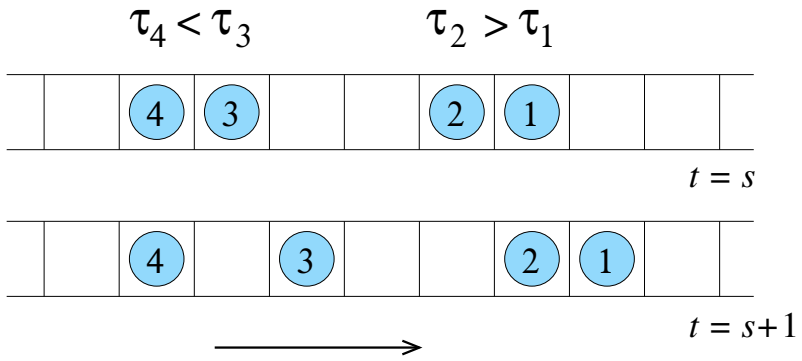

Figure 2.2: Difference of behaviour between a well-ordered and an ill-ordered pair. Here t is a continuous time variable while s is an integer. Particles 1 and 2 can move as a whole because $\tau_1 < \tau_2$ whereas an empty site is needed between particles 3 and 4, as $\tau_3 > \tau_4$.

a sequence a *platoon*. The second case however shows that being in free flow phase requires to have at least one hole for each ill ordered pair. Conversely, it is easy to see that if there are at least as many holes as ill-ordered pairs in the system the free flow phase will be reached. In that case, the current is expected to be $\mathcal{J}^{\mathrm{F}} = \overline{\rho}$.

If there are less holes than ill-ordered pairs, some particles will be blocked at each time step in the stationary state. A realization of disorder in which that occurs will be called a *jammed* realization. In that case, all the well-ordered pairs of particles are compacted into platoons and the stationary state of the system simply consists of a sequence of platoons that have either an empty site between them or not. During a given time step a platoon is allowed to move only if there is an empty site in front of it and all its particles are blocked otherwise, so that only a fraction $(1-\overline{\rho})$ of the platoons move at each time step. The current can therefore be written $\mathcal{J}^{\mathrm{J}} = (1-\overline{\rho})\nu$, where ν is the average size of a platoon.

From what is said in the last paragraph the platoons can then be seen as big particles that are updated in parallel. This shows that there is a connection, although nontrivial, between the jammed phases of parallel and frozen shuffle updates.

At a given density some initial conditions will converge to a free flow stationary state while others will be jammed. Performing the average therefore amounts to counting the number of configurations of each type for given $\overline{\rho}$. This will also give the average platoon length ν.

A pair of particles with no geometry is well -ordered with probability 1/2 and ill-ordered with probability 1/2. As the system is critical when there are as many holes as ill-ordered pairs, in the $L \to \infty$ the critical density must therefore be equal to 2/3. Recurrence relations over the system size

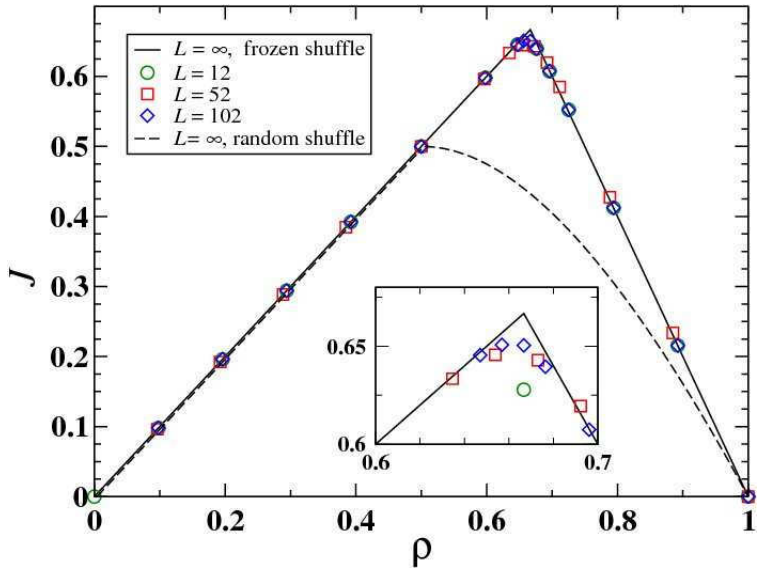

Figure 2.3: Fundamental diagram for frozen shuffle update. The black solid line corresponds to frozen shuffle update in an infinite system. The curve for infinite L is composed of two linear portions linking $(0,0)$ to $(2/3,2/3)$ and $(2/3,2/3)$ to $(1,0)$, the maximal current being attained for a density $\frac{2}{3}$. Symbols represent numerical measurements for finite systems. The finite size corrections can be computed, as shown in Ref. [91]. Frozen shuffle update is compared to random shuffle update, plotted in dashed lines, and clearly shown to be more effective in terms of transport when $\rho > 1/2$.

also enable us to compute finite-size corrections to the $L \to \infty$ behaviour [91]. The corresponding curves are plotted in Fig. 2.3.

2.3 Frozen shuffle update with open boundaries

This section summarizes the findings of Ref. [92].

2.3.1 Injection procedure

We now want to study the same system with open boundaries (OBC). We therefore impose that a particle occupying site L, the exit site, is deleted with probability $\beta < 1$ when it is updated. The deletion procedure itself is independent of the phase of the particle.

Similarly, we would like to create a particle with a certain phase on site 1 with probability $\alpha < 1$ during each time interval of size 1 where site 1, the entrance site, starts empty. In the continuous time picture, the mapping of subsection 2.1.2 suggests creating particles at the entrance with a constant

rate $a > 0$ as long as the entrance site is empty, so that the invariance under time-translations is preserved. Still in continuous time, the probability $K(T)$ that the next particle is created a time $T > 0$ after site 1 is vacated reads

$$K(T) = a\mathrm{e}^{-aT} \qquad T > 0. \tag{2.1}$$

In discrete time, the phase of the created particle will then simply be equal to the fractional part of the time at which it was created. The constant α being defined as the probability that a particle enters during a unit of time where the entrance site starts empty, we easily get

$$\alpha = 1 - \mathrm{e}^{-a}. \tag{2.2}$$

2.3.2 Phase diagram

Similarly to TASEPs with other updates, we expect the system to present a free flow and a jammed flow regime. The maximal current phase is however reduced to one point: the hopping probability being set to 1, the maximal current that the system can convey will be 1 as well.

In the free flow phase the particles move with velocity 1. The continuous time picture of subsection 2.1.2 is therefore valid, and the size of the empty interval between two consecutive particles is equal to the time between the departure of the first particle from the entrance site and the arrival of the second one at the entrance site. Using Eq. (2.1) we show that the average size of the empty interval is equal to a^{-1}, from which we detemine the density and current in the free flow phase,

$$\mathcal{J}^{\mathrm{F}} = \rho^{\mathrm{F}} = \frac{a}{1+a}. \tag{2.3}$$

The current in the jammed phase can be computed in the following way. A particle standing on site L needs on average β^{-1} time steps to exit the system, a platoon of length n will need $n\beta^{-1}$ time steps. There is a hole between two consecutive platoons, so that we must wait one more time step to be back into the initial state. A number n of particles have therefore exited the system in $n\beta^{-1} + 1$ time steps. We denote the average size of a platoon by ν, so that for a number $\mathcal{N}$ of platoons of lengths $n_1,\ldots,n_{\mathcal{N}}$ we have $\sum_i n_i = \mathcal{N}\nu + O(\sqrt{\mathcal{N}})$ particles. The system is in a cyclic state, so that these platoons take a time $\sum_i (n_i\beta^{-1} + 1) = \mathcal{N}(\nu\beta^{-1} + 1) + O(\sqrt{\mathcal{N}})$. The particle current in the jammed phase therefore reads

$$\mathcal{J}^{\mathrm{J}} = \beta\rho^{\mathrm{J}} = \frac{\beta\nu}{\beta+\nu}. \tag{2.4}$$

It is worth underlining that, contrarily to the case of the most common updates, the jammed current $\mathcal{J}^{\mathrm{J}}$ depends not only on the exit probability β but also on the entrance rate a through the structure of the platoons.

A platoon of length n will be formed each time exactly n consecutively injected particles have increasing phases. It does not matter whether the particles are on consecutive sites or not, as the sequence will be compacted once it

reaches the jam. We are therefore lead to consider the decimal part of the delay between two particles $\hat{T} \equiv T - \lfloor T \rfloor$. The variable $\hat{T}$ is equal to the difference of the phases of the two particles that have been injected with a delay T, possibly modulo 1 if the second phase is smaller than the first one. Its distribution is obtained from Eq. (2.1) [92],

$$\hat{P}(\hat{T}) = \frac{a\mathrm{e}^{-a\hat{T}}}{1-\mathrm{e}^{-a}}. \tag{2.5}$$

The average platoon length is then the inverse of the characteristic difference between consecutive phases,

$$\frac{1}{\nu} = \int_{\hat{T}=0}^{1} \hat{P}(\hat{T})\mathrm{d}\hat{T} = 1 + \frac{1}{a} - \frac{1}{1-\mathrm{e}^{-a}}. \tag{2.6}$$

The equation of the transition line between free flow and jammed flow is then $\mathcal{J}^{\mathrm{F}} = \mathcal{J}^{\mathrm{J}}$, which gives $\alpha = \beta$. The system is in free flow phase for $\alpha < \beta$ and in jammed phase for $\alpha > \beta$. What would normally be called maximal current phase can be thought of as reduced to the point $\alpha = \beta = 1$, even though there is no need to introduce such a concept here. The density as a function of α is plotted in Fig. 2.4 for different system sizes, clearly showing the phase transition.

In Fig. 2.5 the density profile is plotted for α crossing the transition. A theoretical explanation based on the so-called domain wall theory was attempted. We delay the explanation of this theory until chapter 3, where it is exposed in great detail. Fig. 2.5 shows that there is a weak but persistent discrepancy between theory and numerics. Its explanation will be one important focus of section 3.2.

2.4 Intersecting unidimensional lanes with open boundaries

We now want to study the case of two open lanes, similar to the one of section 2.3, that intersect on a given site, here the exit site. We will see that the phase diagram of this model can be determined exactly thanks to a remarkable pairing effect. Moreover the obtained expressions of the currents are easily generalizable to the case with arbitrary number of lanes. It also serves as a preliminary for part II, in which the intersection will be enlarged. This system was first considered in Ref. [93].

2.4.1 Intersecting lanes

Here we precisely define the model that we are going to study. We consider an intersection of two one-dimensional open lanes similar to those of section 2.3, as shown in Fig.2.6. The parameters controlling the entrances, α_1 and α_2, and the exits, β_1 and β_2, of both lanes are chosen independently.

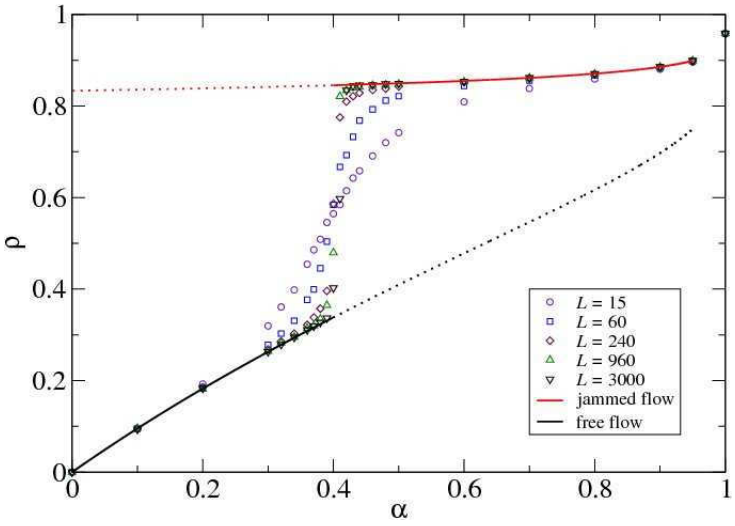

Figure 2.4: Space-averaged density as a function of the entrance parameter α for the open chain with exit probability $\beta = 0.4$. Each symbol corresponds to a system size, while the black and red solid lines are the predictions (2.3) for the free flow phase and (2.4) for the jammed phase, respectively. For critical $\alpha = 0.4$ the density shows a discontinuity in the large L limit.

We are interested in the phase diagram of this model, as a function of the four parameters α_1, α_2, β_1 and β_2. Based on the findings of section 2.3, we expect each of the two lanes to be either in free flow or in jammed phase, which we will denote by FF when the two phases are in free flow, FJ when the first is in free flow and the second is jammed, JF and JJ, similarly. Before deriving the exact phase diagram we will point out an interesting effect specific to frozen shuffle update that is observed in this system.

2.4.2 Pairing effect

Consider the system from Fig.2.7 in the JJ phase. In this phase there are two queues on both lanes.

For the purpose of the demonstration we start at a time when the intersection site is empty, there are therefore two platoons of particles of length n_1 (on lane 1) and n_2 (on lane 2) which will potentially invade the intersection at the next time step. The particles of these platoons are labeled as 1, 2, ..., n_1 and $1'$, $2'$, ..., n_2 as shown in Fig. 2.7(a). If $\tau_1 < \tau_{1'}$ the first particle to hop towards the intersection will be particle 1 (subfigure (b)). Particle 1 then exits with probability β_1 and therefore needs on average β_1^{-1} time steps to exit the system. Now suppose $\tau_{1'} < \tau_2$, so that $1'$ hops towards the intersection at the exact same time step when particle 1 exits the system (c). Particle $1'$

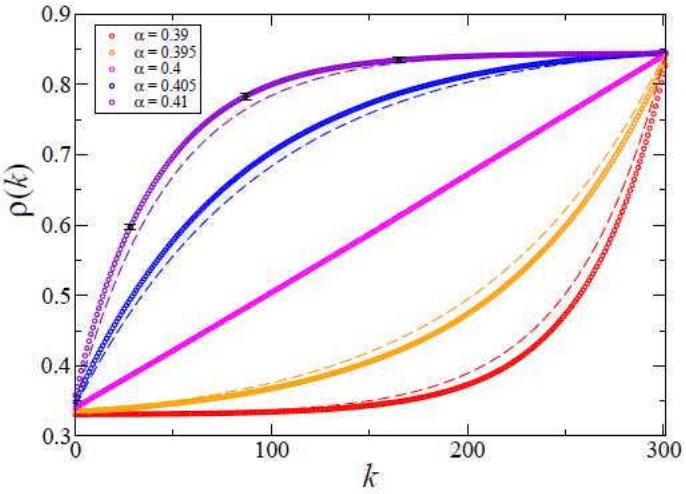

Figure 2.5: Density profile for a system of size $L = 300$ with $\beta = 0.4$ and alpha close to criticality. Data points correspond to simulations and dashed curves to the predictions of the simple domain wall theory exposed in section 3.1. Each simulation had a duration of 8×10^7 time steps. An explanation of the discrepancies between theory and simulations will be given in section 3.2.

then takes on average β_2^{-1} time steps to exit the system. The particle with the lowest phase between 2 and $2'$ then hops to the intersection, and so on (d)-(e). Examination of the dynamics shows that when the last particle of the union of both platoons 1 and 2 exits the system, the intersection site is vacated because the following particles are either blocked or are still 1 site apart from the last exiting particle and will therefore hop forward on a neighbouring site of the intersection.

This examination calls for several comments. First of all, the particles of platoons 1 and 2 hopped towards the intersection site in the order of their phases and without any empty site between them, just as if they were all part of a single big platoon. This natural merging phenomenon between two platoons gives its name to the *pairing mechanism*. The second remark is that the state of the system after platoons 1 and 2 have exited shown in Fig. 2.7(f) is similar to the starting position (a). Indeed figures (a) and (f) both show an empty intersection site with one platoon arriving from each lane, the first particle of the platoon being on the site just before the intersection site. Even though the platoons represented in figures (a) and (f) are different it should be noted that their statistical properties are the same, and are independent. The system is then cyclic in the sense that it can then be described as a sequence of i.i.d. events.

Using this, we can compute the output current. With the notations of

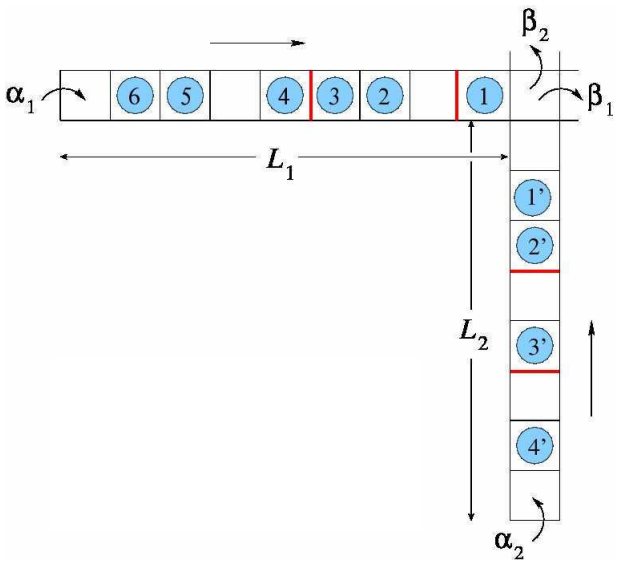

Figure 2.6: The two-lane configuration studied in this section. Particles are represented by blue circles and a heavy red bar represents the end of a platoon, as defined in subsection 2.2. The entrance probabilities are denoted by α_1 and α_2 and the exit probabilities by β_1 and β_2. The two lanes have lengths L_1 and L_2, though it will be of little importance for the following.

Fig. 2.7, n_1 particles exited lane 1 during a time $1 + \frac{n_1}{\beta_1} + \frac{n_2}{\beta_2}$, on average over the realizations of the exit. The system was then back in the starting state. Considering a large number $\mathcal{N}$ of platoons, the central limit theorem ensures that $\mathcal{N}\nu_1$ will exit lane 1 in a time $\mathcal{N}(1+\nu_1\beta_1^{-1}+\nu_2\beta_2^{-1})+O(\sqrt{\mathcal{N}})$ The average current in the JJ phase reads

$$\mathcal{J}_\sigma^{\mathrm{JJ}} = \frac{\nu_\sigma}{1 + \frac{\nu_1}{\beta_1} + \frac{\nu_2}{\beta_2}}, \qquad \sigma = 1, 2, \tag{2.7}$$

where the mean platoon length ν_σ is still given by Eq. (2.6).

This key observation will enable us to determine the full phase diagram of the model in the following subsection 2.4.3.

2.4.3 Phase diagram

Similarly to the OBC case the phase diagram in the stationary state will be determined from the conservation of current in the whole system. Our remaining task is then to compute the current in the FF, FJ and JF phases.

The expressions in the FF phase is simply the same as in Eq. (2.3), as the two systems do not interact enough to disturb the stationary current. We write

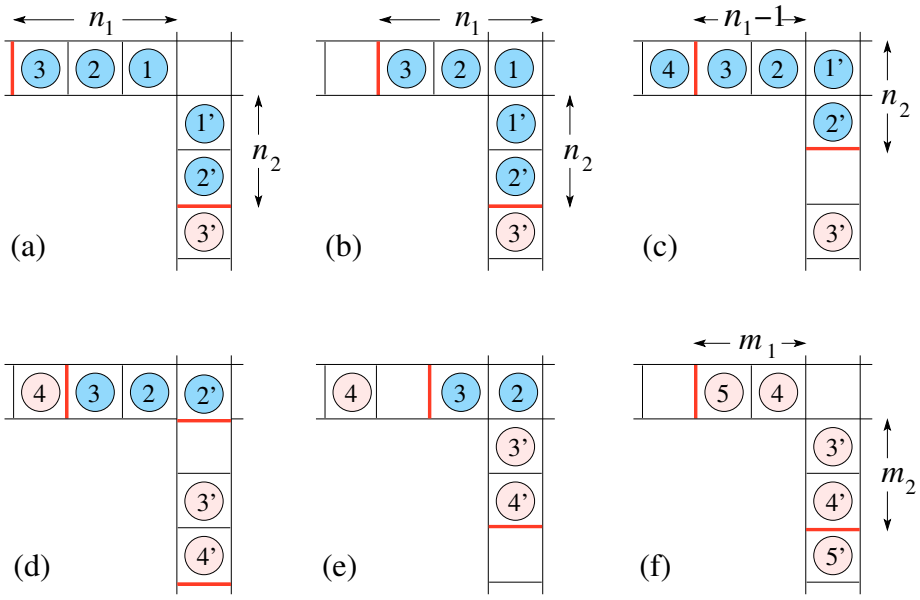

Figure 2.7: Illustration of the pairing mechanism between platoons on a particular case. The dynamics is such that when both lanes are jammed the platoons always exit the system in pairs. The figure is described step by step in the main text.

it once again for clarity,

$$\mathcal{J}_\sigma^{\mathrm{FF}} = \frac{a_\sigma}{1+a_\sigma}, \qquad \sigma = 1, 2, \tag{2.8}$$

with $a_\sigma = -\log(1-\alpha_\sigma)$.

In the FJ phase lane 1 is in free flow so that $\mathcal{J}_1^{\mathrm{FJ}}$ is simply given by Eq. (2.8). For lane 2 we generalize the argument based on the pairing effect by defining μ_1 as the average number of particles that exit on lane 1 during the time needed for a platoon to exit lane 2. We can then write

$$\mathcal{J}_2^{\mathrm{FJ}} = \frac{\nu_2}{1+\frac{\mu_1}{\beta_1}+\frac{\nu_2}{\beta_2}}, \tag{2.9}$$

where μ_1 is determined by $\mathcal{J}_1^{\mathrm{FJ}} = \frac{\mu_1}{1+\frac{\mu_1}{\beta_1}+\frac{\nu_2}{\beta_2}} = \frac{a_1}{1+a_1}$. Of course symmetrical expressions hold in the JF phase.

The equations of the phase boundaries are obtained when two of the currents (2.8), (2.9) and (2.7) are equal. More precisely, $\mathcal{J}^{\mathrm{FF}} = \mathcal{J}^{\mathrm{FJ}}$ gives an equation for the FF/FJ boundary, $\mathcal{J}^{\mathrm{FJ}} = \mathcal{J}^{\mathrm{JJ}}$ gives the FJ/JJ boundary, and the phase diagram is obviously symmetric by exchange of the two lanes. It is plotted in Fig. 2.8. In particular, we find that all the phase boundaries intersect at a four-phase point $\alpha_1 = \alpha_2 = \frac{\beta_1\beta_2}{\beta_1+\beta_2}$.

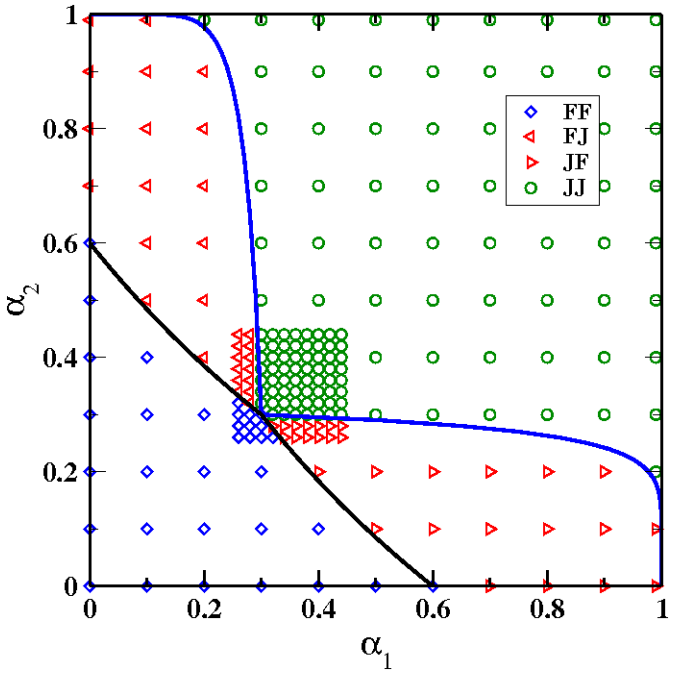

Figure 2.8: Phase diagram of the two-lane system for $\beta_1 = \beta_2 = 0.6$ in the (α_1, α_2) plane. Solid lines represent theoretical predictions and the symbols are the results of numerical measurements. There is a four-phase point for $(0.3, 0.3)$.

More detailed calculations can be done, in particular the density can be deduced from the current in all phases. A more detailed report can be found in Ref. [93].

2.4.4 More than 2 lanes

A natural way of generalizing of the two-lane problem is to consider P lanes. In that case each lane would have its parameters α_σ, β_σ and L_σ for $\sigma = 1, \ldots, P$, and the last site L_σ of each lane σ would be common between all lanes. The previous expressions can be easily generalized to this geometry, because the 'pairing' effect still exists in that case. In this case we denote by $\mathcal{J}^n_{\sigma,F/J}$ the current in a free (jammed) lane, where we keep track of the number n of jammed lanes.

If all the lanes are in free flow the currents simply read

$$\mathcal{J}^0_{\sigma,F} = \frac{a_\sigma}{1 + a_\sigma} \tag{2.10}$$

If there is at least one jammed lane we make use of the variables μ_σ and we

define

$$S_\mu \equiv \sum_{j\in \mathrm{F}} \frac{\mu_j}{\beta_j} \tag{2.11}$$

and

$$S_\nu \equiv \sum_{j\in \mathrm{J}} \frac{\nu_j}{\beta_j}, \tag{2.12}$$

where $\sum_{j\in \mathrm{F/J}}$ means a sum over all the free (jammed) lanes. For the currents we naturally get

$$\mathcal{J}^{n>0}_{\sigma,F} = \frac{\mu_\sigma}{1+S_\mu+S_\nu}, \tag{2.13}$$

$$\mathcal{J}^{n>0}_{\sigma,J} = \frac{\nu_\sigma}{1+S_\mu+S_\nu}. \tag{2.14}$$

The μ_σ are still determined by the fact that the free flow current is equal to the expression (2.10), namely

$$\frac{\mu_\sigma}{\mathcal{J}^0_{\sigma,F}} = 1+S_\mu+S_\nu. \tag{2.15}$$

We can substitute the value of μ_σ given by Eq. (2.15) in Eq. (2.11), which gives an equation for the value of S_μ. Introducing the shorthand notation $S_\mathcal{J} \equiv \sum_{j\in \mathrm{F}} \frac{\mathcal{J}^0_{j,F}}{\beta_j}$, we finally get $S_\mu = \frac{S_\mathcal{J}(1+S_\nu)}{1-S_\mathcal{J}}$ and an expression for μ_σ in terms of the control parameters only,

$$\mu_\sigma = \mathcal{J}^0_{\sigma,F}\frac{1+S_\nu}{1-S_\mathcal{J}}, \tag{2.16}$$

and explicit expressions for the currents of the jammed lanes

$$\mathcal{J}^{n>0}_{\sigma,J} = \nu_\sigma \frac{1-S_\mathcal{J}}{1+S_\nu}. \tag{2.17}$$

Despite the fact that these expressions look complicated, it is not hopeless to try to extract information from them, at least in the simplest cases.

The simplest case occurs when all the lanes have the same parameters α and β. In this case we expect all the lanes to get jammed at the same time by symmetry under permutations. The currents simplify to

$$\mathcal{J}^0_F = \frac{a}{1+a}, \tag{2.18}$$

$$\mathcal{J}^P_J = \frac{\nu}{1+\frac{P\nu}{\beta}}. \tag{2.19}$$

At the jamming point the currents are equal. The equation we need to solve is similar to the single OBC lane with a modified value of the exit parameter, which readily gives the critical point $\alpha = \beta_{\mathrm{eff}}(P) = \frac{\beta}{P}$, as could be guessed

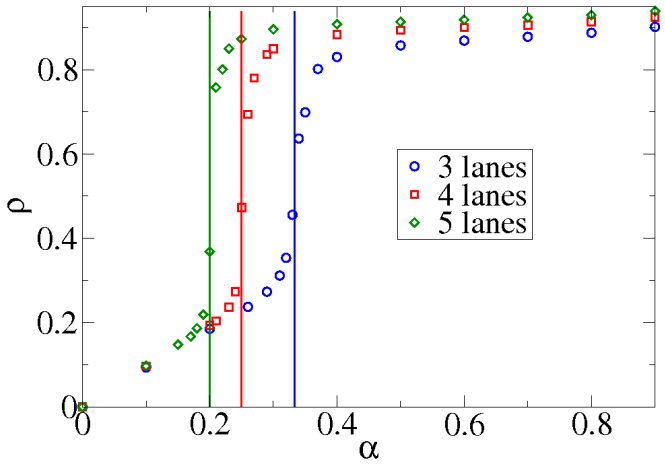

Figure 2.9: Phase transition for systems with P identical lanes for $P = 3, 4, 5$ and $\beta = 1$. Symbols correspond to numerical measurements and the vertical solid lines simply mark the expectedly critical values. Jamming indeed occurs for $\alpha = \frac{1}{P}$.

from symmetry considerations. This simple case has been tested numerically and is shown in Fig. 2.9.

This work has not been pursued further, but leaves some interesting perspectives. One could think of trying to determine which lanes are in free flow and which are in jammed flow in the general case where the P lanes have different α and β constants. In particular it is not clear in which order the successive phase transitions will occur for a given set of parameters. Maybe simplifications occur when $P \to \infty$, a particular kind of thermodynamic limit. Finally, an other appealing direction is the generalization to more complex networks.

Chapter 3

The domain wall picture

Domain wall theory is a generically approximate theory that aims at describing a spatially extended system in terms of homogeneous domains separated by walls. This tool sometimes greatly simplifies the analysis of a problem and enables one to trace out the microscopic structure of the system while keeping only a handful of macroscopic variables. In the case of the TASEP, domain wall has been used to predict static and dynamical quantities in a simple way, at least in a part of the phase diagram and with great success in the case of random sequential update. In particular, the domain wall theory enables to understand the transition between free flow and jammed phase with simple arguments. The first section 3.1 presents the domain wall theory, first in general and then in the specific case of the TASEP with continuous time update.

While it is understood that domain wall fails in certain parts of the phase diagram due to long-range correlations, other discrepancies are observed when the update scheme is changed. In particular, parallel update is widely used in traffic applications and a simple and accurate description of the jamming transition would be of great utility. In section 2.3 we also observed discrepancies between the traditional domain wall theory and the numerics in the density profile of the open TASEP with frozen shuffle update, see Fig. 2.5. Indeed, the success of the traditional domain wall theory in random sequential update is closely related to the absence of correlations between neighbouring sites of the bulk, while we will see that nearest-neighbour correlations are relatively strong in updates with low fluctuations such as parallel or frozen shuffle update.

To understand these discrepancies we present an exact solution of the deterministic TASEP with parallel update in section 3.2. This solution relies on an exact microscopic definition of the domain wall that can easily be compared to the approximate theory of section 3.1. Strikingly, the exact solution shows memory effects that are completely neglected by the approximate domain wall theory and lead to a discrepancy in the density profile similar to the one exhibited in section 2.3. These results are also presented in Ref. [95].

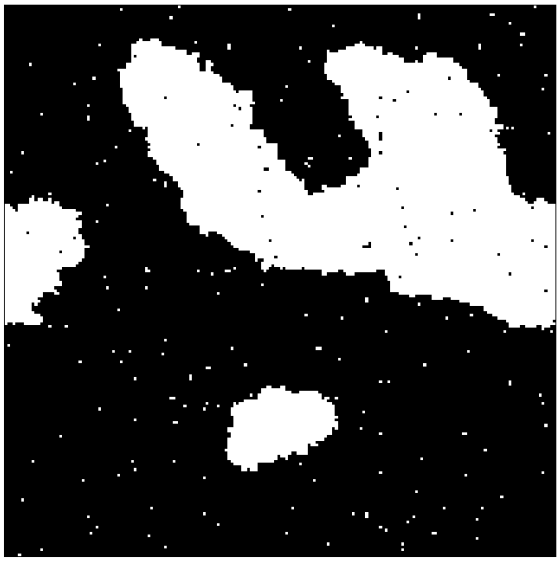

Figure 3.1: Typical configuration of the bidimensional Ising model for a system of size 200 and periodic boundaries. Black sites represent down spins and white ones represent up spins. The systems is roughly divided in black and white domains separated by an interface.

3.1 Domain wall theory

3.1.1 General idea

Domain walls have found their origin in the study of magnetic systems, where it is found that homogeneous zones are separated by interfaces. Over time these concepts have been used in various problems of statistical mechanics [96, 97] or high-energy physics [98, 97], finding applications *e.g.* in gravitation. We however stick to traditions and start with illustrating the main ideas on the most famous model for magnetism: the Ising model.

Consider the two-dimensional ferromagnetic Ising model, say on a square lattice. For large temperatures the equilibrium state of the system is determined by entropic effects: the two-point correlation function decays exponentially with a finite correlation length, so that the magnetization per spin of an infinite system is equal to zero on average. When the temperature goes down energetic effects become more important to the point of dominating the entropic ones, so that the system reaches a critical point where the system gets ordered, the correlation length diverges and the average magnetization per spin becomes nonzero.

In the disordered phase the system is however not completely disordered, as the energetic cost of a configuration in which the spins are uncorrelated is too important. Since the correlation length is finite the equilibrium state should rather consist of homogeneous domains of a size of the order of the correlation length, that will be separated by interfaces also called *domain walls*. In the case of the Ising model the homogeneous domains simply consist of regions where almost all the spins are up or all the spins are down, a domain being characterized only by its macroscopic magnetization. The interaction is nearest-neighbour and the spins can only take two values, so that a domain wall will simply be composed of links where one spin is up and the other is down. In particular the width of a wall is strictly equal to 1 in this case. Fig. 3.1 shows a snapshot of the 2D Ising model for illustration.

Here we also present an analytic illustration of this concept. We consider a one-dimensional model system whose microscopic state is described by a function $u(x,t)$, and where the spatial average of $u(x,t)$ as the order parameter of the system. We suppose that the evolution of this system is described by Burgers' equation

$$\frac{\partial u}{\partial t} = u\frac{\partial u}{\partial x} + \nu\frac{\partial^2 u}{\partial x^2}, \tag{3.1}$$

valid inside the system bounds $-L/2 < x < L/2$ for $t > 0$, where ν has the interpretation of a diffusion constant. We now look for solutions of Burgers' equation where a domain wall is present to use them as a pedagogical example to illustrate the main steps of the reasoning. Requiring that the system is homogeneous near the boundaries here means imposing that the profile $u(x,t)$ becomes flat when x approaches $\pm L/2$; $\frac{\partial u}{\partial x}(\pm L/2, t) = 0$. We write $u(\pm L/2, t) = \overline{u} \pm \Delta u$, where $\overline{u}$ and Δu are fixed control parameters.

We now want to know what the interface between domains looks like. For simplicity we look for a propagating solution of Eq. (3.1) that depends only on $x - vt$ for some constant velocity v. The size of the system being intended to be large, we send L to infinity to avoid complications and suppose that the solution does not change much for L large but finite. For $\Delta u \geq 0$ one then obtains a family of solutions

$$u(x,t) = \overline{u} + \Delta u\frac{2}{\pi}\tanh\left(\frac{\Delta u(x - x_0 + \overline{u}t)}{\pi\nu}\right), \tag{3.2}$$

where x_0 is a constant of integration and v takes the value $-\overline{u}$.

Roughly speaking $u(x,t)$ is therefore equal to one of the two imposed constant values outside of a region of width $\sim \nu$ around $x_0 + vt$. If $\nu \ll \Delta u L$ one can simply think of the system as being separated in two domains characterized by the macroscopic parameters $\overline{u}$ and Δu where $u(x,t) = \overline{u} \pm \Delta u$ depending on the domain. Again for $\nu \ll \Delta u L$ the wall may be considered infinitely thin and is located at $w(t) = x_0 + vt$. In agreement with what we said earlier the motion of the wall is fully determined by the macroscopic characteristics of the domains, as we found $v = -\overline{u}$. Note that in a more usual treatment the

velocity of the wall would be found by using the conservation of mass at the interface, with $-\frac{u^2}{2} - \nu\frac{\partial u}{\partial x}$ being the conserved current.

The order parameter of the system is then simply given by the integral of $u(x,t)$. In our special case the interface is symmetrical so that the domain wall picture gives the same result as the exact calculation to leading order in L. The domain wall calculation is however much simpler. For times such that $|w(t)| < L/2$ we get

$$\begin{aligned}\frac{1}{L}\int_{x=-L/2}^{L/2} u(x,t)\mathrm{d}x &= \frac{1}{L}\int_{x=-L/2}^{w(t)} (\overline{u}-\Delta u)\mathrm{d}x \\ &\quad + \frac{1}{L}\int_{x=w(t)}^{L/2} (\overline{u}+\Delta u)\mathrm{d}x \\ &= \overline{u} + \frac{2w(t)}{L}\Delta u. \end{aligned} \tag{3.3}$$

According to the domain wall picture, for $|w(t)| = L/2$ the wall reaches a boundary and the system reaches a stationary state where u is constant and uniform. In the actual solution a boundary layer of width $\sim \nu/\Delta u$ should be expected near the invaded boundary. The stationary state depends on the sign of v, which depends on the sign of $\overline{u}$. In this regard the system is critical for $\overline{u} = 0$ at any fixed value of Δu, and the domain wall picture provides a dynamical explanation for the phase transition.

In arbitrary dimensions domain walls are hypersurfaces, *e.g.* the domain walls are one-dimensional curves in the 2D Ising model and points for the one-dimensional equation (3.1). Burgers' equation describing the continuous limit of a TASEP with density $\frac{1}{2}(1-u(x,t))$, it comes as no surprise that the domain wall theory can be applied to TASEP. We concentrate on this particular case in the following subsection.

3.1.2 Domain wall theory for TASEP

The TASEP may also be described with a *domain wall theory* (DWT). The idea has been implemented in the case of continuous time by Kolomeisky *et. al* [99] in the following form. The wall separates two homogeneous domains + on the right and − on the left which are fully determined by their densities $\rho_\pm$ and their currents $\mathcal{J}_\pm$. The probability to find the wall at position i at time t, denoted $P_i(t)$, is assumed to obey a master equation of the form

$$\frac{\mathrm{d}P_i(t)}{\mathrm{d}t} = D_+P_{i-1}(t) + D_-P_{i+1}(t) - (D_+ + D_-)P_i(t), \tag{3.4}$$

containing two a priori unknown coefficients D_+ and D_-. These coefficients now have to be linked to the intrinsic characteristics of the domains, in the case of the TASEP the densities and the currents. Mass conservation imposes the value of the drift $\delta \equiv D_+ - D_- = \frac{\mathcal{J}_+ - \mathcal{J}_-}{\rho_+ - \rho_-}$ but an hypothesis on the

fluctuations is needed to determine the diffusion constant $D \equiv \frac{D_+ + D_-}{2}$. In a TASEP, if $\mathcal{J}_- = 0$ we expect to have $D_- = 0$ becasue the particles hop only from left to right. Still in the particular case $\mathcal{J}_- = 0$, this would give $D_+ = \frac{\mathcal{J}_+}{\rho_+ - \rho_-}$. Interpreting the motion of the wall as the result of two independent shot noises coming from the right and the left domains, we get $D = \frac{1}{2}\frac{\mathcal{J}_+ + \mathcal{J}_-}{\rho_+ - \rho_-}$. The probability distribution of the position of the wall gives access to all the properties of the system. For instance, the density profile can be determined using

$$\rho_i(t) = \rho_+ \sum_{k=1}^{i} P_k(t) + \rho_- \sum_{k=i+1}^{L} P_k(t), \tag{3.5}$$

where the choice of putting site i in the + domain is arbitrary and does not make any difference in the large L limit.

For later reference, we also note that in the large system limit Eq. (3.4) becomes a Fokker-Planck equation for a function $\mathcal{P}(x,t)$ that depends on a continuous variable $x \equiv \frac{i}{L} \in [0;1]$, simply by performing a Taylor expansion. This equation reads

$$\frac{\partial \mathcal{P}}{\partial t} = -\frac{\delta}{L}\frac{\partial \mathcal{P}}{\partial x} + \frac{D}{L^2}\frac{\partial^2 \mathcal{P}}{\partial x^2} + O(L^{-3}). \tag{3.6}$$

The derivation of this equation is essentially a simpler case of the passage from Eqs. (3.10) to Eqs. (3.22), so that the reader can check the details there if needed.

This theory works surprisingly well for TASEP with continuous time update for $\alpha, \beta < p/2$, the most important predictions being the nonstationary ones, that are missed by exact solutions in OBC. In this range of parameters domain wall theory successfully predicts dynamical quantities, *e.g.* relaxation times, of the TASEP when its update is continuous time [100, 101, 102] and can be easily adapted to variants with modified kinetics [103, 79, 104, 75] and geometries [78, 105, 106, 107], or be used as a basis for more general discussions [108]. For higher α or β the density-density correlations can decay algebraically [64] so that the hypothesis of an infinitely thin domain wall breaks down and the predictions become incorrect [101, 109, 110, 111].

For other updates, however, observed discrepancies with exact [112, 105] or numerical [92, 113] results call for an adapted DWT such as proposed in Refs. [114, 112] for sublattice parallel update and in Ref. [115] for some particular configurations of a system with parallel update.

In an other approach, some exact equations for domain walls have been written in particular cases by G. Schütz and collaborators. For sublattice parallel update, *i.e.* one updates alternatively the even and the odd links, exact drifts and diffusion coefficients were found in Refs. [112, 114] for an infinite line, and finite-size corrections were proposed in Ref. [114] to study the open boundary case. For deterministic parallel update, a special class of configurations that give rise to a shock have been studied in Ref. [115] for an infinite line. We stress the fact that the configurations studied in Ref. [115] are different from those

found in an usual open TASEP with deterministic parallel update, so that the dynamics of the shock studied by the authors of Ref. [115] is different from what we will find in section 3.2. Finally, we note that in Ref. [112] a general formula for the diffusion coefficient is conjectured, that reads

$$D = \frac{\mathcal{J}_+ + \mathcal{J}_-}{\rho_+ - \rho_-}\left(1 - \left(\frac{\delta}{2}\right)^2\right). \tag{3.7}$$

We now turn on to the exact solution of the open TASEP with deterministic parallel update.

3.2 Domain wall theory for the deterministic case with parallel update

In the case of the frozen shuffle update the expressions of the currents and the densities in each phase are given by Eqs. (2.3), (2.4) and (2.6). Domain wall theory as presented in the previous subsection 3.1.2 should in principle be applicable. Discrepancies were however observed, as shown in Fig. 2.5. Indeed with frozen shuffle update important correlations between neighbouring sites exist, contrarily to the case of continuous time update, that are *a priori* not taken into account in the domain wall theory. We have seen that both the free flow and the jammed phase of the frozen shuffle update look like those of the parallel update. In this latter case discrepancies are observed as well, and we shall show that the short range correlations indeed explain the discrepancies.

Here we turn our interest towards parallel update, under which all the hopping, entrance and exit operations are performed at the same time. In parallel update exact expressions for the stationary state have already been found [70, 116], but here we write exact closed dynamical equations whose variables are essentially the position and the velocity of a domain wall. From there discrepancies between the exact solution and the approximate theory of subsection 3.1.2 are made very explicit in a scaling limit where the system is close to criticality and large at the same time. In this last case all the subtleties are contained in the diffusion coefficient alone, which is shown not to agree with the approximate one. Moreover, parallel update shares a lot of properties with frozen shuffle update, so that this exact calculation also provides a qualitative explanation for the discrepancies of Fig. 2.5.

3.2.1 Structure of the system: the flag

A precise microscopic definition of the domain wall is possible when one uses deterministic parallel update, and more generally when all the particles of the free flow phase move with a velocity exactly 1. Let us define the *flag* as being located on the same site as the leftmost particle that has ever been blocked. If no particle in the system has ever been blocked, the flag is located on a virtual site $L + 1$. The update rule being deterministic in the bulk, it is easy to see that if no particle is blocked at the exit the motion simply consists of a

translation of the particles 1 site to the right at each time step, and no particle is ever blocked. Consequently, a particle can be blocked only if its predecessor has already been blocked. This shows by induction that all the particles to the right of the flag have already been blocked. By construction, no particle to the left of the flag has ever been blocked. These observations show that the flag separates two qualitatively different regions to be identified with the *free flow domain* on the left and the *jammed domain* on the right. The 'velocity' of the flag $a = \pm 1, 0$ is defined as the value of the last hop of the flag to the right, *i.e.* is -1 if the flag hopped to the left, 0 if it did not move, $+1$ if it hopped to the right.

There are simple correlations between the occupation probabilities of the sites in the free flow domain coming directly from the injection rule at the entrance boundary. More precisely we have that if site i is empty then site $i-1$ is occupied with probability α, and if site i is occupied then site $i-1$ is empty for sure. After ensemble average, in the free-flow domain the occupations $\rho_i(t)$ obey the following recurrence relations

$$\rho_{i-1}(t) = \alpha(1 - \rho_i(t)). \tag{3.8}$$

Similar relations hold in the jammed domain, making use of the particle-hole symmetry.

3.2.2 Time evolution of the flag

It turns out that the coupled evolution of the position and of the velocity of the flag constitutes a Markov process. Indeed, let us examine the microscopic dynamics of the flag. If the flag is on site i we know for sure that there is a particle on i. The flag will hop to the right if and only if $i-1$ and $i+1$ are empty, hop to the left whenever site $i-1$ is occupied (because the particle standing on $i-1$ will be blocked by the one on i) and stand still otherwise.

Let us evaluate the probabilities of each of these events. Examination of the structure of the jammed domain shows that, before the flag hops, site $i+1$ is occupied with probability $1-\beta$ no matter the velocity of the flag. Site $i-1$ is occupied with probability α if $a = 0$ or -1 but it is necessarily empty if $a = 1$, the particle carrying the flag having just freed this site. This last remark clearly shows that there is a correlation between the flag velocity at two successive time steps.

We define $P_i^a(t)$ as the probability that the flag is on site $i = 1, 2, \ldots, L+1$, having hopped $a = 0, \pm 1$ sites to the right at the last time step. It turns out that the evolution equations can be written in terms of $P_i^1(t)$ and the combination

$$P_i^{-10}(t) \equiv P_i^{-1}(t) + P_i^0(t) \tag{3.9}$$

only. The bulk equations read

$$\begin{aligned} P_i^{-10}(t+1) &= \alpha P_{i+1}^{-10}(t) + (1-\alpha)(1-\beta)P_i^{-10}(t) \\ &\quad + (1-\beta)P_i^1(t), \\ P_i^1(t+1) &= (1-\alpha)\beta P_{i-1}^{-10}(t) + \beta P_{i-1}^1(t), \end{aligned} \tag{3.10}$$

for $2 \leq i \leq L-1$ and $3 \leq i \leq L$, respectively. At the left boundary one has to be careful that no particle can come from the site 0, which gives $P_1^1(t) = 0$ for all times. On the neighbouring sites we have

$$\begin{aligned} P_1^{-10}(t+1) &= \alpha P_2^{-10}(t) + (1-\beta) P_1^{-10}(t), \\ P_2^1(t+1) &= \beta P_1^{-10}(t). \end{aligned} \tag{3.11}$$

The right boundary requires more attention. When the flag stands on the virtual site $L+1$ its dynamics depends on the occupation of site L, which depends on the number of time steps the flag has spent on $L+1$ in a row. To see this, let us define R_u (and S_u) as the probability that the flag stood on site $L+1$ for $u = 0, 1, 2, \ldots$ time steps in a row and that site L is occupied (empty). The average occupation of site L conditioned by the fact that the flag has spent u time steps on site $L+1$ then reads $r_u = \frac{R_u}{R_u + S_u}$.

If the flag has been on site $L+1$ for u time steps and L is empty, there is simply a probability α that it will be filled and $(1-\alpha)$ that it will be vacated. If site L is occupied either the particle on L exits with probability β or it stays blocked at the exit. In the first case the flag does not move and we know site L will be empty in the next time step, whereas in the second case the flag hops to L and leaves $L+1$, so that there is a loss of probability. The R_u and S_u therefore obey the first-order recurrence

$$\begin{aligned} R_{u+1} &= \alpha S_u \\ S_{u+1} &= (1-\alpha) S_u + \beta R_u. \end{aligned} \tag{3.12}$$

When the flag hopped towards $L+1$ site L was necessarily empty, which gives the initial condition $R_1 = \alpha$ and $S_1 = 1-\alpha$ or equivalently $R_0 = 0$ and $S_0 = 1$. Diagonalizing the transfer matrix of Eqs. (3.12) gives the eigenvalues $\lambda_\pm = \frac{(1-\alpha) \pm \sqrt{(1-\alpha)^2 + 4\alpha\beta}}{2}$ and the occupation

$$r_u = \alpha \frac{\lambda_+^u - \lambda_-^u}{(1-\lambda_-)\lambda_+^u - (1-\lambda_+)\lambda_-^u}. \tag{3.13}$$

The probability that the flag stays on $L+1$ has therefore to be split in an infinite number of probabilities $P_{L+1}^{-10} = \sum_{u=1}^{\infty} P_{L+1,u}^{-10}$, the integer u accounting for this memory effect. The equations for the flag near the right boundaries finally read

$$\begin{aligned} P_L^{-10}(t+1) &= \sum_{u=1}^{\infty} (1-\beta) r_u P_{L+1,u}^{-10}(t) \\ &\quad + (1-\alpha)(1-\beta) P_L^{-10}(t) + (1-\beta) P_L^1(t), \\ P_{L+1,1}^{-10}(t+1) &= P_{L+1}^1(t), \\ P_{L+1,u}^{-10}(t+1) &= (1-(1-\beta) r_{u-1}) P_{L+1,u-1}^{-10}(t), \quad u \geq 2. \end{aligned} \tag{3.14}$$

Eqs. (3.10), (3.11) and (3.14) constitute the master equation for the position and the velocity of the flag, with an unusual memory effect for $i = L+1$. With these one can check probability conservation $\sum_{i=1}^{L+1} \sum_{a=0,\pm 1} P_i^a(t) = 1$.

The definition of the flag explicitly breaks particle-hole symmetry. A 'flag of the holes' could be defined by the rightmost hole that has ever been blocked. One can however show that the flag of the holes is always to the left of the flag of the particles, and that they can only be separated by a 'maximal current' structure of the form $\dots 0101010 \dots$ in which particles and holes alternate [117]. The probability to have this alternating structure on a length $2l$ can however be seen to be proportional to $\min(\alpha, \beta)^l$, so that the two flags are at an average distance negligible with respect to the size of the system for large L. Moreover, we are going to be able to compute exactly the density profile without any reference to the flag of the holes.

Here we comment on the relation between the flag we introduced and the second-class particle introduced by Derrida *et al.* [118] as shock markers in continuous time. These latter particles will be denoted by the symbol $\frac{1}{2}$. The dynamical rules are the following: if a second-class particle sits to the right of a (first-class) particle (configuration $\dots 1\frac{1}{2}\dots$) their position are exchanged as if the second-class particle were a hole, and symmetrically if the local configuration is $\dots \frac{1}{2}0\dots$ the second-class particle hops as if it were a particle.

Suppose now that on the coarse-grained level we have a shock configuration where the density goes from ρ_- to ρ_+ when the coordinate x increases. The velocity of the shock is still given by mass conservation $\delta = \frac{\mathcal{J}_+ - \mathcal{J}_-}{\rho_+ - \rho_-} = 1 - (\rho_+ + \rho_-)$ in continuous time, using the values of Table. 1.1. The second-class particle is expected to move with velocity $1 - 2\rho(x)$. It is then easy to show that the second-class particle will be attracted to the position of the shock when the density increases monotonically from ρ_- to ρ_+. This observation has enabled the authors of Ref. [118] to compute the density profile of the shock by Matrix Product Ansatz.

Things are not that simple in parallel update. Indeed one has to decide where the second-class particle goes when the case $\dots 1\frac{1}{2}0\dots$ occurs. A general way of solving the problem that preserves the coupling between the second-class particle and the shock is to decide that in the $\dots 1\frac{1}{2}0\dots$ case the second-class particle hops to the right with some probability q and to the left with probability $1-q$. This would give a continuous family of second-class particles which still tend to hop to the right of holes and to the left of particles. The two extreme deterministic choices $q = 0$ and $q = 1$ would be tightly bound to the flag of the holes and the flag of the particles, respectively. Intuitively, any choice of $0 < q < 1$ would result in a second-class particle performing a biased random walk between the positions of the flags. We also mention that a marker very closely related to both the flag and a 'second-class particle' with $q = 1$ was introduced in section 5 of Ref.[115]. The authors however do not use it in their calculations.

Of course all these markers should give the same results as the flag after coarse-graining, as all of them should stay exponentially close. The flag is located at the position of the shock by definition, which gives it an advantage compared to second-class particles. The structure of the shock is also

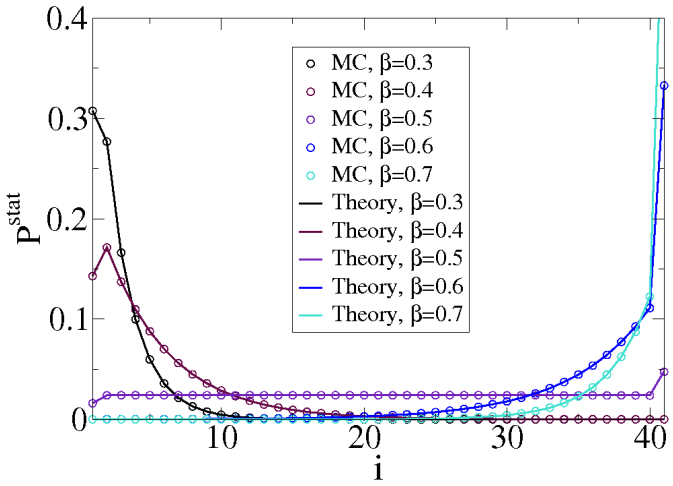

Figure 3.2: Stationary probability distribution of the position of the flag $P_i^{\rm stat}$ for $\alpha = 0.5$ and varying β in a system of size $L = 40$. Lines are the analytical predictions from Eq. (3.15) and empty circles are the result of Monte-Carlo simulations. The distribution is exponential apart from particular values on the two extremal sites. For $\beta < \alpha$ the wall is most likely located near the entrance and the jammed domain invades the bulk while for $\beta > \alpha$ the situation is reversed. In the critical case $\alpha = \beta$ the probability distribution is flat.

greatly simplified when expressed in terms of the flag, so that the master equation (3.10), (3.11) and (3.14) is simpler to write in terms of the flag.

3.2.3 Stationary state

In the stationary state Eqs. (3.10), (3.11) and (3.14) give

$$\begin{aligned} P_1^{1,\rm stat} &= 0 \\ P_i^{-10,\rm stat} &= \beta^{-1} P_{i+1}^{1,\rm stat} = \frac{1}{Z}\left(\frac{\beta}{\alpha}\right)^{i-1} \qquad 1 \le i \le L \\ P_{L+1}^{-10,\rm stat} &= \frac{1}{Z}\,\frac{1+\alpha\beta}{1-\beta}\left(\frac{\beta}{\alpha}\right)^{L} \\ P_{L+1,u}^{-10,\rm stat} &= \frac{\prod_{l=1}^{u-1}(1-(1-\beta)r_l)}{\sum_{u'=1}^{\infty}\prod_{l=1}^{u'-1}(1-(1-\beta)r_l)} P_{L+1}^{-10,\rm stat}, \end{aligned} \tag{3.15}$$

where we used the fact that

$$1-(1-\beta)r_l = \frac{(1-\lambda_-)\lambda_+^{l+1} - (1-\lambda_+)\lambda_-^{l+1}}{(1-\lambda_-)\lambda_+^{l} - (1-\lambda_+)\lambda_-^{l}}$$

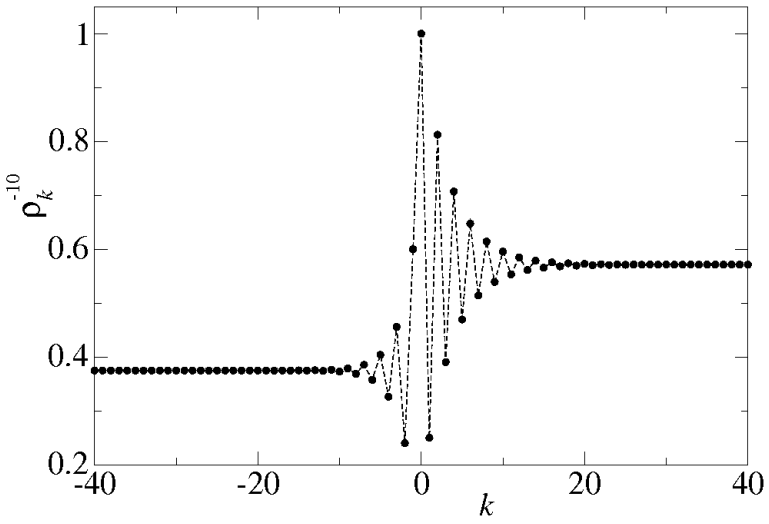

Figure 3.3: Flag dependent density profile ρ_k^{-10} for $\alpha = 0.60$ and $\beta = 0.75$. The flag is located at $k = 0$. For $k \to \mp\infty$ the density tends to the bulk values $\frac{\alpha}{1+\alpha}$ and $\frac{1}{1+\beta}$ as $\sim (-\alpha)^{|k|}$ on the left and as $\sim (-\beta)^k$ on the right. Dotted lines are guides to the eye.

to compute

$$\sum_{k=0}^{\infty} \prod_{l=0}^{k} (1 - (1-\beta) r_l) = \frac{1+\alpha\beta}{\alpha(1-\beta)}. \tag{3.16}$$

Eq. (3.15) shows that for $\alpha \neq \beta$ the stationary position distribution of the flag is exponential with a localization length $\pm\frac{1}{\log(\beta/\alpha)}$. At $\alpha = \beta$ a transition occurs between free flow phase, for $\alpha < \beta$ and jammed phase, for $\alpha > \beta$. The flag position distribution is shown in Fig. 3.2 for $\alpha = 0.5$ and different values of β on both sides of the transition. It should be stressed here that the flag not only provides a coarse-grained definition of the position of the wall but also a microscopic one which allows for direct measurements of the $P_i^{a,\mathrm{stat}}$. These measurements are of course in perfect agreement with the above exact equations.

3.2.4 Density profile

As is done in the usual domain wall theory, we would now want to predict the density profile with the help of the flag. A microscopically exact way to do so is to define the *flag-dependent density profiles* ρ_k^a, *i.e.* the partial density profiles indexed by the supposedly known position and velocity of the flag. With this notation $k = 0$ corresponds to the site of the flag which is always occupied when the flag is in the bulk. On the right boundary site $L + 1$ some

complications arise due to the infinite memory, forcing us to define the infinite family $\rho^a_{k,u}$.

As an example, we can compute ρ_k^{-10} for $k < 0$ as follows. The fact that the velocity of the flag is 0 or -1 implies that the occupation of site $k = -1$ is equal to α. Now as the sites to the left of the flag belong to the free flow domain we can use the recurrence relation (3.8) to compute all the $\rho^{-10}_{k<0}$. We get

$$\rho^{-10}_{k<0} = \alpha \frac{1-(-\alpha)^k}{1+\alpha}. \tag{3.17}$$

Similar expressions are obtained for $\rho^{-10}_{k>0}$ and ρ^1_k. Both of these functions start from $\rho^a_0 = 1$ and exhibit damped oscillations with characteristic length $\frac{1}{\log\alpha}$ (or $\frac{1}{\log\beta}$) for $k < 0$ (or $k > 0$) before finally reaching their limit $\frac{\alpha}{1+\alpha}$ (or $\frac{1}{1+\beta}$), respectively. The function ρ_k^{-10} is shown in Fig. 3.3.

The exact average density profile is simply obtained by averaging over the states of the flag,

$$\begin{aligned} \rho_j(t) &= \sum_{i=1}^{L} \sum_{a=-10,1} \rho^a_{j-i} P^a_i(t) + \rho^1_{j-(L+1)} P^1_{L+1}(t) \\ &+ \sum_{u=1}^{\infty} \rho^{-10}_{j-(L+1),u} P^{-10}_{L+1,u}(t). \end{aligned} \tag{3.18}$$

A plot of this profile is shown in Fig. 3.4. It confirms that expression (3.18) is exact for systems of any size.

3.2.5 Scaling limit

In the large L limit all these expressions simplify to give a more intuitive picture of the system, which turns out to be a true domain wall picture. We therefore define the continuous space variable $x \equiv \frac{i}{L} \in [0;1]$ and the accordingly rescaled probability distributions $\mathcal{P}^a(x,t) \equiv L P^a_i(t)$. The factor L ensures that $\int_0^1 (\mathcal{P}^{-10}(x,t) + \mathcal{P}^1(x,t))dx = 1$ for all t. When Taylor expanding all quantities around $x = i/L$ in Eqs. (3.10) we get a system of two differential equations. We start by introducing new functions

$$\mathcal{P} = \mathcal{P}^{-10} + \mathcal{P}^1, \tag{3.19}$$

the position distribution of the flag irrespective of its velocity, and

$$\mathcal{Q} \equiv \frac{(1-\beta)\mathcal{P}^1 - \beta(1-\alpha)\mathcal{P}^{-10}}{1-\alpha\beta}, \tag{3.20}$$

a function quantifying the weighted difference between $\mathcal{P}^1$ and $\mathcal{P}^{-10}$.

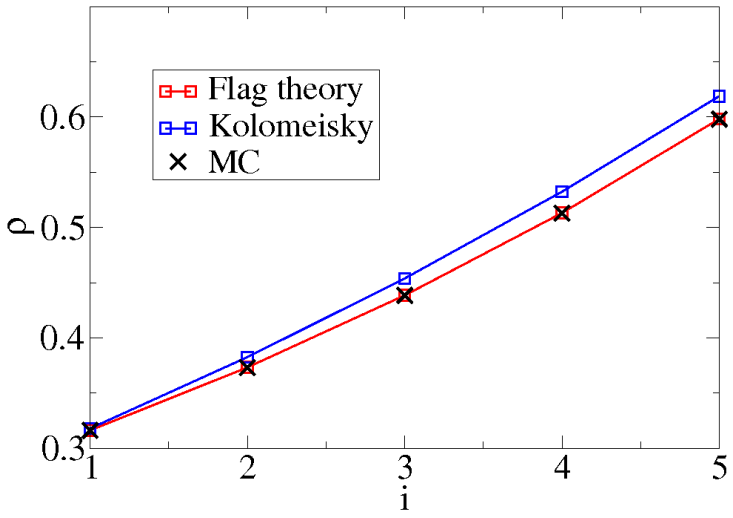

(a) $L = 5$

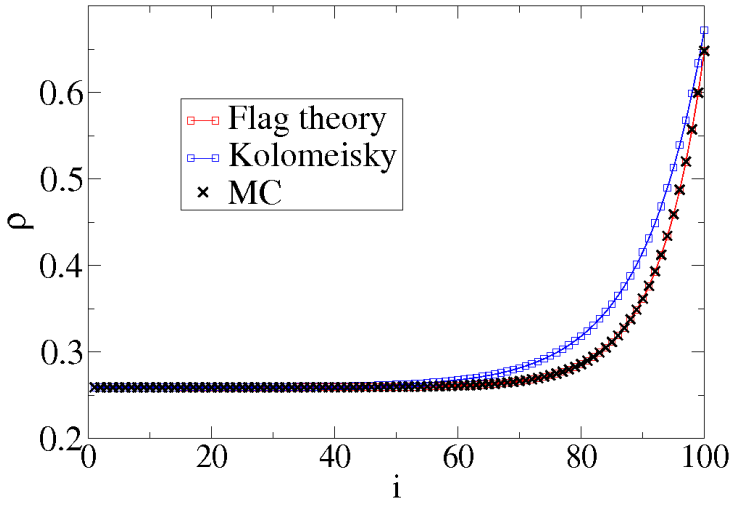

(b) $L = 100$

Figure 3.4: Stationary density profile for $\alpha = 0.35$, $\beta = 0.4$ and $L = 5$ (up) and 100 (down). The numerics (black crosses) are compared to the flag theory (red squares) and the more standard domain wall theory *à la* Kolomeisky *et al.* described in section 3.1 (blue squares).

Further defining $\Delta_t A(t) \equiv A(t+1) - A(t)$ for any quantity A, the drift $\delta \equiv \frac{\beta-\alpha}{1-\alpha\beta}$ and a partial diffusion coefficient $D_1 \equiv \frac{\alpha+\beta-2\alpha\beta}{2(1-\alpha\beta)}$, we get

$$\begin{aligned}\Delta_t \mathcal{P} &= -\frac{\delta}{L}\frac{d\mathcal{P}}{dx} + \frac{D_1}{L^2}\frac{d^2\mathcal{P}}{dx^2} - \frac{(1+\beta)\alpha}{L}\frac{d\mathcal{Q}}{dx} \\ &\quad -\frac{(1-\beta)\alpha}{2L^2}\frac{d^2\mathcal{Q}}{dx^2} + O(L^{-3}), \end{aligned} \tag{3.21a}$$

$$\begin{aligned}\Delta_t \mathcal{Q} &= -(1-\alpha\beta)\mathcal{Q} - \frac{\beta(1-\alpha^2)(1-\beta)}{L(1-\alpha\beta)^2}\frac{d\mathcal{P}}{dx} \\ &\quad +\frac{\alpha\beta(\beta-\alpha)}{L(1-\alpha\beta)}\frac{d\mathcal{Q}}{dx} + O(L^{-2}), \end{aligned} \tag{3.21b}$$

where the time 'derivative' is still discrete.

Eq. (3.21b) shows that on timescales $\gg 1$ the fast $\mathcal{Q}$ will adiabatically follow the slower $\mathcal{P}$, taking the value $-\frac{\beta(1-\beta)(1-\alpha^2)}{L(1-\alpha\beta)^3}\frac{d\mathcal{P}}{dx} + O(L^{-2})$. Combining it with equation (3.21a) and after defining $D_2 \equiv \frac{\alpha\beta(1-\alpha^2)(1-\beta^2)}{(1-\alpha\beta)^3}$ and $D \equiv D_1 + D_2$ we are able to write an equation for the probability distribution of the position of the flag only,

$$\Delta_t \mathcal{P} = -\frac{\delta}{L}\frac{d\mathcal{P}}{dx} + \frac{D}{L^2}\frac{d^2\mathcal{P}}{dx^2} + O(L^{-3}), \tag{3.22}$$

where we state again that

$$\begin{aligned} D &= D_1 + D_2, \\ D_1 &= \frac{\alpha+\beta-2\alpha\beta}{2(1-\alpha\beta)}, \end{aligned} \tag{3.23}$$

$$D_2 = \frac{\alpha\beta(1-\alpha^2)(1-\beta^2)}{(1-\alpha\beta)^3}. \tag{3.24}$$

After the rescaling it can be easily shown that the flag-dependent density profiles all become step functions as the oscillations occur on a finite number of sites and therefore disappear in the large L limit. Equation (3.22) is therefore an evolution equation for the position distribution of a true domain wall, and the drift coefficient δ is of course equal to the expression expected from mass conservation. The discrepancy with the domain wall theory exposed in section 3.1 therefore manifests itself in a very simple way: the value of the diffusion coefficient D is different from the value $\frac{1}{2}\frac{\mathcal{J}_+ + \mathcal{J}_-}{\rho_+ - \rho_-}$ predicted by the traditional approach, and as a consequence the decay length of the stationary distribution differs as well. Qualitatively one would expect that the discrepancy between the exact value of D and the predictions of Kolomeisky *et al.* comes from the memory effect in the motion of the flag. It is however not clear if it is possible to separate such contributions. In particular D_1 and D_2 taken separately do not have a clear interpretation. It may also be noted that D is not equal to the right-hand side of Eq. (3.7), conjectured after the study of some other exactly solvable cases.

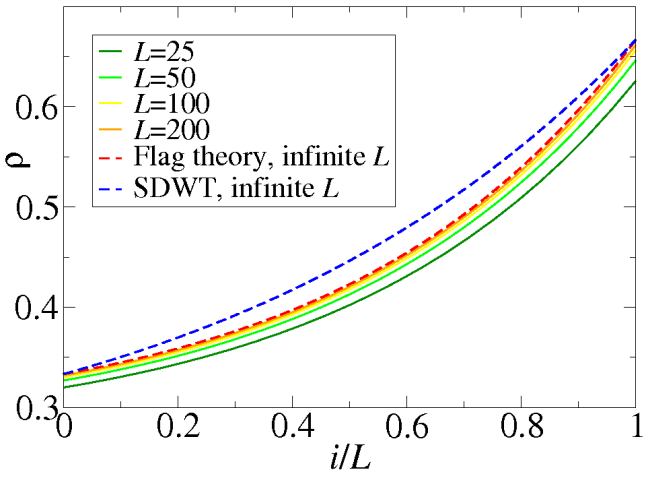

Figure 3.5: Stationary density profile in the scaling limit for $\beta = 0.5$ and $c = 1$. Blue dotted line: domain wall theory *à la* Kolomeisky, section 3.1. It is distinctly different from the red dashed line, obtained from Eq. (3.25) and representing the flag theory. Continuous lines: Monte-Carlo simulations for different lengths L converging to the flag theory prediction.

The discrepancy between the two theories is even better appreciated when taking the scaling limit in which none of the terms in Eq. (3.22) disappear, namely $\tau \equiv tL^{-2}$, $c \equiv L(\beta - \alpha)$ and D fixed. For $L \to \infty$ we get

$$\partial_\tau \mathcal{P} = -\frac{c}{1-\beta^2}\partial_x \mathcal{P} + \frac{\beta}{1-\beta^2}\partial_x^2 \mathcal{P}. \tag{3.25}$$

The stationary state of Eq. (3.25) is compared to the predictions of Eq. (3.6) in the same scaling limit and to numerical simulations in Fig. 3.5.

To summarize, we defined a new marker called the flag, that traces the position of the wall by definition on a microscopic level. Exact closed evolution equations have been written for this flag that involve not only the flag position but also its velocity, thereby exhibiting a memory of one time step. From these equations dynamical quantities can in principle be extracted. However, we focused on the stationary state, deriving the position distribution of the flag followed by the exact density profile. Finally, we took a scaling limit in which the discrepancy between exact and traditional domain wall theories was made very simple.

Even though a similar solution for frozen shuffle update seems out of reach, it can be observed to exhibit the same kind of behaviour as parallel update. The free flow phases in parallel or frozen shuffle update are qualitatively the same because the particles do not interact, making the precise updating scheme

unimportant. In the jammed phase it has been argued in section 2.1 that the platoons of frozen shuffle update can be seen as big particles updated in parallel, without making the correspondence more precise. In both phases both updates share the same qualitative properties, so that the same memory effect can be expected to appear with frozen shuffle update. This would explain the discrepancy of Fig. 2.5.

Part II

Intersecting traffic flows

In part I we have gained deeper understanding of traffic-relevant updates in (quasi-)one-dimensional systems. We shall now turn our interest towards bidimensional problems. The main goal of part II is to study the behaviour of pedestrian-like particles in a crossing of two perpendicular incoming corridors.

To begin this part II, we turn our interest towards pedestrians. There are many examples of problems with two intersecting flows in pedestrian experiments and numerical studies, which are most of the time perpendicular but tend to show the same behaviour for a generic angle. Indeed, in these situations it has been observed that pedestrians tend to segregate into stripes. Reproducing this pattern may therefore be required from any given pedestrian model, and (perpendicularly) intersecting flows may serve as a test situation to assess the validity of the model. This phenomenon has also been observed in the physics literature. The Biham-Middleton-Levine (BML) model [39] is a very simplified model for car traffic in a city, featuring two intersecting flows. In the paper a snapshot can be found where the striped pattern appears.

In both the pedestrian and the BML-related studies, the striped pattern is clearly observed but is not systematically studied. In the pedestrian community the striped pattern is part of 'common knowledge', has been known for decades [37, 38] and can be easily observed with the eye, but has never been the object of quantitative measurements. For example, the precise shape of the stripes can still be cast in doubt [119] with no quantitative evidence contradicting the statement. The inventors of the BML model focus on the jamming transition in their paper [39], and no explanation is given for the striped pattern.

Reaching a quantitative explanation of this phenomenon will be the first focus of part II. For this we will define our own model, which roughly consists of two wide perpendicular lanes that intersect and is defined more precisely in section 4.2. While the intersection model still clearly belongs to the realm of statistical physics, we also put it in the perspective of pedestrians in intersecting flows. Along the whole part II we will of course discuss the relevance of our main conclusions to pedestrians.

Although the evolution rules of the model look very simple, we will see that the striped pattern appears in the free flow phase of our model. With periodic boundary conditions we explain the pattern thanks to mean-field-like equations in the first part of chapter 5. After this partial validation of the model we stay focused on the pattern formation and go from periodic to open boundary conditions. In this last case we observe a more subtle secondary non-linear instability called the 'chevron' effect.

The whole chapter 6 will then be devoted to finding a satisfying explanation to this phenomenon. Our strategy will be borrowed from soft matter studies. The main idea is to decompose complex interactions between many particles into a sum of two-particle interactions, this idea being often used *e.g.* in colloidal suspensions. While describing effective interactions between such out-of-equilibrium agents is generally difficult in fluid mechanics, in our case the system will prove simple enough to provide the first example where the effective interaction can be calculated exactly in an out-of-equilibrium sys-

tem. This calculation will give both an analytical characterization and a clear picture of the pattern we seek to explain. For the particularly simple alternating parallel update, we will even see that we will be able to go back from individual interactions to a global pattern in an exact way, thus justifying the approximations made earlier.

We shall finish this part by discussing the hypotheses of the model by relaxing some of them, which will of course have implications for the relevance of our findings to pedestrians. We will also see that our considerations in the stationary state can be applied to transient states as well.

Chapter 4

Pedestrians and cars in intersections

Throughout part II we shall be interested in intersecting traffic flows. Before enlarging the intersection we studied in section 2.4 we will study some of the previous works that motivate this qualitative jump. Intersections of pedestrian flows have been widely studied in the pedestrian traffic community, both in experiments and in numerical models. The important presence of intersections constitutes a strong motivation to study two-dimensional generalizations of the models presented in part I. The results from pedestrian studies however stay at the level of the qualitative observation from where little quantitative observation can be extracted, and we will show that a simplified model enables us to make precise predictions about the pattern formation. In the following we will therefore interest ourselves in the Biham-Middleton-Levine (BML) model [39]. Originally designed to study car traffic in a city, the BML is a very simple model of particles on a lattice that keeps only the most important features observed in systems of intersecting flows, and is very similar to what we are going to obtain by enlarging the lanes of section 2.4. The results found by Biham *et al.* in Ref. [39] concern mainly the jamming transition and will be reviewed. Many extensions that have been developed over the years will be presented as well. All this will be done in the first section 4.1.

In the second section 4.2, the intersection model that will be the focus of most of part II is clearly defined. We are interested in an instability that occurs in free flows of pedestrians, so the jammed phase of the model will be of limited relevance to us. For completeness, we shall however summarize Ref. [120], in which the jammed phase is studied.

4.1 Literature

4.1.1 Pedestrian experiments and numerics

The validation of a numerical model for pedestrians depends on how well the model reproduces the experimentally known features of pedestrian motion. They include simple features as the free walking speed of a pedestrian or the density of a crowd of people, which are often used to calibrate the parameters. Among these one also finds the fundamental diagram of pedestrians, which seems however less meaningful for pedestrians than for *e.g.* cars because of a high variability in individual characteristics. However the most important is that the collective behaviour of the pedestrians in the model is in agreement with what is indeed observed in experiments. These requirements include pattern formation and are most of the time qualitative. Of particular importance to us will be the formation of diagonal stripes in perpendicularly intersecting pedestrian flows, a phenomenon very close to the lane formation observed in counter-propagating flows of pedestrians [20, 121, 21, 33] or in other physical systems involving lattice gases [45] or colloidal mixtures [122]. Other instances of these collective phenomena could be given, in a slightly different class of models, by oscillations at a bottleneck [123], stop-and-go waves in queuing scenarios or the very popular faster-is-slower effect in evacuation scenarios at high density involving humans [124, 84, 19, 125] or even ants [126], an effect under which the more a single individual wants to exit the room, the slower the whole crowd will manage to exit.

Some of those experiments have been performed in the frame of the PEDIGREE project, in which my supervisor C.Appert-Rolland participated. The situations studied concerned for example pedestrians walking around a circle without overtaking each other [12, 13, 14, 26] or situations where conflicts between pedestrians occur.

In this whole chapter of the thesis the focus will be on perpendicularly intersecting traffic flows. Here we review the experiments and the simulations of intersecting pedestrian flows and the main results of relevance to us. We start with the experiments.

4.1.2 Pedestrians in intersections

The first reported experimental study of crossing pedestrian flows was performed by Naka in 1977 [37]. He found that when two directed flows intersect they tend to form stripes perpendicular to the sum of the two walking speeds at their intersection. This was confirmed by Ando *et al.* in 1988 [38]. These two papers were however written in Japanese. A sketch from Ando's article made it to the rest of the world, which is shown in Fig. 4.1. People who did not master Japanese had to wait until 2002 to see the scheme of Ando used in an article written in English by Hughes [32]. In this article he introduces a simple PDE model for pedestrian flows and only uses Fig. 4.1 as an illustration with little explanation. Helbing *et al.* then used it again in a review article [127].

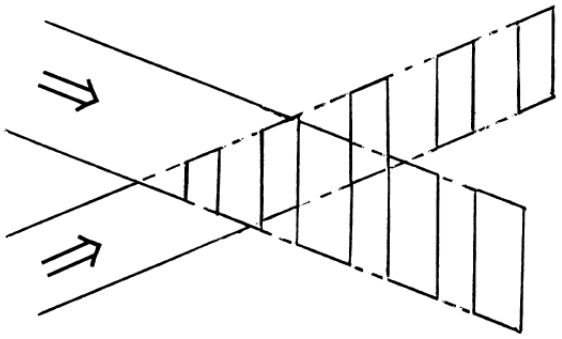

Figure 4.1: Sketch from Ando *et al.*'s article [38] edited by Hughes [32]. A diagonal pattern is formed in the intersection of two pedestrian flows.

This story is taken from a talk of the TGF'13 conference [119].

Some quantitative experiments have been performed since then. Hoogendoorn *et al.* [10] conducted walker experiments in 2003 for several geometries including corridors with unidirectional flow, corridors with counter-propagating flows and perpendicular intersections. In this last case the walkers were divided in two perpendicular straight flows and stripe formation has been visually observed on snapshots of the experiment, see Fig. 4.2. However, no quantitative measurements specific to this pattern formation such as *e.g.* correlation functions were presented. They also observed that the standard deviation of the empty zone distribution is larger in the intersection than in the corridors because of conflicts, *i.e.* two pedestrians willing to step towards the same spot. In that situation one of them decelerates almost without changing direction and may speed up when the conflict is resolved. The variability of individual speeds is then larger, hence the variability of the empty zone distribution.

Other experiments have been conducted. One of them was performed by some students of the École Polytechnique in Palaiseau, France in 2010 [128]. Again the participants were divided in two perpendicular intersecting flows and the whole experiment was video-recorded from the top. The flows were not necessarily of equal size, however stripe formation seemed to occur regardless of the ratio of participants in the main flow, see the snapshot of Fig. 4.3. The number of experiments was however small, which prevents us from giving a more quantitative meaning to the previous statement.

Some more recent experiments were performed in Ref. [129] but have no specific results on the formation of stripes. In Ref. [119] stripe formation is studied. One of the conclusions of these experiments is that the stripes look more like 'bubbles' than stripes. Up to now there is however no quantitative way to support this statement or the opposite.

As part of the PEDIGREE project some experiments on intersecting flows

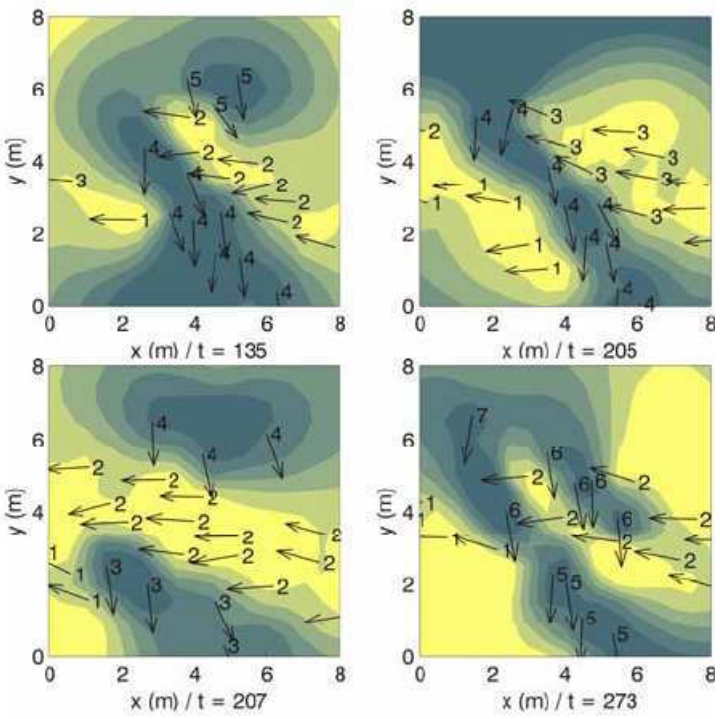

Figure 4.2: Formation of diagonal stripes in a pedestrian crossing experiment. The colors indicate the average direction of the pedestrians. Taken from [10].

have been conducted, however these experiments concern intersections of three flows at an angle of 60°. The trajectories of the pedestrians have been extracted but they have not been exploited yet. It is however doubtful that stripes could be observed in this context, as numerical simulations of intersections with three species show more complicated patterns [130].

From the numerical side, a model for pedestrians has been designed by Hoogendoorn *et al.* [21]. The basic feature of this complicated agent-based model is that each pedestrian minimizes a cost function by predicting the behaviour of the other pedestrians and choosing a walking strategy, which is implemented via a feedback loop. Among other phenomena stripe formation in perpendicularly intersecting flows is observed, see Fig. 4.4. The authors however note that the formation of stripes depends critically on the parameters of the model, in particular the pedestrians should rather decelerate than change directions when there is a conflict for the pattern to be observed.

Two simpler models were proposed by Yamamoto *et al.* [131], still in continuous space. The first one is an ODE particle model similar to Newtonian dynamics and the second one a continuous PDE model in the spirit of fluid

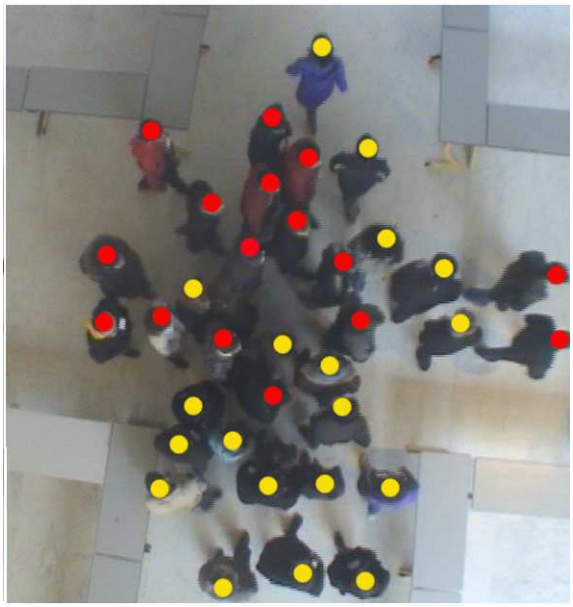

Figure 4.3: Snapshot form the experiment done at the École Polytechnique. Two groups of pedestrians of equal size come from the left and the bottom of the picture. Pedestrians walking towards the top are highlighted with a yellow dot and those going to the right carry a red dot.

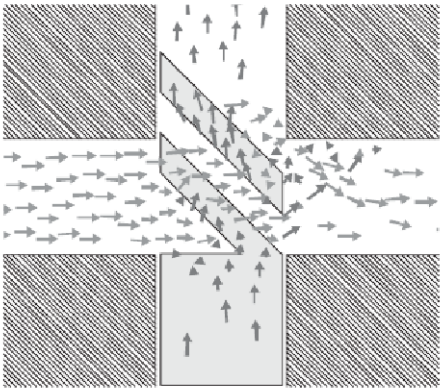

Figure 4.4: Result of simulations performed by Hoogendoorn and Bovy [21]. The small arrows represent pedestrians by their velocities and again a diagonal pattern is visible, that has been highlighted by dark stripes in the picture.

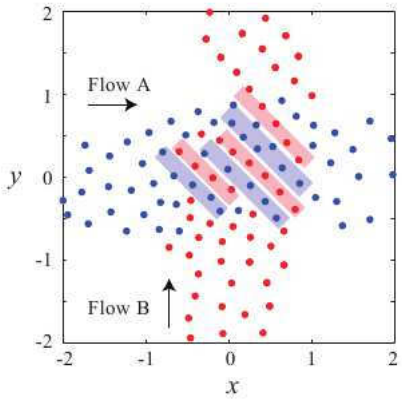

Figure 4.5: Simulation of crossing flows using the particle model of Yamamoto and Okada [131].

dynamics. In both cases diagonal stripes are observed, as shown in Figs. 4.5 and 4.6. The authors also remark that the output flow is very high when the pedestrians are organized into these stripes. They even propose that the entrance flow at crossings could be monitored to artificially help creating stripes in order to maximize the flow.

4.1.3 The BML model

In this subsection we focus on a particular instance of intersecting flows, namely the Biham-Middleton-Levine (BML) model introduced in 1992 in Ref. [39]. The BML model is indeed very similar to the one that will be introduced in section 4.2. Here we will therefore define it precisely and review the findings of the authors of the original paper and subsequent works, and the variants that have been proposed.

The BML model is a simple model of car traffic in a city. The city is represented by a square lattice of size $M \times M$ with periodic boundary conditions in both directions. Each node of the lattice represents a four-way intersection and each link represents a portion of a street between two intersections. Cars are modeled by particles hopping on this lattice. Each particle has a fixed preferred direction which is either east or north. Particles are then enabled to hop towards their preferred direction when they are updated. The number of particles of each type is chosen equal, so that the only macroscopic control parameter is the conserved total particle density $\overline{\rho} \in [0; 1/2]$. At initial time $M^2\overline{\rho}$ particles of each type are then dropped on randomly chosen sites of the system. Finally, the update scheme is completely deterministic and is equiva-

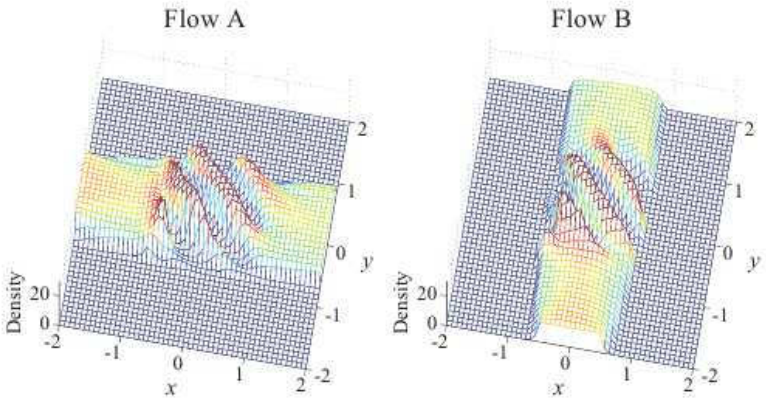

Figure 4.6: Simulation of crossing flows using the continuous model of Yamamoto and Okada [131].

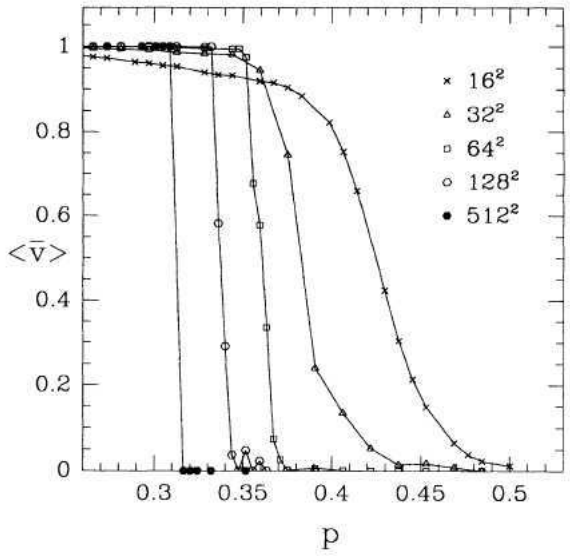

Figure 4.7: Ensemble average velocity as a function of the total density for different system sizes in the BML model. The velocity changes rapidly from 1 to 0 with increasing concentration. The location of the transition however depends strongly on the system size. Taken from [39].

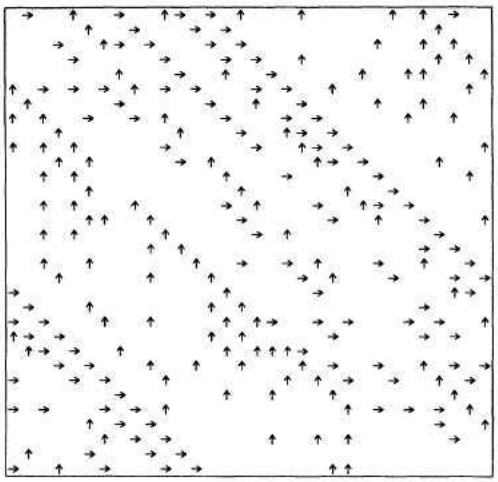

Figure 4.8: Snapshot of a typical configuration in the low-density phase of the BML model. In this phase the average velocity of the particles is equal to 1. Particles are represented by arrows pointing east or north depending on their hopping direction. In Ref. [39] the authors remark the organization of the particles into stripes.

lent to the alternating parallel update to be defined in subsection 4.2.2: each species of cars stands still half of the time because of traffic lights.

The main finding of Ref. [39] concerns a jamming transition that occurs when the density $\overline{\rho}$ increases, which has an obvious interpretation in terms of car traffic. Evidence for this transition is provided by measurements of the ensemble-averaged velocity of the particles. As shown in Fig. 4.7 the ensemble-averaged velocity converges either to zero or to one depending on the value of $\overline{\rho}$. As the system size goes up the transition gets sharper, however the authors could not estimate the critical value of $\overline{\rho}$ for an infinite system, because the transition keeps occurring for smaller and smaller densities even at the maximal simulated size $M = 512$. In particular, it is not clear whether this critical value is finite for an infinite system.

Of more interest to us are the snapshots of the system presented in Figs. 4.8 and 4.9, showing typical configurations of the system in free and jammed phase, respectively. In Fig. 4.8 the authors remark that the particles are self-organized in alignments in the free flow phase but do not try to measure or to explain this effect. In the jammed state shown by Fig. 4.9 the particles are all blocked along a diagonal wrapped around the system.

It should also be noted that the BML system is not ergodic. The stationary state of the system, free flow or jammed, depends not only on the density of particles in each lane, but also on their precise starting positions. For example,

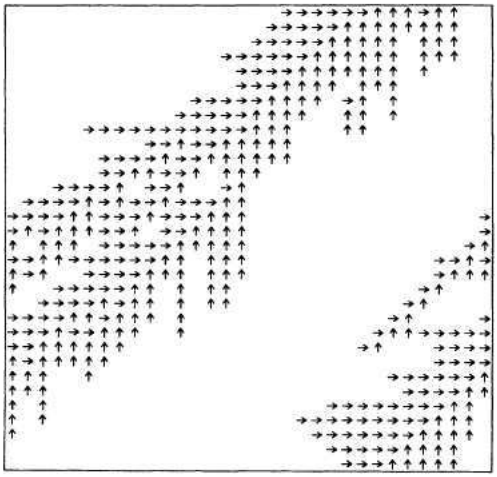

Figure 4.9: Typical jammed configuration of the BML model. The average velocity is 0, as the particles are organized in such a way that they are all blocked. Taken from [39].

a jammed system can be obtained for densities as low as $\overline{\rho} = \frac{1}{M}$, since particles can be arranged on a long diagonal of width 2 similar to Fig. 4.9. Conversely, free flowing systems can be obtained for rather high densities. The results presented in *e.g.* Fig. 4.7 are ensemble averages.

4.1.4 Variants of BML

In 1994 Tadaki *et al.* studied the same BML model, still with PBC, and showed the existence of an other jammed phase different from the one shown in Fig. 4.9 for even higher densities [132]. For very high densities particles do not even have the time to get organized into a jammed diagonal but the system is close to frozen in its initial state. A snapshot is shown in Fig. 4.10.

A theoretical explanation of the jamming transition was attempted in Refs. [133, 134] for a generalization of the BML model with stochastic turns. The authors write exact equations for the two density fields of particles of each type and truncate the BBGKY-like hierarchy by factorizing the two-point correlation functions. They end up with a system of equations that are used to study the jamming transition. An instability of the uniform density state is then exhibited by a linear stability analysis of the equations, thus explaining qualitatively the jamming transition. An alternative system of PDEs is then proposed in continuous space, that basically leads to the same conclusions as the original discrete equations.

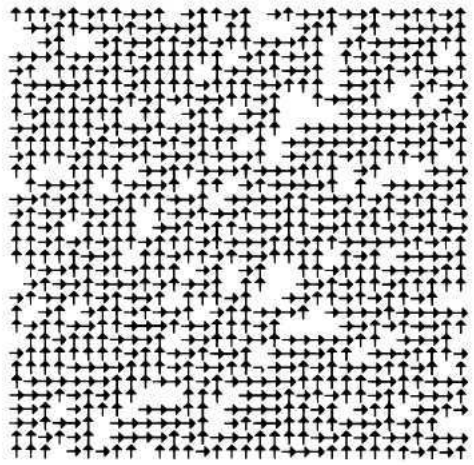

Figure 4.10: Typical configuration in the 'frozen' high-density state where the particles stay very close to their initial configuration. Taken from [132].

Several variants of this model have been studied in the literature.

In 1996 Tadaki replaced the periodic boundaries by open boundaries [135]. In his model particles are injected probabilistically at the west and south boundaries and exit the system deterministically at the east and north boundaries. However the focus is once again on the jamming transition. Even if mean-field arguments are presented the paper is to a large extent numerical, the main quantity of interest being the power spectrum of the exit current. The author also remarks that due to the probabilistic injection of the particles local jammed clusters can be created even in the free flow phase.

In 2005 D'Souza presented a more detailed study of the jamming transition [136] of the BML model in PBC, extending his analysis to the case where the two periodic directions do not have the same length. The jammed phase is described in terms of simple yet very powerful geometric quantities, such as the winding number of a jammed diagonal around a given direction of the lattice. This analysis is however very specific to the update scheme and many of the considered phenomena may be finite-size effects. To my knowledge it still is the most precise analysis of the jamming transition of the BML model.

While the results mentioned above have been obtained mainly for the jamming transition, the findings of Ding *et. al* [137, 138] in the free flow phase will be of interest to us. The authors replaced parallel update by the random sequential one, and they consider both PBC and OBC. While the focus is still on the jamming transition, the authors state that they do not observe the diagonal striped pattern from Fig. 4.8 anymore, as a typical system in the free flow

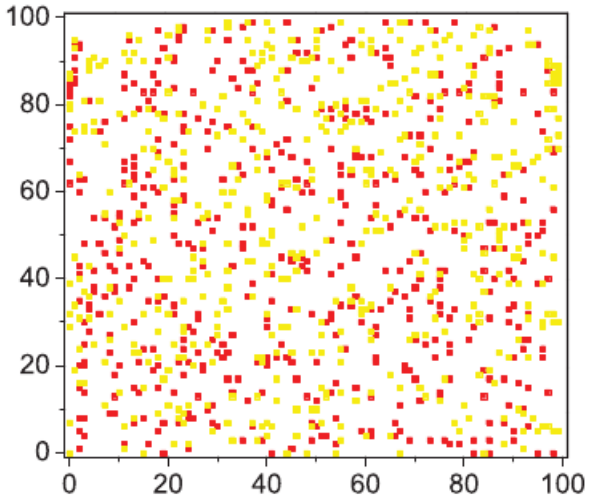

Figure 4.11: Typical configuration in the low-density state with random hopping rates. The diagonal pattern disappears. Taken from [137].

state looks like Fig. 4.11. This result tends to show that the striped pattern appears only in systems where the fluctuations are relatively low, and confirms that random sequential update is not relevant for pedestrians.

In the same spirit as the previous article Ding *et al.* enabled a fraction of the cars to move with velocity 2, interpreting this phenomenon as a violation of the traffic lights [139] by outlaw drivers. In this case the formation of stripes is observed in the free flow phase, the stripes however having slopes -2 and $-1/2$ when there are enough violators. Fig. 4.12 illustrates this phenomenon.

Yann Chiffaudel, at that time a bachelor student, did his internship during the months of May and June 2013 at the LPT under the direction of Henk Hilhorst. He studied numerically the formation of diagonals in the free flow phase of rectangular periodic systems and found that when the aspect ratio of the rectangle is not a simple fraction the system goes to a stationary state where the ratio of the winding numbers of the diagonals around the two directions is still a simple fraction, but the usually unimpeded particles get periodically blocked. During his internship, numerical results were also obtained on an hexagonal crossing with 3 species of particles, that show patterns more complicated than stripes [130].

More variants have been studied in various contexts. Peruani *et al.* considered the much more complicated case of a lattice occupied by four types of particles, each going in one of the four directions [140]. Chowdhury *et al.* put some road sections between the intersections of the BML model to reproduce

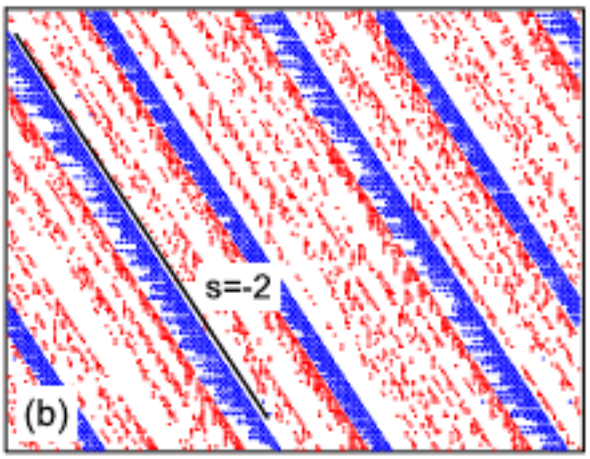

Figure 4.12: Stripes with slope -2 observed in Ref. [139] when some cars move with velocity 2.

more realistically the structure of a Manhattan-like city [57].

These preliminary results in mind, we turn on to the definition of the model that will be the main focus of the next chapters 5, 6 and 7.

4.2 The intersection model

Here we simply define the intersection model to be studied in the next chapters and discuss its relevance and simplifying choices of parameters. The jamming transition will not be studied in this thesis for it has already been studied previously in Ref. [120], however the main findings will be reviewed in the last subsection 4.2.3.

4.2.1 Geometry

In this section a model that incorporates all the important features of intersecting perpendicular flows is defined. Although being very similar to the BML model, we will not study the jamming transition but the structure of the free flow phase, more precisely the pattern formation. In the following it shall be referred to as *the particle model* or *the model* for short, as opposed to the mean-field equations introduced in subsection 5.1.3.

We model a *street* by simply taking a number M of identical noninteracting open TASEPs of length $L+M$ side by side. All the properties of this street are

of course well-known from section 2.3 for the case of the frozen shuffle update and from previous literature [66] for a lot of other updates.

A crossing is then modeled as the intersection of two such streets, as shown in Fig. 4.13. In principle the streets are parametrized by two sets of values $(\alpha_{\mathcal{E}}, \beta_{\mathcal{E}}, L_x + M_x, M_y)$ and $(\alpha_{\mathcal{N}}, \beta_{\mathcal{N}}, L_y + M_y, M_x)$ that represent the entrance probability per time step, the exit probability per time step, the length and the width of the street, respectively. In this notation the symbols $\mathcal{E}$ and $\mathcal{N}$ stand for the two types of particles 'east' and 'north', and x and y are the eastward and northward coordinates. In the following we will almost always consider a symmetric intersection $\alpha_{\mathcal{E}} = \alpha_{\mathcal{N}} \equiv \alpha$, $\beta_{\mathcal{E}} = \beta_{\mathcal{N}} \equiv \beta$, $M_x = M_y \equiv M$ and $L_x = L_y \equiv L$. We will see that these choices capture the main ingredients of the pattern formation. Results for asymmetric intersections presented in section 7.1 will show the same qualitative behaviour. The bold region highlighted in Fig. 4.13 is called the *intersection square*, or *intersection* for short, and contains $M \times M$ sites. The two outer parts of size $L \times M$ will be called the *entrance lanes*.

The sites of the intersection will be labeled either with a vector $\mathbf{r}$ or with their components (i, j) in the natural basis $\mathbf{e}_x$ and $\mathbf{e}_y$ with the integers $i, j = 1, \ldots, M$. The symmetric choices of the parameters then imply that on average the system is invariant under a swap of the directions $x \leftrightarrow y$ together with a swap of the particle types $\mathcal{E} \leftrightarrow \mathcal{N}$.

In the intersection the two types of particles $\mathcal{E}$ and $\mathcal{N}$ are present. The $\mathcal{E}$ particles ($\mathcal{N}$ particles) enter the intersection from the western (the southern) boundary, hop towards the east (the north) and exit the intersection at its eastern (northern) boundary, respectively. Particles of type $\mathcal{E}$ (of type $\mathcal{N}$) will from now be represented by blue right-pointing triangles (orange up-pointing triangles) in all the figures *e.g.* in Fig. 4.13.

As our primary interest is pedestrians we want the motion to be as regular as possible. We then set the hopping probability of the particles equal to unity $p = 1$, similarly to part I of the thesis. If a lane is not jammed the bulk motion of the particles in it then simply consists of a translation with velocity 1, according to the continuous mapping of section 2.1.2. This shows that the behaviour of the system in the intersection square should not depend on the value of L. In Ref. [120] it is shown how to account for the dynamics of the entrance lanes in the free flow and in the jammed phase, hence allowing simulations for a truly infinite system. The idea is to reduce the entrance lanes to entrance sites. Each entrance site is associated to two dynamical variables: the position of the first incoming particle on the lane and the number of times the particle has been blocked. The evolution of these variables is deduced form the properties of the free flow phase. This description does however not account for the boundaries and therefore works only in the true $L \to \infty$ limit.

The intersection square will therefore be our primary focus. Note that Fig.4.13 corresponds to the case where both directions have open boundaries, as studied in section 5.2. Periodic boundaries can also be applied in either direction, in which case the parameters α and β are simply replaced by the initial density of particles on a given lane. The model can then be studied on

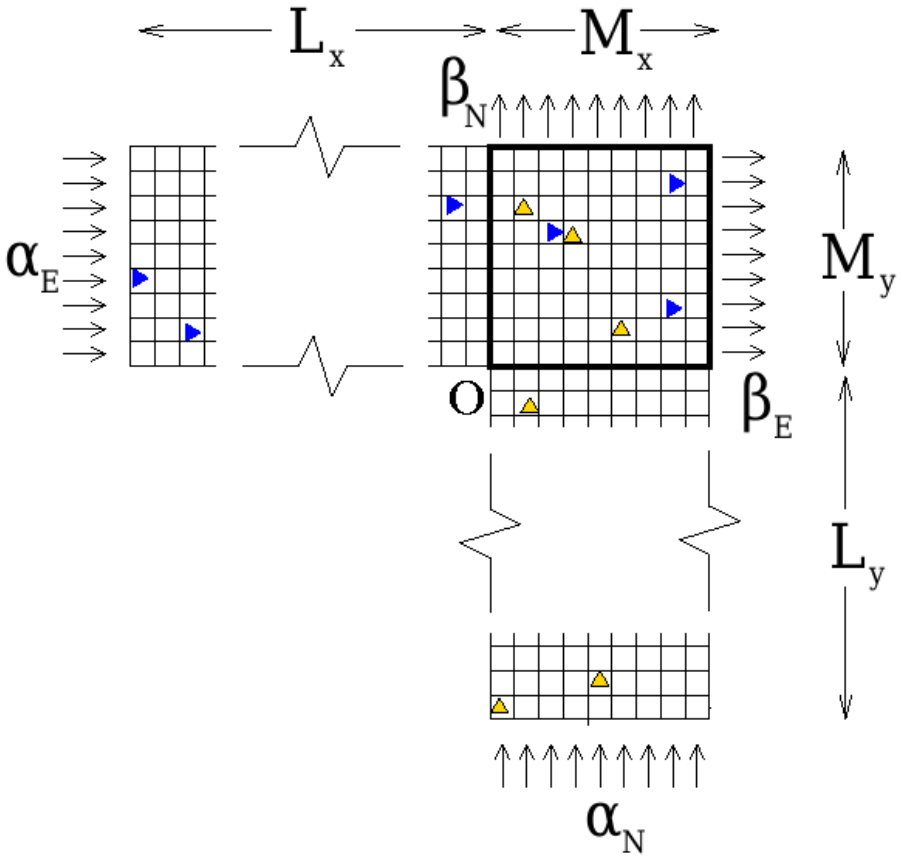

Figure 4.13: The intersection of two streets of width M_x and M_y is an $M_x \times M_y$ rectangle which is emphasized by the bold line. The other parameters of the model are the lengths of the entrance lanes L_x and L_y, the entrance probabilities per time step $\alpha_{\mathcal{E}}$ and $\alpha_{\mathcal{N}}$, and the exit probabilities per time step $\beta_{\mathcal{E}}$ and $\beta_{\mathcal{N}}$. Eastbound or $\mathcal{E}$ particles are represented by the blue right-pointing triangles whereas northbound $\mathcal{N}$ particles are represented by the orange up-pointing triangles. The origin is denoted by the symbol '**O**'. In the following we shall mainly restrict ourselves to the symmetric case $M_x = M_y$, as anticipated here, having also $L_x = L_y$, $\alpha_{\mathcal{E}} = \alpha_{\mathcal{N}}$ and with the choice $\beta_{\mathcal{E}} = \beta_{\mathcal{N}} = 1$.

the torus (section 5.1) and on a cylinder (chapter 7) as well.

Finally, we want to isolate the effects of the geometry, which we are interested in, from other phenomena that could disturb the flow of pedestrians. In particular, we choose to eliminate the well-understood queues that may propagate from the exit boundaries by using the deterministic exit rate $\beta = 1$. Unless otherwise stated this choice of the parameters will be used in the following, so that only two parameters of the model remain: the length of the side of the intersection square M and the entrance probability per time step α.

4.2.2 Update scheme and relevance to pedestrians

As already argued in subsection 2.1.1 the best update schemes for simulating pedestrians are expectedly frozen shuffle update and parallel update. These one-dimensional update schemes now have to be generalized to two dimensions if we want to apply them to our intersection problem. In two dimensions there is in particular a need to solve the *conflicts*, *i.e.* the case when two particles try to hop towards the same site at the same time. Having both particles hopping to the same site is forbidden by the exclusion principle, so that we need a prescription to determine if the first particle, the second one, or none of them will hop.

The case of the frozen shuffle update is pretty easily dealt with, as the phases $\{\tau_P\}$ define a natural priority order on the particles: two particles can never have the same phase. We therefore do not need any further prescription to employ frozen shuffle update in more than one dimension.

When using parallel update all the particles are updated at the same time, which means that conflicts between two pedestrians that target the same site at the same time can possibly occur. To solve them we replace parallel update by *alternating parallel update*, which means that we update all the $\mathcal{E}$ particles in parallel, followed by all the $\mathcal{N}$ particles, followed by the $\mathcal{E}$ particles again and so on. This update is still highly regular and provides a pretty natural generalization of parallel update to higher dimensions.

Other mechanisms could be thought of to solve conflicts in cellular automata updated in parallel, which may have an important physical relevance in *e.g.* pedestrian evacuation models. In particular, the conflict resolution mechanism is crucial if one wishes to reproduce the faster-is-slower effect in the simulations [84]. Experimentally, this effect has never been clearly observed in groups of pedestrians at sufficiently low density, and understanding what role conflicts play in real-life situations is still an open question. Back to the simulations, many ideas have been tried, most of them including the idea of pedestrians being either cooperative or competitive.

If n particles attempt to hop on the same site, the winner could simply be chosen among the candidates with uniform probability $1/n$ for each [60, 34]. In our case this would however break the deterministic character of the bulk dynamics, which we do not want. An evolution of the latter rule would be to introduce a friction parameter μ which quantifies the probability that none of the candidates hop [84] to model non-cooperative behaviour between pedestri-

ans in an evacuation context. In even more sophisticated models the friction parameter can depend on the number of conflicting pedestrians [35, 19] or more complicated instances of game theory can be employed [86]. Pedestrians can also have varying internal states, instances of these models being given by making each pedestrian either cooperative or competitive [85] or more simply employing random or frozen shuffle update, the phase being considered as an internal state.

Both frozen shuffle and alternating parallel update belong to a more general class of update schemes which is parametrized by the joint distribution of the phases of the particles. More precisely, each time a particle is created a phase must be associated to it. In frozen shuffle update the phase of the new particle is determined only by the phase of the last injected particle at the same site via the exponential kernel from Eq. (2.1). Alternating parallel update is obtained by giving the same phase to all the particles of the same type, say $\tau_{\mathcal{E}} = 0$ for the $\mathcal{E}$ particles and $\tau_{\mathcal{N}} = 1/2$ for the $\mathcal{N}$ particles. For this last case to be well-defined we have to use the convention according to which a particle hopping towards a site occupied by a particle having the same phase gets blocked.

A further generalization would allow the phases to vary from one time step to another, which would include random shuffle update but exclude the more 'site-oriented' continuous time and random sequential updates. Interpreting the phase in terms of step cycle, it looks interesting to design an update scheme in which the phases have their own dynamics, which would of course be coupled to the spatial dynamics of the particles. Such an hybrid shuffle update is under study in a collaboration between C. Appert-Rolland, C. Arita and myself.

In our model no lane changes are allowed. Even though changing lanes seems a pretty natural reaction of pedestrians when there is a conflict, Ref. [10] indicates that the main reaction of pedestrians in case of conflict is to slow down. In reality of course the reaction of a typical pedestrian is a combination of decelerating and moving around the obstacle pedestrian blocking him. In this model the introduction of lane changes is expected to partially or totally blur the pattern formation we are going to be interested in, as taking the hopping probability $p < 1$ does (see section 7.2). This is a priori not relevant, as striped patterns indeed are observed in pedestrian experiments. In a statistical mechanics framework, imposing the absence of lane changes and the equality $p = 1$ can be seen as taking the zero-temperature limit of *e.g.* the Ising model, where the collective effects appear in their purest form thanks to the absence of fluctuations.

Another point of criticism could concern the parameter range that will be used. In the following chapters 5 and 7 we will study intersections of typical size $M \gtrsim 100$ and of particle density of a given type $\rho^{\mathcal{E},\mathcal{N}} \simeq \alpha \sim 0.1$. This size may seem too big, as having 100 pedestrians walk side by side would already correspond to a street of width $\sim 100 \times 50\text{cm} = 50\text{m}$. We however have to bear in mind that the interactions between pedestrians responsible for the pattern formation we are going to study depend on the density, so that the relevant control parameter is the average number of interactions a pedestrian undertakes when going through the whole intersection. In the simulations we

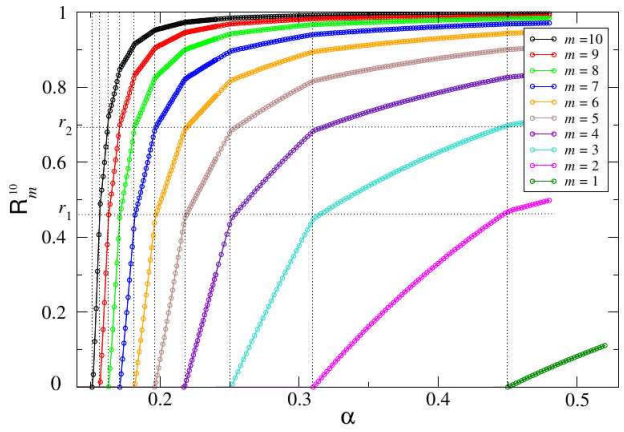

Figure 4.14: Reflection coefficient $R_m^{10}(\alpha)$ for $M = 10$ and $m = 1, 2, ..., 10$. The lines connecting the points are meant to guide the eye. The thin dotted vertical lines correspond to the critical points on the α axis. The thin dotted horizontal lines are the approximate levels at which the curves have their first and second discontinuity of slope. Taken from [120].

have to stay in a weakly interacting regime to ensure that the intersection is still in free flow phase. A pedestrian going through the intersection then interacts approximately $\rho^{\mathcal{E},\mathcal{N}} M \gtrsim 10$ times with other pedestrians in our range of parameters. For a weakly crowded street with 0.5^{-2}ped/m^2, in which motion is still possible for real pedestrians, this corresponds to a minimal width $0.5^2 \times 10\text{m} = 2.5\text{m}$, which clearly includes the realistic parameter range.

4.2.3 Jamming transition

An important feature of the BML model is its jamming transition, that can be shown from Fig. 4.7 to occur for densities $\rho^{\mathcal{E},\mathcal{N}}$ of the order of 0.17 for an intersection with $M = 512$. Some results relative to this transition have already been outlined in subsection 4.1.3. With the open boundary conditions presented in subsection 4.2.1 the jamming behaviour is a little different from what was found in the BML model with PBC. Before dealing with the central theme of this thesis, pattern formation in free flow phase, we shall briefly review the jamming transition of the intersection model in OBC and present soe illustrations. This analysis that was carried out by H.J. Hilhorst and C. Appert-Rolland in Refs. [120] and [141], where further elements can be found.

The authors first get rid of the finite-size effects by implementing an algorithm equivalent to taking $L = \infty$. The lanes are labeled by an integer $m = 1, 2, \ldots, M$ from the outer lanes inward. The current $\mathcal{J}_m^M$ exiting the lanes

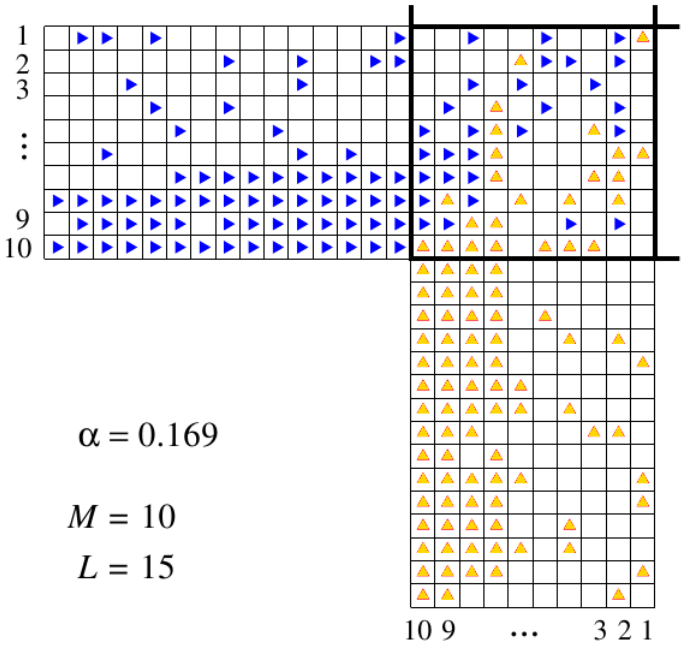

Figure 4.15: Snapshot of an intersection square of linear size $M = 10$ and for injection probability $\alpha = 0.169$. For this value of α lanes 1 to 7 are in the free flow and 8, 9 and 10 in the jammed flow phase. Taken from [120].

is measured, and corresponding reflection coefficients are defined, $R_m^M \equiv 1 - \frac{\mathcal{J}_m^M}{\mathcal{J}^{\mathrm{F}}}$, with $\mathcal{J}^{\mathrm{F}}$ given by Eq. (2.3). With this notation lane m being in free flow (jammed) is equivalent to $R_m^M = 0$ (or to $R_m^M \neq 0$), respectively.

For small enough $M \lesssim 24$ their measurements can be summarized in Figs. 4.14 and 4.15. Fig. 4.14 shows that the reflection coefficients become nonzero one at a time for some given values of α called α_m^M, here for $M = 10$. When the entrance current increases from 0 each lane undergoes a separate jamming transition, starting with the inner ones. The jamming transition of the whole intersection can then be considered to be of second order. It seems that a slope discontinuity can be observed for all the reflection coefficients of the already jammed lanes at each new transition, as seen in Fig. 4.14. Fig. 4.15 is a snapshot of such a system where the 3 inner lanes of each street are jammed, so that a 'crystallized' square occupies the southwest of the intersection.

These numerical results leave a lot of questions open. In particular, an analytical argument giving the critical points α_m^M or at least how they scale with the parameters m and M is missing. The behaviour of the principal

critical point α_M^M is unknown as well, in particular it is not known whether $\alpha_M^M \to 0$ in the $M \to \infty$ limit.

For greater sizes $M \gtrsim 24$ the nature of the phase transition changes and a tricritical point is found [141]. For these large intersections a local jam is nucleated somewhere inside the intersection, which may grow while propagating towards the southwest corner. The germ arriving at the corner may cause a large number of lanes to be blocked at the same time, contrarily to what was observed for $M \lesssim 24$. The intersection can however stay in free flow for a very long time before this germ nucleates and grows, so that the system can be considered to be in a metastable state. This first-order phase transition is illustrated in Fig. 4.16.

In the further sections we are not going to study this jamming transition, rather we will choose α and M so that we stay in the free flow phase. The average current in each (OBC) lane will then simply be equal to the free flow current $\mathcal{J}^{\mathrm{F}}$ from Eq. (2.3).

The following sections are devoted to the analysis of pattern formation in the free flow phase. In chapter 5 the PBC and the OBC case are studied whereas chapter 7 deals with some variants.

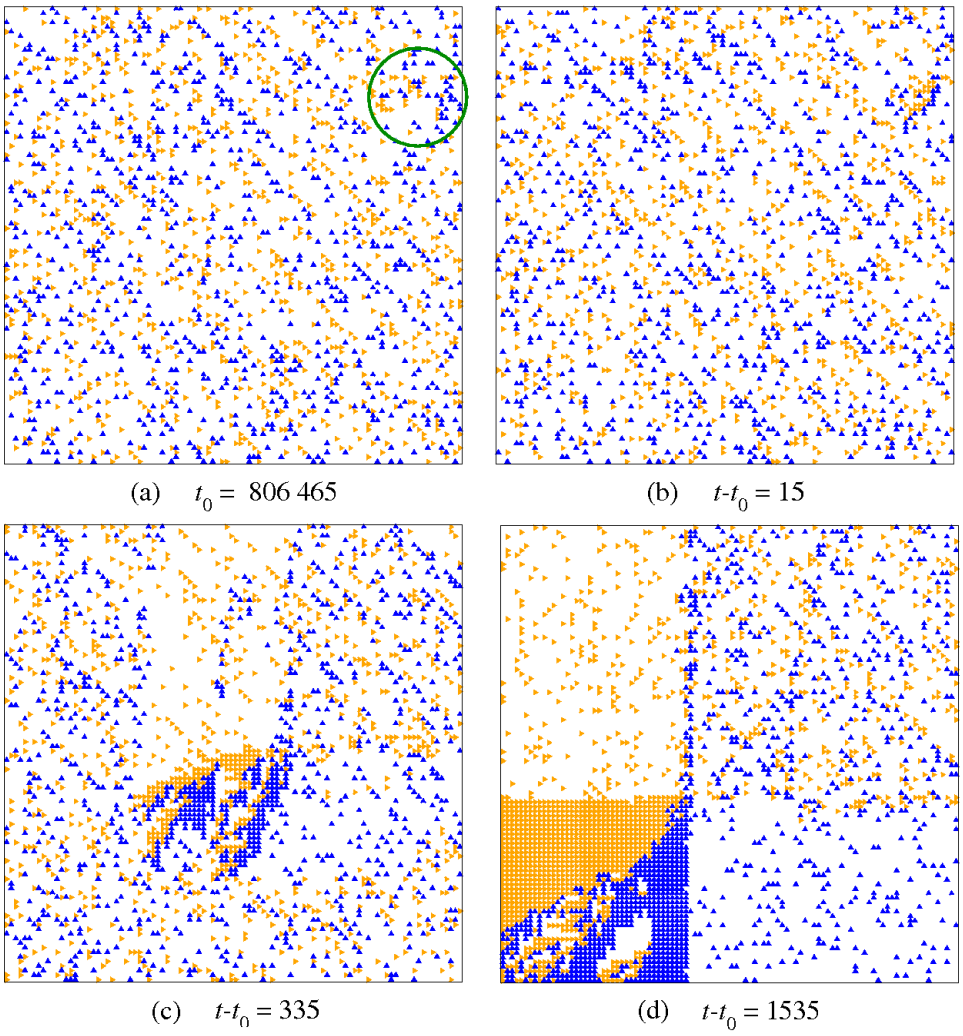

Figure 4.16: Example of formation of a jam in large intersection squares, with frozen shuffle update, $\alpha = 0.08729$ and $M = 100$. (a) The system has stayed in the free flow state for a long time. There is only a small jam in the upper right region, emphasized by the green circle. (b) While the jam would usually quickly evaporate, this one persists longer than expected. (c) The jam grows because of the arrival of particles at the bottom and left sides, the departure of particles at the top right tip of the jam not being fast enough to compensate for the arrivals. The jam grows and effectively propagates towards southwest. (d) When the jam reaches the southwest boundary several lanes get blocked simultaneously, the transition therefore becoming of first order.

Chapter 5

Pattern formation

After having reviewed the jamming transition of the intersection model, we finally study the case of interest to us and to pedestrians, namely the free flow phase. The problem with open boundaries does not possess any symmetry other than the exchange of particle types. We therefore allow ourselves to add translational symmetry to the model in the first section 5.1, as we consider periodic boundary conditions. This modification will simplify the phenomenology and the analytics, serving as a basis to understand the more complicated OBC case. We will see that the stationary state simply consists of alternating diagonal stripes of both particle types, that can be explained analytically by a simple linear stability analysis of nonlinear mean-field-type equations. The coherence between the results obtained from the particle system and the equations *a posteriori* justifies the relevance of these equations, that we will be able to use again in the following.

The OBC case is studied in sections 5.2 and 5.3. Translational invariance is lost and, while the particles still self-organize into alternating stripes, the angle of the stripes is not 45° anymore but depends on the position in the intersection, resulting in what we call the chevron effect. In section 5.2 the phenomenology is first presented. The linearized mean-field equations are then studied with open boundaries, mimicking the linear stability analysis of subsection 5.1.5. After a long calculation we obtain explicit formulas for many interesting quantities that characterize the propagation of a perturbation, however we do not find the chevron effect. The explanation is then delayed to chapter 6, as we first focus on performing quantitative measurements of the chevron effect in section 5.3. Indeed, the effect may seem clear to the eye but it is not so straightforward to reproduce the natural visual procedure in an algorithm. We therefore define two ways of locally measuring the angle of the stripes, that are compared and found to be in good agreement.

All these results can be found in Refs. [142, 143, 144] and have also been presented at conferences [145, 146].

5.1 Periodic boundary conditions: diagonal stripes

5.1.1 Periodic boundary conditions

Here we precisely define the periodic boundary conditions (PBC).

Imposing periodic boundary conditions in direction x means that the target site of an $\mathcal{E}$ particle hopping from any of the sites (M, j) with $j = 1, \dots, M$ is site $(1, j)$, *i.e.* the $\mathcal{E}$ particle hops towards $(1, j)$ if $(1, j)$ is empty and does not move otherwise. With these boundary conditions it is readily seen that the number of particles on each row j is conserved, so that the initial $\mathcal{E}$ particle density $\rho^{\mathcal{E}}$ replaces the entrance probability per time step $\alpha_{\mathcal{E}}$ on the same lane. It should also be noted that imposing periodic boundary conditions in direction x renders the system statistically translationally invariant along the x direction. Of course an equivalent definition holds for the y direction. In particular, the system is non ergodic.

In this section 5.1 we study the intersection with periodic boundaries in both the x and y directions. In this case there is translational invariance along the x and the y direction, in other words all the sites of the intersection are statistically equivalent. This will also simplify the Fourier analysis that will be performed later in subsection 5.1.5, to be compared with the equivalent calculation in OBC from subsection 5.2.3.

We note that with this choice of boundary conditions the model is exactly equivalent to the type I BML model [39] if parallel update is used. In the PBC case simulations were performed for frozen shuffle update and the results are presented in the following subsection 5.1.2.

5.1.2 Numerical observations

Simulations were performed with PBC in both directions and frozen shuffle update, the control parameters being the size of the system M and the density of particles of each type.The simulations were performed by Chloé Barré, who did her bachelor internship on the intersection with PBC at the LPT in may and june 2012 under the direction of Henk Hilhorst [147].

In the simulations, at the initial time the same number $\overline{\rho}M^2$ of particles of each type are dropped on random sites of the intersection and the phases of the particles are drawn uniformly. As there are no boundaries the evolution of the system is then completely deterministic. It should be noted that this preparation of the system does not ensure that the number of $\mathcal{E}$ particles ($\mathcal{N}$ particles) is the same on each row (column) but simply constrains the overall density of each particle type on the whole system. We stress again the fact that the system is not ergodic, so that the number of particles on each lane will remain fixed for the whole realization. Averages will therefore be taken over ensembles with fixed total number of particles of each kind.

For most initial conditions the system reaches a stationary state after a transient time of the order of a few system sizes. Mimicking the analysis of Biham *et al.*, these stationary states can roughly be divided into two classes

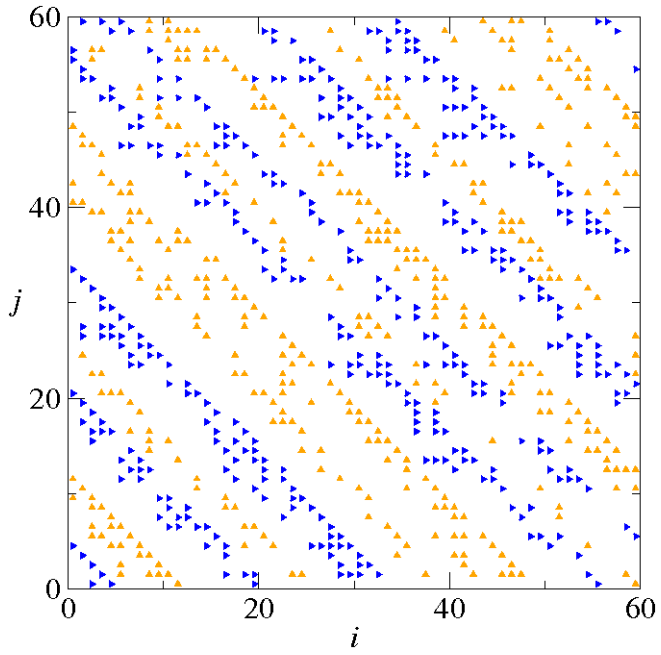

Figure 5.1: Snapshot of the stationary state of a particle simulation with frozen shuffle update and periodic boundary conditions, for system size $M = 60$ and particle density $\overline{\rho} = 0.1$. Particles of the same type are aligned along diagonals in the $(1, -1)$ direction. These diagonals have a width of a few lattice distances. The simulation was carried out by Chloé Barré, who also prepared this figure.

in which the velocity of the particles is either close to 0 (jammed) or to 1 (free flow). Fig. 5.1 shows a typical free flow stationary state. Similarly to what happens with alternating parallel update, the system self-organizes into a pattern of alternating diagonals of $\mathcal{E}$ and $\mathcal{N}$ particles with a pretty irregular wavelength between 5 and 15 lattice distances. Note that the wavelength is on average smaller in the case of alternating parallel update (see Fig. 4.8). This comes from the fact that particles updated in parallel need to keep an empty site in front of them in order to move with velocity 1 whereas with frozen shuffle update an empty site in front of each platoon is enough. In Fig. 5.1 platoons play the role of big particles, increasing the wavelength.

The pattern being clearly identified, we now turn on to an analytic explanation of this pattern in subsection 5.1.3

5.1.3 The mean-field equations

To explain this pattern, we will write the exact evolution equations of the system. These equations will help us motivate the introduction of mean-field

equations, in the sense that the two-body correlations will be approximated by one-body functions. For frozen shuffle update the exact evolution equations are rather complicated, as the evolution of the density on a single site may depend on an arbitrary large number of phases of the other particles. The same qualitative patterns are however obtained with alternating parallel update, and in this case the evolution equations are much simpler to write. We will therefore start from the exact evolution equations for alternating parallel update.

We define $n_t^{\mathcal{E},\mathcal{N}}(\mathbf{r}) = 0, 1$ as the occupation of site $\mathbf{r}$ at time t, *i.e.* $n_t^{\mathcal{E},\mathcal{N}}(\mathbf{r}) = 1$ iff site $\mathbf{r}$ is occupied by an $\mathcal{E}$ particle ($\mathcal{N}$ particle) at time t. The simple exclusion constraint then reads

$$n_t^{\mathcal{E}}(\mathbf{r}) n_t^{\mathcal{N}}(\mathbf{r}) = 0 \tag{5.1}$$

for all $t > 0$ and $\mathbf{r}$ in the intersection. For alternating parallel update with the arbitrary choice of phases $\tau_{\mathcal{E}} = 0$ and $\tau_{\mathcal{N}} = 1/2$ the evolution equations read

$$\begin{aligned} n_{t+1}^{\mathcal{E}}(\mathbf{r}) &= [1 - n_t^{\mathcal{E}}(\mathbf{r}) - n_{t+1/2}^{\mathcal{N}}(\mathbf{r})] n_t^{\mathcal{E}}(\mathbf{r} - \mathbf{e}_x) \\ &\quad + [n_t^{\mathcal{E}}(\mathbf{r} + \mathbf{e}_x) + n_{t+1/2}^{\mathcal{N}}(\mathbf{r} + \mathbf{e}_x)] n_t^{\mathcal{E}}(\mathbf{r}), \\ n_{t+1/2}^{\mathcal{N}}(\mathbf{r}) &= [1 - n_{t-1/2}^{\mathcal{N}}(\mathbf{r}) - n_t^{\mathcal{E}}(\mathbf{r})] n_{t-1/2}^{\mathcal{N}}(\mathbf{r} - \mathbf{e}_y) \\ &\quad + [n_{t-1/2}^{\mathcal{N}}(\mathbf{r} + \mathbf{e}_y) + n_t^{\mathcal{E}}(\mathbf{r} + \mathbf{e}_y)] n_{t-1/2}^{\mathcal{N}}(\mathbf{r}) \end{aligned} \tag{5.2}$$

for $t \in \mathbb{N}$ and $\mathbf{r}$ in the intersection. In this section, Eqs. (5.2) are supplemented with the periodic boundary conditions

$$\begin{aligned} n_t^{\mathcal{E}}(M+1, j) &\equiv n_t^{\mathcal{E}}(1, j) \qquad j = 1, \ldots, M, \\ n_t^{\mathcal{N}}(i, M+1) &\equiv n_t^{\mathcal{N}}(i, 1) \qquad i = 1, \ldots, M. \end{aligned} \tag{5.3}$$

It seems impossible to solve Eqs. (5.2) and (5.3) exactly, as they give rise to a BBGKY-like hierarchy in which correlations of $n+1$ variables systematically appear in the evolution equation for the n^{th} correlation function.

We will therefore perform coarse-graining approximations in a spirit similar to *e.g.* block renormalization of the Ising model, where the system is divided in mesoscopic blocks whose state is specified by an continuous magnetization field averaged over the block. In our case we will replace the discrete-valued $n_t^{\mathcal{E},\mathcal{N}}(\mathbf{r})$ by continuous density fields $\rho_t^{\mathcal{E},\mathcal{N}}(\mathbf{r})$. We can however not define these continuous fields as mesoscopic spatial averages because we are interested in structures at the scale of the lattice distance. The evolution equations for the $\rho_t^{\mathcal{E},\mathcal{N}}(\mathbf{r})$ will therefore be based on Eqs. (5.2), but the $\rho_t^{\mathcal{E},\mathcal{N}}(\mathbf{r})$ will be interpreted as continuous versions of the $n_t^{\mathcal{E},\mathcal{N}}(\mathbf{r})$ in a rather imprecise sense, as a simple time or ensemble averaging would smear out the stripes.

If we take an average of Eqs. (5.2) two-point correlations appear that need to be dealt with. Remember that we are in the free flow phase, which makes the average density of the system $\overline{\rho}$ rather small and will determine which approximations we will make. The following discussion holds independently of the boundary conditions.

Consider an $\mathcal{E}$ particle. We will show that the correlation between the presence of the $\mathcal{E}$ particle and the possible presence of a $\mathcal{N}$ particle targeting the same site as the $\mathcal{E}$ particle is negligible. If there were only $\mathcal{E}$ particles in the system the rows would be completely independent. The only correlations between the $\mathcal{E}$ particle considered and other $\mathcal{E}$ particles from different rows are therefore a consequence of the presence of the $\mathcal{N}$ particles, which gives a supplementary factor $\sim \overline{\rho}$ compared to what would be expected if the rows were in direct contact. The result is therefore a negligible contribution to the correlations we are interested in. There is a strong correlation between a $\mathcal{E}$ particle and the other $\mathcal{E}$ particles in the same row. The typical distance between two consecutive particles of a lane however scales like $\overline{\rho}^{-1}$, therefore there is very little chance that a given column still has the memory of the passage of the previous particle when the current one passes. This analysis shows that two particles of types $\mathcal{E}$ and $\mathcal{N}$ colliding are to the highest order uncorrelated. Terms of the form $n^{\mathcal{E}} n^{\mathcal{N}}$ will then simply become $\rho^{\mathcal{E}} \rho^{\mathcal{N}}$ in the equations for $\rho_t^{\mathcal{E},\mathcal{N}}(\mathbf{r})$.

We now turn to the second type of terms, the correlators between particles of the same type. A collision between two $\mathcal{E}$ particles can occur only if they are consecutive particles on the same row. In the undisturbed free flow phase however no collisions occur, which shows that another particle, of type $\mathcal{N}$, should be involved in such collisions. Indeed, the $\mathcal{N}$ particle is needed to slow down the first $\mathcal{E}$ particle, so this first $\mathcal{E}$ particle may eventually block the second one. The probability that two $\mathcal{E}$ particles are close enough to ensure that the second one gets blocked on a given site if the first one is grows like $\overline{\rho}^2$ to leading order and the probability to have a $\mathcal{N}$ particle blocking the first one scales like $\overline{\rho}$, so that the probability for the whole process goes like $\overline{\rho}^3$. Terms of the type $n^{\mathcal{E}} n^{\mathcal{E}}$ are then simply neglected in the equations for $\rho_t^{\mathcal{E},\mathcal{N}}(\mathbf{r})$.

Finally, we perform one last approximation: we suppose that both fields $\rho_t^{\mathcal{E},\mathcal{N}}(\mathbf{r})$ are updated at the same time. The behavior of the system is expected not to be altered too much by this simplification, as the alternating update is only used for solving conflicts. Combining all these arguments gives what we will call the *mean field* equations for the density fields,

$$\begin{aligned} \rho_{t+1}^{\mathcal{E}}(\mathbf{r}) &= [1-\rho_t^{\mathcal{N}}(\mathbf{r})]\rho_t^{\mathcal{E}}(\mathbf{r}-\mathbf{e}_x) + \rho_t^{\mathcal{N}}(\mathbf{r}+\mathbf{e}_x)\rho_t^{\mathcal{E}}(\mathbf{r}), \\ \rho_{t+1}^{\mathcal{N}}(\mathbf{r}) &= [1-\rho_t^{\mathcal{E}}(\mathbf{r})]\rho_t^{\mathcal{N}}(\mathbf{r}-\mathbf{e}_y) + \rho_t^{\mathcal{E}}(\mathbf{r}+\mathbf{e}_y)\rho_t^{\mathcal{N}}(\mathbf{r}). \end{aligned} \tag{5.4}$$

In this section, Eqs. (5.4) are still complemented with the periodic boundary conditions

$$\begin{aligned} \rho_t^{\mathcal{E}}(M+1,j) &\equiv \rho_t^{\mathcal{E}}(1,j) \qquad j=1,\dots,M, \\ \rho_t^{\mathcal{N}}(i,M+1) &\equiv \rho_t^{\mathcal{N}}(i,1) \qquad i=1,\dots,M. \end{aligned} \tag{5.5}$$

5.1.4 Properties of the equations

A full solution of Eqs. (5.4) and (5.5) still seems hard to obtain. We can however make some remarks that will either be useful later in the treatment of these

equations or that may support the fact that these equations capture the main ingredients of the particle system.

We first notice that the $2M$ numbers of $\mathcal{E}$ particles on each row and of $\mathcal{N}$ particles on each column are conserved by the dynamics, as we have from Eqs. (5.4) and (5.5) that

$$\begin{aligned} \sum_{j=1}^{M} \rho_{t+1}^{\mathcal{E}}(i,j) &= \sum_{j=1}^{M} \rho_{t}^{\mathcal{E}}(i,j) \qquad i = 1,\ldots,M, \\ \sum_{i=1}^{M} \rho_{t+1}^{\mathcal{N}}(i,j) &= \sum_{i=1}^{M} \rho_{t}^{\mathcal{N}}(i,j) \qquad j = 1,\ldots,M, \end{aligned} \tag{5.6}$$

for all t, which is in total agreement with what we know from the particle system. This also implies that the total mass of each type is conserved.

Secondly we notice that a uniform constant density for each particle type $\rho_t^{\mathcal{E},\mathcal{N}}(\mathbf{r}) = \overline{\rho}^{\mathcal{E},\mathcal{N}}$ solves Eqs. (5.4) and (5.5). According to equations (5.6) the $\overline{\rho}^{\mathcal{E},\mathcal{N}}$ are determined by the initial condition. Here we will stick to the symmetric initial conditions and simply take $\overline{\rho}^{\mathcal{E}} = \overline{\rho}^{\mathcal{N}} \equiv \overline{\rho}$. This solution does however not have an interpretation in terms of the particle system as the only homogeneous states of the particle system consist of a completely empty or a completely full lattice.

Another class of solutions can be guessed from the equations. These solutions are characterized by the fact that all the quadratic terms in the equations vanish at all times because the two density fields are never nonzero at the same time. When this separation occurs $\rho^{\mathcal{E},\mathcal{N}}$ then propagate to the east (the north) with velocity 1, as Eqs. (5.4) become $\rho_{t+1}^{\mathcal{E}}(\mathbf{r}) = \rho_t^{\mathcal{E}}(\mathbf{r} - \mathbf{e}_x)$ and $\rho_{t+1}^{\mathcal{N}}(\mathbf{r}) = \rho_t^{\mathcal{N}}(\mathbf{r} - \mathbf{e}_y)$. One can show that for a square toroidal intersection this mode is stable if the density fields are segregated into diagonals with a slope -1. There is then a clear parallel between this solution of the equations and the diagonals observed in Fig. 5.1 with the particle model.

It has to be stressed that even if the equations (5.4) seem to naturally incorporate the simple exclusion principle in the dynamics, there is no strict restriction similar to Eq. (5.1) for the $\rho^{\mathcal{E},\mathcal{N}}$ variables in general. This may cause some divergences in the density fields to appear which will be discussed later in subsection 5.2.3 along with the numerical resolution of these equations. For now we simply treat Eqs. (5.4) and (5.5) analytically.

5.1.5 Linear stability analysis

In this section we perform a linear stability analysis of the mean-field equations with periodic boundaries around the constant uniform densities solution.

We write $\rho_t^{\mathcal{E},\mathcal{N}}(\mathbf{r}) \equiv \overline{\rho} + \delta\rho_t^{\mathcal{E},\mathcal{N}}(\mathbf{r})$, where $\overline{\rho}$ is determined by the initial condition and the $\delta\rho^{\mathcal{E},\mathcal{N}}$ are supposed to be small. We then linearize Eqs. (5.4)

to get the *linearized equations*

$$\begin{aligned}\delta\rho^{\mathcal{E}}_{t+1}(\mathbf{r}) &= (1-\overline{\rho})\delta\rho^{\mathcal{E}}_t(\mathbf{r}-\mathbf{e}_x) - \overline{\rho}\delta\rho^{\mathcal{N}}_t(\mathbf{r}) \\ &\quad +\overline{\rho}\delta\rho^{\mathcal{E}}_t(\mathbf{r}) + \overline{\rho}\delta\rho^{\mathcal{N}}_t(\mathbf{r}+\mathbf{e}_x), \\ \delta\rho^{\mathcal{N}}_{t+1}(\mathbf{r}) &= (1-\overline{\rho})\delta\rho^{\mathcal{N}}_t(\mathbf{r}-\mathbf{e}_y) - \overline{\rho}\delta\rho^{\mathcal{E}}_t(\mathbf{r}) \\ &\quad +\overline{\rho}\delta\rho^{\mathcal{N}}_t(\mathbf{r}) + \overline{\rho}\delta\rho^{\mathcal{E}}_t(\mathbf{r}+\mathbf{e}_y).\end{aligned} \tag{5.7}$$

We now define the Fourier transforms

$$\hat{\delta\rho_t^{\mathcal{E},\mathcal{N}}}(\mathbf{k}) \equiv \sum_{\mathbf{r}} \delta\rho_t^{\mathcal{E},\mathcal{N}}(\mathbf{r})\mathrm{e}^{\mathrm{i}\mathbf{k}.\mathbf{r}}, \tag{5.8}$$

where the sum goes over all the sites of the intersection. The components of the wavevectors $\mathbf{k} = (k_x, k_y)$ are quantized by the conditions $\mathrm{e}^{Mik_x} = \mathrm{e}^{Mik_y} = 1$ but in the following we shall treat them as continuous variables of the interval $[0; 2\pi[$. In the Fourier space Eqs. (5.7) become

$$\begin{aligned}\hat{\delta\rho_t^{\mathcal{E}}}(\mathbf{k}) &= [(1-\overline{\rho})\mathrm{e}^{\mathrm{i}k_x} + \overline{\rho}]\hat{\delta\rho_t^{\mathcal{E}}}(\mathbf{k}) + \overline{\rho}(\mathrm{e}^{-\mathrm{i}k_x} - 1)\hat{\delta\rho_t^{\mathcal{N}}}(\mathbf{k}), \\ \hat{\delta\rho_t^{\mathcal{E}}}(\mathbf{k}) &= [(1-\overline{\rho})\mathrm{e}^{\mathrm{i}k_y} + \overline{\rho}]\hat{\delta\rho_t^{\mathcal{N}}}(\mathbf{k}) + \overline{\rho}(\mathrm{e}^{-\mathrm{i}k_y} - 1)\hat{\delta\rho_t^{\mathcal{E}}}(\mathbf{k}).\end{aligned} \tag{5.9}$$

To determine whether there is an instability we compute the eigenvalues of the matrix $\begin{pmatrix} A(k_x) & B(k_x) \\ B(k_y) & A(k_y) \end{pmatrix}$, with $A(k) \equiv (1-\overline{\rho})\mathrm{e}^{\mathrm{i}k} + \overline{\rho}$ and $B(k) \equiv \overline{\rho}(\mathrm{e}^{-\mathrm{i}k} - 1)$. The characteristic polynomial reads

$$\chi(\mu) = \mu^2 - (A(k_x) + A(k_y))\mu + [A(k_x)A(k_y) - B(k_x)B(k_y)], \tag{5.10}$$

thus the eigenvalues

$$\mu_\pm(\mathbf{k}) = \frac{A(k_x) + A(k_y)}{2} \pm \sqrt{\left(\frac{A(k_x) - A(k_y)}{2}\right)^2 + B(k_x)B(k_y)}. \tag{5.11}$$

Examination shows that $|\mu_-(\mathbf{k})| < 1$ for all $\mathbf{k}$, we therefore focus on $\mu_+(\mathbf{k})$. Guided by the numerics, we look for a maximum of $|\mu_+(\mathbf{k})|$ on the diagonal $k_x = k_y$. The eigenvalue then reads

$$\mu_+(k_x, k_x) = 2\overline{\rho} + (1 - 2\overline{\rho})\cos(k_x) - \mathrm{i}\sin(k_x) \tag{5.12}$$

and its squared norm

$$|\mu_+(k_x, k_x)|^2 = 1 + 4\overline{\rho}[\overline{\rho} + (1 - 2\overline{\rho})\cos(k_x) - (1 - \overline{\rho})\cos^2(k_x)]. \tag{5.13}$$

An extremum is obtained for $\mathbf{k} = (k_x^*, k_x^*)$ such that $\frac{d}{dk_x}|\mu_+(k_x, k_x)|^2 = 0$. This gives

$$\cos(k_x^*) = \frac{1 - 2\overline{\rho}}{2 - 2\overline{\rho}}, \tag{5.14}$$

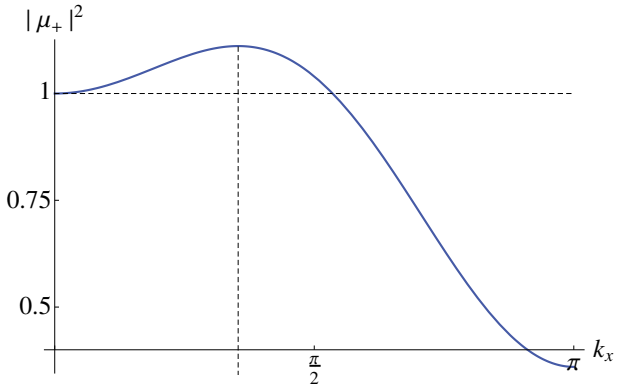

Figure 5.2: Plot of the squared 'growth factor' $|\mu_+(k_x, k_x)|^2$ for $0 \leq k_x \leq \pi$. We took $\overline{\rho} = 0.1$, which gives $\cos(k_x^*) = 4/9$ or $k_x^* = \arccos(4/9) \simeq 1.11024$ if we choose k_x^* in the $[0; \pi)$ interval, and $|\mu_+(k_x^*, k_x^*)|^2 = 10/9 = 1.111\ldots$. The vertical dashed line shows the value of k_x^* while the horizontal dashed line is constant equal to 1. The curve is symmetric with respect to $k_x = \pi$, so that an other maximum is located at $2\pi - k_x^*$.

from which we get the simple formula

$$|\mu_+(k_x^*, k_x^*)|^2 = \frac{1}{1-\overline{\rho}} > 1, \tag{5.15}$$

which proves the existence of an instability. The curve defined by Eq. (5.13) is plotted in Fig. 5.2.

The maximal instability occurs along the $(1, 1)$ direction with wavelength

$$\lambda_{\mathrm{PBC}} = \frac{\sqrt{2}\pi}{k_x} = \frac{\sqrt{2}\pi}{\arccos\left(\frac{1-2\overline{\rho}}{2-2\overline{\rho}}\right)} = 3\sqrt{2} - \frac{3\sqrt{6}}{\pi}\overline{\rho} + O(\overline{\rho}^2), \tag{5.16}$$

which seems close to what can be observed in Fig. 4.8 for the case of parallel update, at least in certain regions. In the case of frozen shuffle update we have seen that transport is more efficient, as particles tend to create platoons. The wavelength is therefore larger than what Eq. (5.14) predicts, as can be seen on Fig. 5.1. The eigenvalues corresponding to the maximal instability come in complex conjugate pairs, as replacing k_x by $2\pi - k_x$ leaves Eq. (5.13) unchanged and simply reverses the sign of the sine in Eq. (5.12). Both terms combine into a cosine, so that the instability propagates. The dominant wavevector being on the diagonal, the instability propagates in the $(1, 1)$ direction, in agreement to what was observed in the particle model. The mean-field equations therefore explain the pattern formation in the particle model.

5.1.6 Discussion and extensions

In subsection 5.1.3 mean-field equations were motivated from those of the particle model previously defined in section 4.2 and were proved in subsections 5.1.4 and 5.1.5 to explain the main feature of the particle model in free flow phase, namely the formation of a pattern of diagonal stripes.

Even though the preceding analysis seems pretty convincing, the full nonlinear mean-field equations were solved numerically as well for comparison with the linear analytical results. Numerical resolution of the equations shows that the solution tends to a stationary state that consists of alternating stripes. In each stripe only one of the density fields is nonzero, and between them empty zones exist where both fields vanish. The whole pattern then propagates diagonally, as each type of stripe propagates eastward or northward with velocity 1.

There are two main conclusions to this study of the diagonal pattern with periodic boundary conditions.

The first one concerns the correspondence between the particle model and the equations. They have been proved to have the same qualitative behavior, which leads us to think that the postulated mean-field equations give a satisfying description of the particle model for both update schemes we use. Conversely, the equations are expected to constitute the mean-field description of a larger class of systems, the particle model with frozen shuffle and alternating parallel update simply being two instances of this class. It is then no surprise to observe similar phenomena in more complicated models [21, 131] or in experiments [10].

The second conclusion can be summarized like follows: the PBC study is an important preliminary to the subtler OBC analysis. Indeed, here we have defined equations that will still be useful in the following. We also observed the segregation of the two types of particles into diagonal stripes with an angle exactly 45°, which has been proved to be a linear effect.

After this preliminary we therefore focus on the open intersection, which is done in the following section 5.2.

5.2 Open boundary conditions: the chevron effect

The particle model will now be simulated with open boundary conditions (OBC). In this section numerical observations of the so-called chevron effect are presented in subsection 5.2.1. The linearized mean-field equations are analyzed with open boundaries, mimicking the analysis of section 5.1. The final result is expressed in terms of a Green function that gives informations about the wavelength or the velocity of the instability, but fails to account for the chevron effect. After that, methods for measuring the angle of the stripes are designed and measurements are presented in section 5.3. The chevron effect will be explained in a more physical way in the following chapter 6.

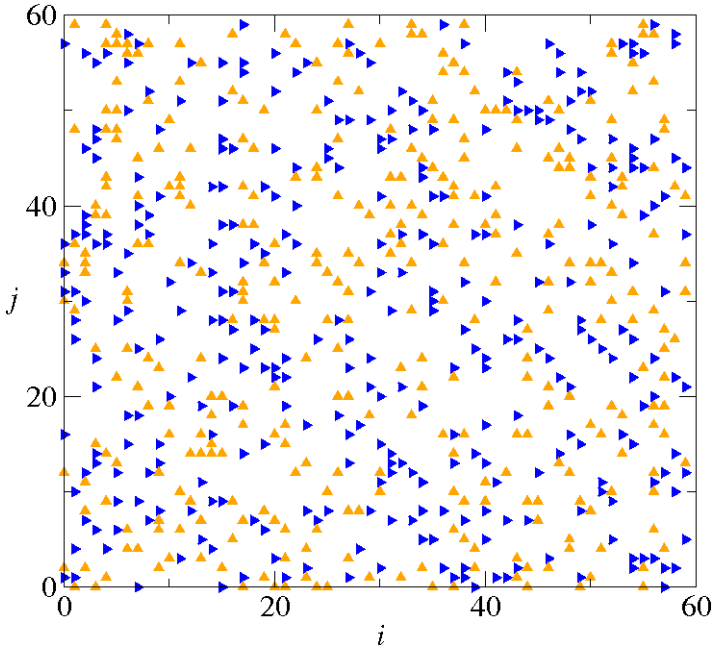

Figure 5.3: Snapshot of the stationary state of the intersection square in a particle simulation with open boundary conditions for $\alpha = 0.09$ and $M = 60$. The blue particles come from the left and the orange ones from the bottom. Obtained with frozen shuffle update.

5.2.1 Numerical observations

Here we present the principal observations that have been made on numerical simulations of the particle system with open boundaries as shown in Fig. 4.13. Similarly to what happens in one dimension, the open system is ergodic so that the initial condition has *a priori* little importance.

In the simulations the system is empty at the initial time so that the first particle to reach an exit site does so after a time $\sim L + M$. In the free flow phase a stationary state is then reached quickly after that moment, in which the dynamics is stationary and the macroscopic properties of the system are constant if they are averaged over many cycles. In this cyclic state the value of L has been shown in section 4.2 to be unimportant.

We start with the small system of size $M = 60$ shown in Fig. 5.3. Near the entrance sites the particles seem to fill the intersection square in a random fashion. From our previous knowledge of the diagonal patterns in PBC we can however guess the emergence of such an organization further from the boundaries. This observation motivates the study of larger systems. For $M = 640$ a typical stationary state is shown by Fig. 5.4.

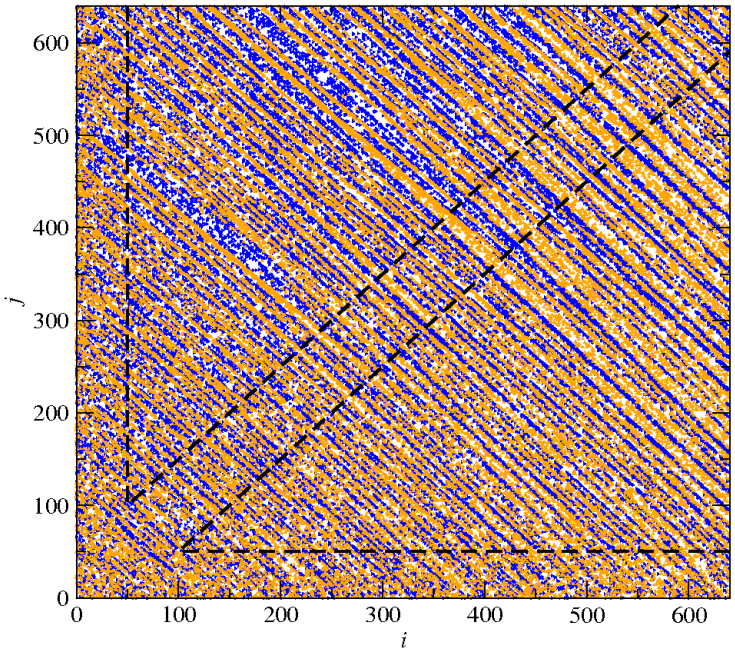

Figure 5.4: Snapshot of the stationary state of the intersection square of a particle system with $M = 640$ and $\alpha = 0.09$ and subject to frozen shuffle update. When propagating in the system particles progressively self-organize into a diagonal pattern. Along the two entrance boundaries there are disordered boundary layers of width $\xi \approx 50$. The black dashed lines roughly delimit the two triangular regions.

Along the entrance boundaries we still observe a disordered zone, whose size is expected not to depend on M. Indeed in the free flow phase the information almost propagates only downstream up to exponential terms in the density, so that for example sites $(40, 50)$ of two different intersections with $M = 60$ and $M = 640$ are almost statistically identical for the same value of α. This motivates the introduction of a *penetration length* $\xi(\alpha)$ that does not depend on M. The length $\xi(\alpha)$ is not defined very precisely here, but can be thought of as the characteristic length needed by disordered particles to self-organize. From Figs. 5.3 and 5.4 we see that $\xi(0.09) \sim 50$. For $\alpha \to 0$ the length ξ diverges roughly as α^{-1}, which is consistent with the intuitive idea that the 'organization' of the particles is proportional to the number of collisions they have undertaken. More precise measurements are presented in subsection 7.3.1 in the numerical resolution of the mean-field equations.

After this penetration zone $i, j \gtrsim \xi(\alpha)$ stripes similar to those observed in PBC can be clearly distinguished in Fig. 5.4. A closer look at Fig. 5.4 however reveals an inhomogeneity of the intersection. Excluding the penetration zones, the intersection may roughly be divided into two triangular zones separated by

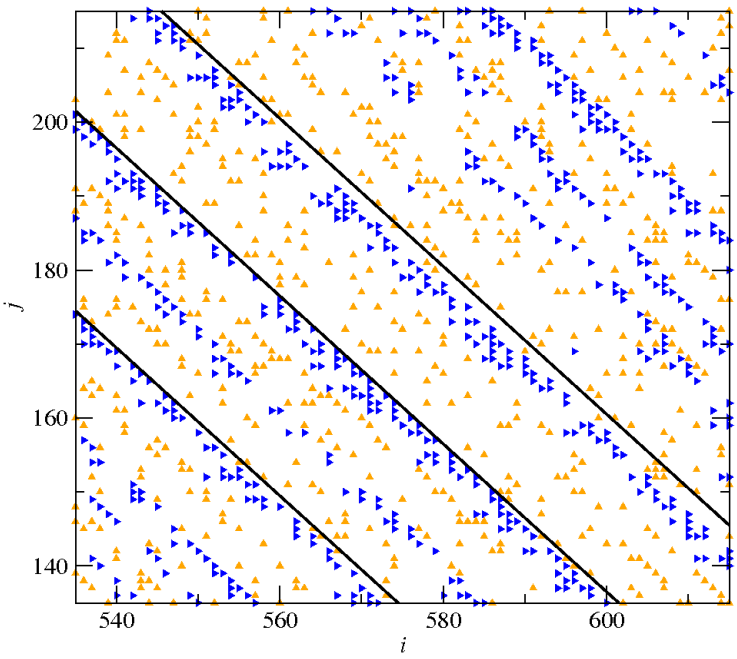

Figure 5.5: Zoom on a region of the lower triangle of Fig. 5.4 showing the chevron pattern. This snapshot has been taken for $M = 640$ and $\alpha = 0.09$, the blue right-pointing triangles are the eastbound particles and the orange up-pointing triangles are the northbound ones. The black solid lines are at an angle of 45° and highlight the fact that there is a negative chevron angle $\Delta\theta$. Moreover the eastbound particles appear to be confined, statistically, to narrower strips than the northbound ones.

the main diagonal. On a global picture like Fig. 5.4 the inhomogeneity is best noticed by looking at the colors of the triangles: the *upper triangle* ($j \gtrsim i$) looks more blue whereas the *lower triangle* ($i \gtrsim j$) looks more orange.

Several features can be observed in Fig. 5.5, which shows a zoom on a region of the lower triangle of Fig. 5.4. The most prominent effect is the asymmetry in the organization of the two particle types. In the lower triangle $\mathcal{E}$ particles seems to be organized in very compact diagonals, occupying a very small fraction of space, whereas $\mathcal{N}$ particles occupy all the rest of space in a very random fashion. This explains why the lower triangle looks orange. A second observation concerns the alignments of $\mathcal{E}$ particles. The angle of these alignments with respect to the vertical axis is found to be slightly lower than 45°, as is emphasized by the black solid lines in Fig. 5.5.

Of course, a symmetrical behaviour occurs in the upper triangle, where $\mathcal{N}$ particles are organized into alignments of angle larger than 45° and $\mathcal{E}$ particles are disorganized. With these angles of inclination the straight stripes turn into chevrons. We shall thus call the described set of correlated phenomena the

chevron effect, as the most straightforward way to quantify this effect is to measure the chevron angle. Using alternating parallel update instead of frozen shuffle the effect is also present, which supports the generality of the effect. In fact the chevron effect is even stronger, as alternating parallel update is more regular. In contrast to the OBC case, in PBC this chevron effect was forbidden by translational symmetry.

To make things precise we write the angle of the stripes with respect to the vertical as $\theta(\mathbf{r}) \equiv 45^\circ + \Delta\theta(\mathbf{r})$. In section 5.3 we will show how to measure $\Delta\theta(\mathbf{r})$. Before that we will however draw our attention over the mean-field equations, for which we want to know whether the chevron effect exists or not. We first mimic the linear stability analysis performed in PBC in section 5.1 for the open system. After that the nonlinear mean-field equations will also be simulated.

5.2.2 OBC for the mean-field equations

Here we define open boundary conditions for the mean-field equations. The geometry will be slightly different from the particle model insofar as the equations in the entrance lanes will not be simulated. Instead we will simply specify the behaviour of the boundary sites, *i.e.* the effective sites having i or j equal to 0 or $M+1$. Along with the bulk equations (5.4) the boundary conditions define unambiguously the behaviour of the intersection.

The easiest part to deal with is the exit boundary. OBCs in the particle system are equivalent to taking the sites beyond the exit boundary empty at all times, so that we may simply set

$$\begin{aligned} \rho_t^{\mathcal{E}}(M+1,j) &\equiv 0 \qquad j=1,\dots,M, \\ \rho_t^{\mathcal{N}}(i,M+1) &\equiv 0 \qquad i=1,\dots,M. \end{aligned} \tag{5.17}$$

Whereas the desired correspondence between the particle model and the mean-field equations fixes the exit boundary condition, there are several ways to impose a stochastic boundary condition at the entrance. Here we choose to model the entrance with

$$\begin{aligned} \rho_t^{\mathcal{E}}(0,j) &\equiv \overline{\eta} + \eta_t^{\mathcal{E}}(j) \qquad j=1,\dots,M, \\ \rho_t^{\mathcal{N}}(i,0) &\equiv \overline{\eta} + \eta_t^{\mathcal{N}}(i) \qquad i=1,\dots,M, \end{aligned} \tag{5.18}$$

where the $\eta_t^{\mathcal{E},\mathcal{N}}(k)$ are i.i.d. random variables of average 0. In the numerical resolution we took for the $\eta_t^{\mathcal{E},\mathcal{N}}(k)$ a uniform distribution between $-\frac{\overline{\eta}}{2}$ and $\frac{\overline{\eta}}{2}$.

Note here that the parameter $\overline{\eta}$ replaces the entrance probability per time step α in the OBC particle system or the average initial density $\overline{\rho}$ for the PBC particle system and equations. The constant $\overline{\eta}$ therefore determines the overall density of the system and plays the role of a control parameter. The $2M$ random variables $\eta_t^{\mathcal{E},\mathcal{N}}(k)$ constitute the noise, which does not necessarily have a small amplitude but at least self-averages to zero. Note also that, as in the particle system, the conservation of the number of particles in each lane, translated by Eq. (5.6), is lost.

From the arguments of subsection 4.2.1 it should still be clear that in the free flow phase the entrance lanes evolve in a very simple way and may be reduced to a single site each with little effect on the rest of the intersection. The precise distribution of the $\eta_t^{\mathcal{E},\mathcal{N}}(k)$ may however raise objections. Here we made the arbitrary choice of a uniform distribution. One could argue that a better correspondence would be given by, say, a binary distribution where $\overline{\eta} + \eta_t^{\mathcal{E},\mathcal{N}}(k) = 1$ with probability $\overline{\eta}$ and 0 otherwise. This kind of discrete distributions is however very particular, and almost all reasonable initial distributions are expected to be forgotten rather quickly because of the collisions. We have therefore chosen what seems to be a typical case, bearing in mind that the precise probability distribution of the entrance noise is expected to be unimportant.

We now turn on to the linear stability analysis of the equations.

5.2.3 Linear stability analysis

Here we perform the linear stability analysis of the equations in OBC. If there was no noise a solution of the mean-field equations would be given by $\rho_t^{\mathcal{E},\mathcal{N}}(\mathbf{r}) = \overline{\eta}$ for all $t > 0$ in the whole quarter plane $i \geq 0$,$j \geq 0$, provided we modify the exit boundary conditions $\rho_t^{\mathcal{E}}(M+1,j) = \rho_t^{\mathcal{N}}(i,M+1) = \overline{\eta}$, which we do throughout the current subsection.

Linearized around this solution $\rho_t^{\mathcal{E},\mathcal{N}}(\mathbf{r}) \equiv \overline{\eta} + \delta\rho_t^{\mathcal{E},\mathcal{N}}(\mathbf{r})$ the mean-field equations (5.4) become similar to Eqs. (5.7) with $\overline{\rho}$ replaced by $\overline{\eta}$, that we reproduce here for clarity

$$\begin{aligned}
\delta\rho_{t+1}^{\mathcal{E}}(\mathbf{r}) &= (1-\overline{\eta})\delta\rho_t^{\mathcal{E}}(\mathbf{r}-\mathbf{e}_x) - \overline{\eta}\delta\rho_t^{\mathcal{N}}(\mathbf{r}) \\
&\quad +\overline{\eta}\delta\rho_t^{\mathcal{E}}(\mathbf{r}) + \overline{\eta}\delta\rho_t^{\mathcal{N}}(\mathbf{r}+\mathbf{e}_x), \\
\delta\rho_{t+1}^{\mathcal{N}}(\mathbf{r}) &= (1-\overline{\eta})\delta\rho_t^{\mathcal{N}}(\mathbf{r}-\mathbf{e}_y) - \overline{\eta}\delta\rho_t^{\mathcal{E}}(\mathbf{r}) \\
&\quad +\overline{\eta}\delta\rho_t^{\mathcal{N}}(\mathbf{r}) + \overline{\eta}\delta\rho_t^{\mathcal{E}}(\mathbf{r}+\mathbf{e}_y),
\end{aligned} \tag{5.19}$$

for $i > 1$,$j \geq 1$ and $i \geq 1$,$j > 1$, respectively. At the entrance the equations are perturbed by the noise and read

$$\begin{aligned}
\delta\rho_{t+1}^{\mathcal{E}}(1,j) &= (1-\overline{\eta})\eta_t^{\mathcal{E}}(j) - \overline{\eta}\delta\rho_t^{\mathcal{N}}(1,j) \\
&\quad +\overline{\eta}\delta\rho_t^{\mathcal{E}}(1,j) + \overline{\eta}\delta\rho_t^{\mathcal{N}}(2,j), \\
\delta\rho_{t+1}^{\mathcal{N}}(i,1) &= (1-\overline{\eta})\eta_t^{\mathcal{N}}(i) - \overline{\eta}\delta\rho_t^{\mathcal{E}}(i,1) \\
&\quad +\overline{\eta}\delta\rho_t^{\mathcal{N}}(i,1) + \overline{\eta}\delta\rho_t^{\mathcal{E}}(i,2).
\end{aligned} \tag{5.20}$$

Because of the loss of translational invariance the linear stability analysis of the equations is much more tedious in OBC than in PBC. The intermediate steps can be found in appendix A, a more complete version being in preparation [144].

Regrouping the density fields in a vector $\delta\rho_t$ and the noises in an other vector η_t, equations (5.19) and (5.20) may be written in a more compact form

$$\delta\rho_{t+1} = \mathbf{M}\delta\rho_t + (1-\overline{\eta})\eta_t, \tag{5.21}$$

for some $2M^2 \times 2M^2$ matrix $\mathbf{M}$ that depends only on $\overline{\eta}$, and where the last term η_t is zero everywhere except on the entrance boundaries. Eq. (5.21) can generically be solved in terms of Green functions,

$$\begin{aligned}\delta\rho^{\mathcal{E}}_{i,j}(t) &\equiv \sum_{t'=0}^{t-1}\Big[\sum_{j'=1}^{\infty} G^{\mathcal{E}\mathcal{E}}_{i,j;j'}(t-t')\eta^{\mathcal{E}}_{j'}(t') + \sum_{i'=1}^{\infty} G^{\mathcal{E}\mathcal{N}}_{i,j;i'}(t-t')\eta^{\mathcal{N}}_{i'}(t')\Big],\\ \delta\rho^{\mathcal{N}}_{i,j}(t) &\equiv \sum_{t'=0}^{t-1}\Big[\sum_{i'=1}^{\infty} G^{\mathcal{N}\mathcal{N}}_{i,j;i'}(t-t')\eta^{\mathcal{N}}_{i'}(t') + \sum_{j'=1}^{\infty} G^{\mathcal{N}\mathcal{E}}_{i,j;j'}(t-t')\eta^{\mathcal{E}}_{j'}(t')\Big]\end{aligned} \tag{5.22}$$

After some algebraic manipulations detailed in appendix A, we obtain

$$\begin{aligned}G^{\mathcal{E}\mathcal{E}}_{i,j;j'}(t-t') &= 4\int_{q=0}^{\pi}\int_{p=0}^{\pi}\frac{dq}{\pi}\frac{dp}{\pi}\frac{1}{2\pi\mathrm{i}}\oint_{\Gamma_0}\frac{dz}{z^{t-t'}}g_{i,j;j'}(\zeta(z);q,p) \qquad (5.23)\\ G^{\mathcal{E}\mathcal{N}}_{i,j;i'}(t-t') &= 4\int_{q=0}^{\pi}\int_{p=0}^{\pi}\frac{dq}{\pi}\frac{dp}{\pi}\frac{1}{2\pi\mathrm{i}}\oint_{\Gamma_0}\frac{dz}{z^{t-t'}}\frac{\zeta(z)^2 a_p^2}{c^2}g_{j,i;i'}(\zeta(z);q,p)\end{aligned}$$

with

$$\begin{aligned}g_{i,j;j'}(\zeta;q,p) &\equiv \frac{(\sin((j'+1)p) - a_p\sin(j'p))\sin(q)}{(\zeta^{-1}-\cos(q)^2)^{1/2}(\zeta^{-1}-\cos(p)^2)^{1/2}} \qquad (5.24)\\ &\times \frac{(\zeta a_q)^i(\zeta a_p)^{j-j'}\sin(iq)\sin(jp)}{1-c^{-4}\zeta^4(a_q)^2(a_p)^2},\end{aligned}$$

$\zeta(z) \equiv \frac{(1-\overline{\eta})z}{1-\overline{\eta}z}$, $a_q(\zeta) \equiv \cos(q) + \mathrm{i}(\zeta^{-1} - \cos^2(q))$, $c \equiv \sqrt{\frac{1-\overline{\eta}}{\overline{\eta}}}$, and Γ_0 runs counterclockwise around the origin. Of course symmetrical expressions hold for $G^{\mathcal{N}\mathcal{N}}_{i,j;i'}(t-t')$ and $G^{\mathcal{N}\mathcal{E}}_{i,j;j'}(t-t')$. Here we are interested in the asymptotic properties of the Green functions (5.23) when $t \to \infty$ with $i, j \sim t$ while keeping i',j' and t' finite. These properties will be determined by the behaviour of $z^{-t}g_{j,i;i'}(\zeta(z);q,p)$, so that we may study both Green functions together.

We expect the perturbation to propagate along the direction $(1,1)$. We therefore stay in the vicinity of the diagonal, letting $i = vt + u\sqrt{t}$ and $j = vt - u\sqrt{t}$. At fixed time t, the parameter v is to be understood as a (balistically) rescaled coordinate along the diagonal $i = j$, while u is a (diffusively) rescaled coordinate in the transverse direction. The path integral over z is evaluated using the residue theorem, and the integrations over q and p can then be performed by saddle-point techniques. More details can be found in appendix A. This finally gives, in the $t \to \infty$ limit

$$G^{\mathcal{E}\mathcal{E}}_{vt+u\sqrt{t},vt-u\sqrt{t};j'}(t-t') \sim \mathrm{e}^{t\mathcal{G}^s_+(v,u)} + \mathrm{e}^{t\mathcal{G}^s_-(v,u)}, \tag{5.25}$$

where some amplitudes that depend on $\overline{\eta}$, v, j' and t' and algebraic factors in t have been omitted.

The physical picture is the following. First of all there exists a critical velocity $v^* \equiv \frac{\sqrt{1-\overline{\eta}}}{2}$ such that for $v > v^*$ the $\mathcal{G}_\pm$ are both real and the Green

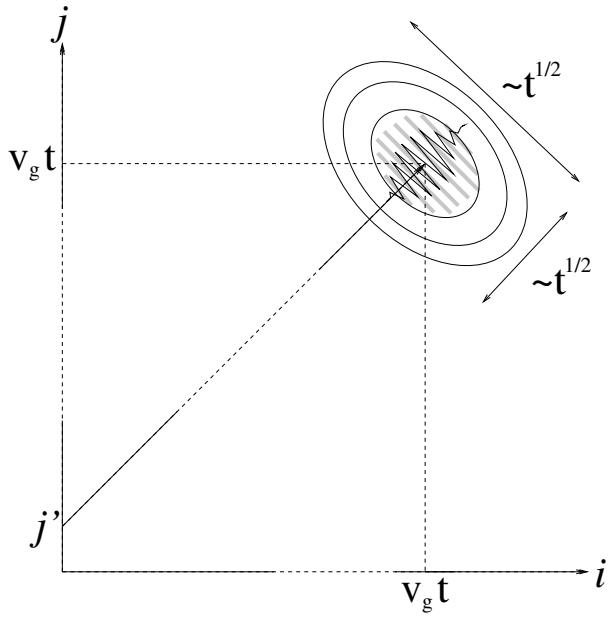

Figure 5.6: Schematic representation of the Green function $G^{\mathcal{E}\mathcal{E}}_{i,j;j'}(t)$ of the linearized equations (5.19). The Green function looks like a wavepacket centered on the point $i = j = v_g t$, located on the diagonal. The wavepacket is Gaussian, so that its widths both scale like $t^{1/2}$. At smaller spatial scales the Green function looks like a wave propagating along the diagonal direction. This is represented here by the wavefronts, that are perpendicular to the diagonal.

function simply decays exponentially without oscillating. This corresponds to a flow of particles invading a uniform background. Here we are more interested in the other case. For $v < v^*$ the two functions $\mathcal{G}_\pm$ are complex conjugate and combine, so that the Green function looks like a Gaussian wavepacket, which is illustrated in Fig. 5.6.

We can then write

$$G^{\mathcal{E}\mathcal{E}}_{vt+u\sqrt{t},vt-u\sqrt{t};j'}(t-t') \sim \mathrm{e}^{t\psi(v)}\mathrm{e}^{-\frac{(i+j)^2}{2t\sigma_\perp^2}}\cos(\omega(v,u)t - \mathbf{k}(v,u).\mathbf{r} - \phi(v,u)), \tag{5.26}$$

where $\sigma_\perp$ is the transversal width of the gaussian wavepacket and can be expressed as functions of $\overline{\eta}$ only. The function $\psi(v)$ represents the amplitude of the wavepacket along the diagonal and reads

$$\begin{aligned}\psi(v) &= \log 2 - \frac{1}{2}\log(1+c^2) - \frac{1}{2}(1-2v)\log(1-2v) \\ &\quad -\frac{1}{2}(1+2v)\log(1+2v) + 2v\log c.\end{aligned} \tag{5.27}$$

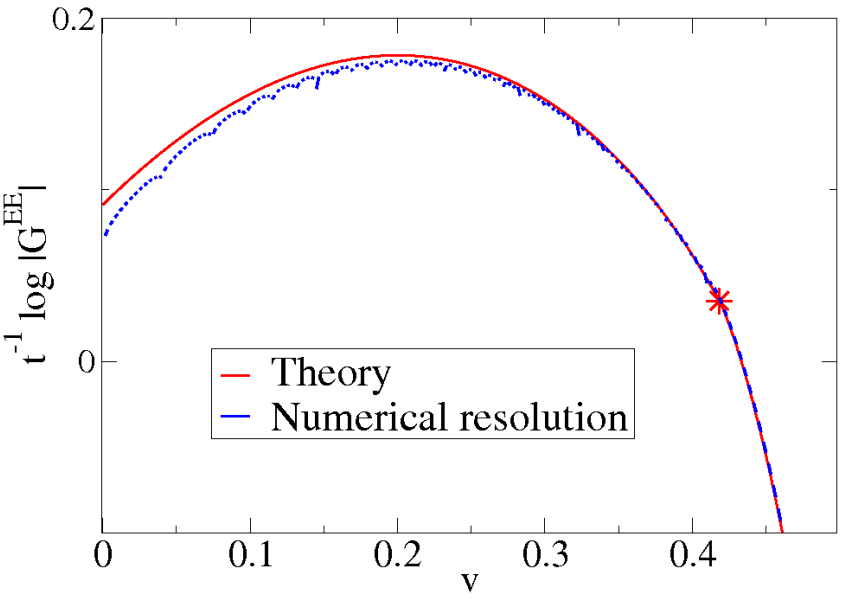

Figure 5.7: Amplitude of the wave packet measured numerically (blue) and the analytical prediction from Eq. (5.27) (red), in the $t \to \infty$ limit. The parameters are $t = 400$ and $\overline{\eta} = 0.3$, and a prefactor has been adjusted to make the agreement between the curves as good as possible. The slope is discontinuous for $v = \frac{\sqrt{1-\rho}}{2} \simeq 0.418$ here, which is emphasized by a red star.

It is plotted in Fig. 5.7.

The factors $\omega(v,u)$, $\mathbf{k}(v,u)$ and $\phi(v,u)$ depend of course on $\overline{\eta}$ but also on the spatial variables v and u, and are therefore to be interpreted as the local pulsation, wavevector and phase of the wave, respectively. We have

$$\mathbf{k}(v,u) = \arctan\left(\frac{\sqrt{c^2-(1+c^2)4v^2}}{2v}\right)(\mathbf{e}_x + \mathbf{e}_y), \tag{5.28}$$

i.e. the perturbation propagates in the $(1,1)$ direction, and $\phi(u,v) \sim u^2$ does not account for the chevron effect. There is therefore no chevron effect in the linearized mean-field equations. Numerical simulations of the linearized equations (5.19) and (5.20) confirm that there is no chevron effect in the linearized problem.

The full nonlinear equations (5.4) were however solved numerically. In this case the chevrons are indeed observed, as shown in Fig. 5.8. This supports again the close correspondence between equations and particle system and the generality of the chevron effect.

A comment is needed about the stability of equations (5.4). When solved numerically they develop an instability, which is more and more frequent with

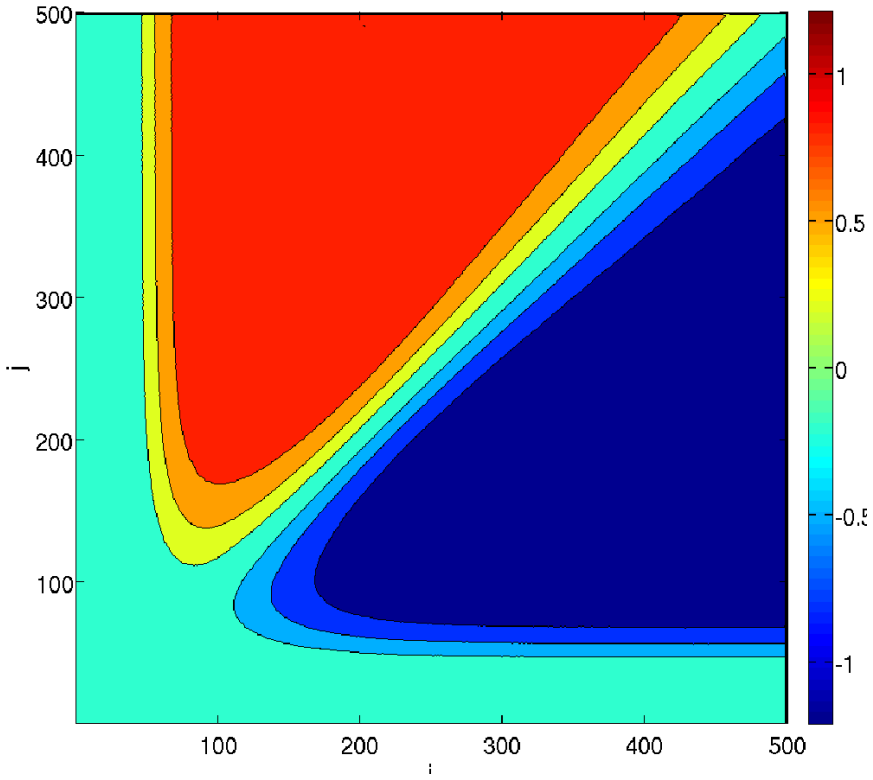

Figure 5.8: Level plot of the stationary chevron angle $\Delta\theta(\mathbf{r})$ in degrees in the system of nonlinear mean-field equations (5.4), obtained wit hthe velocity ratio method. The parameters are $M = 500$ and $\overline{\eta} = 0.06$.

increasing $\overline{\eta}$. The instability starts with one of the density fields becoming negative at a particular site. The instability then propagates and amplifies, the density fields attaining arbitrarily large values. This instability is suppressed if one adds higher order terms in the evolution equation, *e.g.* replaces $\rho^{\mathcal{N}}$ by $1 - \mathrm{e}^{-\rho^{\mathcal{N}}}$ in the first of Eqs. (5.4) and $\rho^{\mathcal{E}}$ by $1 - \mathrm{e}^{-\rho^{\mathcal{E}}}$ in the second one. The presence of these higher order terms ensures that both density fields stay positive at all times and does not alter the phenomena discussed here.

The main conclusion of this study is that the chevron effect is a nonlinear effect which seems hard to explain analytically with the mean-field equations. The fact that the chevron effect is observed with the mean-field equations as well as with the particle system supports again the mean-field equations as an approximate theory of the particle system but does not constitute an explanation. An exact and very intuitive microscopic calculation in terms of effective interactions will be the focus of section 6.3. For now we focus on how

to measure precisely the angle $\Delta\theta(\mathbf{r})$.

5.3 Open boundary conditions: measurements of $\Delta\theta$

5.3.1 Methodology

We now want to achieve quantitative measurements of $\Delta\theta(\mathbf{r})$, which will be done here by to different methods.

The first is the *crest algorithm*, which is most easily defined for the system of equations. Given the values of the density fields $\rho_t^{\mathcal{E},\mathcal{N}}(\mathbf{r})$ on each site $\mathbf{r}$, we will to construct a curve following the crests of the density field of the organized type of particle, $\mathcal{N}$ in the upper triangle and $\mathcal{E}$ in the lower one. To determine the average inclination angle of the stripes in the whole system we can apply the following algorithm.

Take a site (k,k) on the diagonal of the intersection and determine which of $\rho_t^{\mathcal{E}}(k,k)$ and $\rho_t^{\mathcal{N}}(k,k)$ is larger. In the following we will suppose that $\rho_t^{\mathcal{E}}(k,k) > \rho_t^{\mathcal{N}}(k,k)$, the inverse case being treated symmetrically. The $\mathcal{E}$ particle density being larger we construct the crest in the zone where the $\mathcal{E}$ fields are well organized, namely the lower triangle. Site (k,k) being the first site of the crest, the second one will be the one having the largest $\rho^{\mathcal{E}}$ value between $(k+1,k)$, $(k+1,k-1)$ and $(k,k-1)$. More generally, if the n^{th} site of the crest is (i,j) the $(n+1)^{th}$ will be chosen among $(i+1,j)$, $(i+1,j-1)$ and $(i,j-1)$ for having the largest $\rho^{\mathcal{E}}$ value. This procedure will go on until the crest reaches the (southern or eastern) boundary of the system. The angle of the alignments is then simply given by the angle of the vector linking both ends of the crest after averaging over all the crests of $\mathcal{E}$ particles. An example of this construction is shown in Fig. 5.9.

When trying to measure a global value of the angle it can also be useful to exclude the penetration layers that form in the system. The algorithm can indeed easily be adapted to give local values of the angle, by simply considering the ensemble average of the slope of the crest of the organized species of particles at a given point.

This method can also easily be generalized to the particle system, in which the density fields only take the values 0 and 1, by applying some diffusion steps to the density fields. In practice 3 diffusion steps were applied where each site distributes 0.1 of its mass to its four neighbours.

The second method, called the *velocity ratio method*, is based on a simple hypothesis. If the stripes are supposed to be impenetrable then there is a clear link between the angle of the stripes and the individual velocities. Let $v^{\mathcal{E},\mathcal{N}}(\mathbf{r})$ be the average velocities of eastward and northward particles in the stationary state. The angle of the chevrons is constrained on each site by the ratio of the velocities,

$$\tan(\theta(\mathbf{r})) = \frac{v^{\mathcal{N}}(\mathbf{r})}{v^{\mathcal{E}}(\mathbf{r})}. \tag{5.29}$$

In the particle model the velocities can easily be measured, as they can straight-

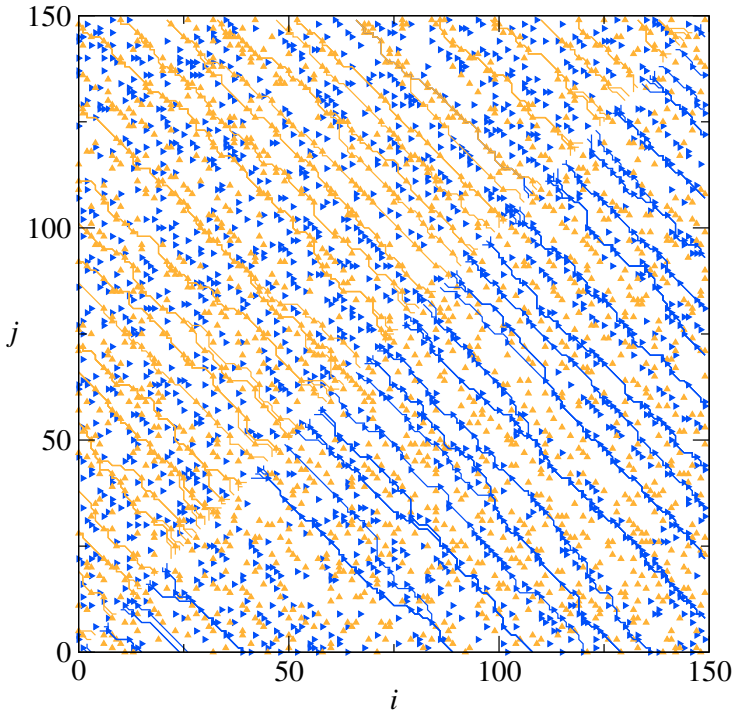

Figure 5.9: Snapshot of the intersection square for a particle system with $\alpha = 0.09$ and $M = 150$, obtained with frozen shuffle update. Superimposed are the crests constructed by means of the crest algorithm described in the main text.

forwardly be expressed in terms of the microscopic variables,

$$v^{\mathcal{E},\mathcal{N}}(\mathbf{r}) \equiv \frac{\langle n^{\mathcal{E},\mathcal{N}}(\mathbf{r})(1 - n^{\mathcal{E}}(\mathbf{r} - \mathbf{e}_{x,y}) - n^{\mathcal{N}}(\mathbf{r} - \mathbf{e}_{x,y}))\rangle_{\text{stat}}}{\langle n^{\mathcal{E},\mathcal{N}}(\mathbf{r})\rangle_{\text{stat}}}, \tag{5.30}$$

where $\langle . \rangle$ denotes an average over the histories of the entrance sites and the subscript stat reminds that it is taken in the stationary state. Note that with OBC, and contrarily to the PBC one, the system is ergodic, which enables us to measure time averages instead of ensemble averages in Eq. (5.30). The equations. (5.4) may be interpreted as local conservation equations. Writing each conserved current as a product between the density and the particle velocity, we get for the average velocities

$$v^{\mathcal{E},\mathcal{N}}(\mathbf{r}) \equiv \langle 1 - \rho^{\mathcal{N},\mathcal{E}}(\mathbf{r})\rangle_{\text{stat}}. \tag{5.31}$$

Both methods have advantages and drawbacks. The crest construction is a static construction based on short-range interactions, which aims at isolating the main features seen with the eye. It however has the disadvantages of being

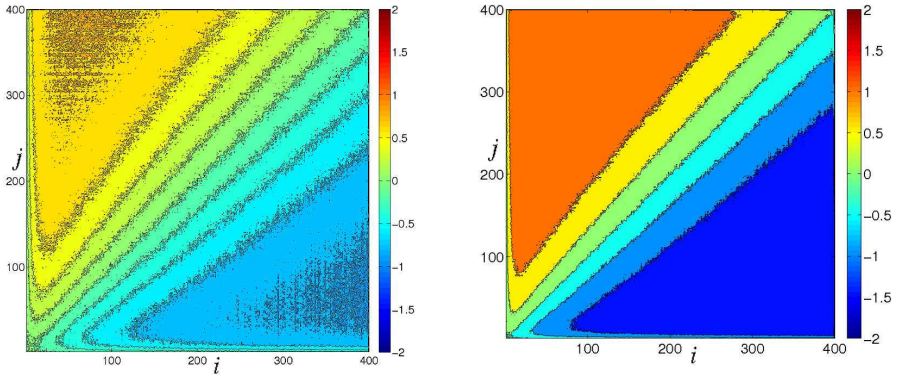

(a) $\alpha = 0.03$ (b) $\alpha = 0.05$

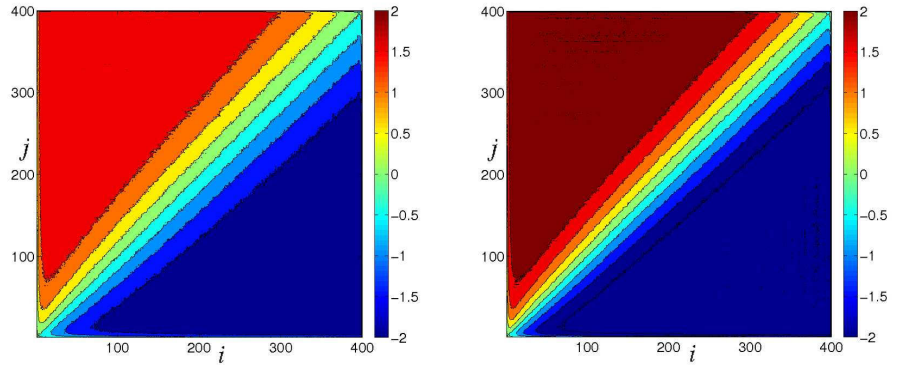

(c) $\alpha = 0.07$ (d) $\alpha = 0.09$

Figure 5.10: Measurements of $\Delta\theta(\mathbf{r})$ for the particle model with $M = 400$ and alternating parallel update, for different values of the entrance parameter $\alpha = 0.03, 0.05, 0.07$ and 0.09.There is a plateau value $\pm\Delta\theta_0$ that increases with α, whereas the size of the boundary layers tends to diminish.

largely arbitrary. Indeed, we could choose to make steps of more than 1 site when constructing a crest, to consider also the 'disorganized' density field and so on. On the other hand, it seems quite plausible that the impenetrability hypothesis at the root of the velocity ratio method is true, but it should nevertheless be checked. Apart from that the velocity ratio method seems solid, as it provides a purely local completely unambiguous way of measuring the angle directly from the microscopic variables.

On the basis of these arguments we choose to use Eq. (5.29) as a definition for the inclination angle, keeping in mind that the measured values should be interpreted as an angle only outside of the boundary layers of width $\xi(\alpha)$.

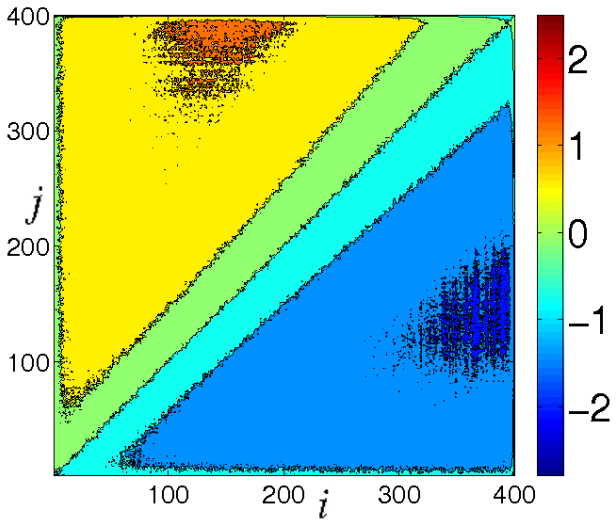

Figure 5.11: Level plot of the space dependent chevron angle $\Delta\theta(\mathbf{r})$ (in degrees) in the stationary state for frozen shuffle update obtained by the velocity ratio method on an open square lattice of size $M = 400$ with $\alpha = 0.09$.

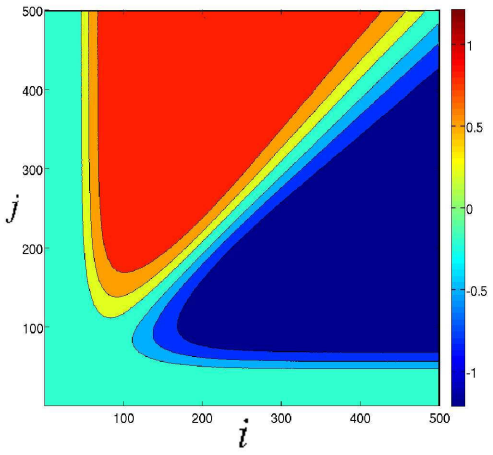

Figure 5.12: Level plot of the space dependent chevron angle $\Delta\theta(\mathbf{r})$ (in degrees) in the stationary state, obtained from the mean field equations (5.4) by the velocity ratio method on a square lattice of size $M = 500$ with open boundary conditions and with $\overline{\eta} = 0.06$.

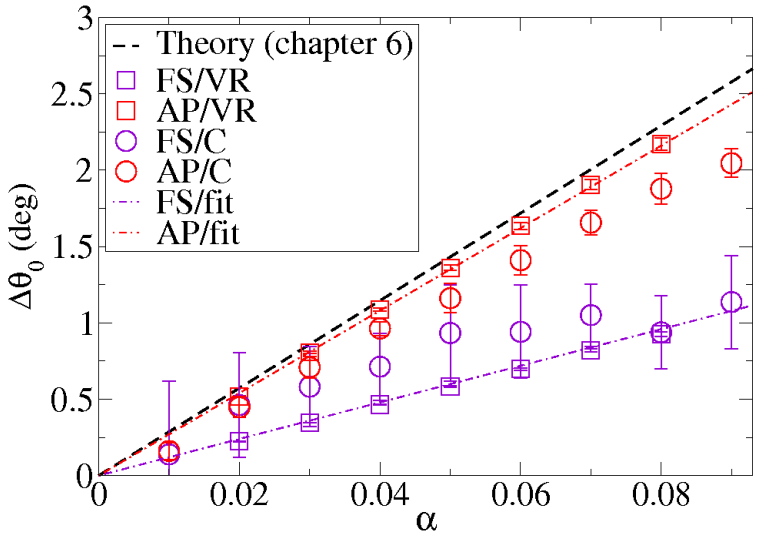

Figure 5.13: Chevron angle $\Delta\theta_0$ as a function of α for open boundary conditions, obtained for the frozen shuffle (FS) and alternating parallel (AP) updates and by the two measurement methods described in subsection 5.3.1, the velocity ratio (VR) and the crests (C) method. The system size is $M = 640$. The purple and red dashed-dotted lines represent the linear fits $\Delta\theta_0 \simeq c\alpha$ of the measurements obtained with the velocity ratio method, and with $c = 12°$ for frozen shuffle and $27°$ for alternating parallel update. The solid black line is the theoretical prediction from section 6.3.

5.3.2 Measurements

The angle $\Delta\theta(\mathbf{r})$ has been measured for various parameters and models, some of these measurements being presented in Figs. 5.10, 5.11 and 5.12. On these figures we see that $\Delta\theta(\mathbf{r})$ seems to reach a constant value $\pm\Delta\theta_0$ when far enough from the boundaries in the upper (lower) triangle, respectively. We call $\Delta\theta_0$ the *plateau angle*, which may *a priori* depend on the entrance probability per time step α. Measurements of $\Delta\theta_0(\alpha)$ are shown in Fig. 5.13. Numerically we found that in the particle system $\Delta\theta_0 \simeq c\alpha$ with $c = 12°$ for frozen shuffle update and $c = 27°$ for alternating parallel update and for the mean-field equations $\Delta\theta_0 \simeq c'\overline{\eta}$ with $c' = 21°$.

A natural related question is whether this stationary state can be maintained in the $M \to \infty$ limit. Particle simulations were performed up to system sizes $M = 2900$. Fig. 5.14 shows the measured chevron angle for sites of the straight line $\frac{i}{j} = \tan(3\pi/8)$, right in the middle of the lower triangular region, for $M = 2200$. These measurements seem to support the claim that $\Delta\theta_0$ can indeed be obtained as the $|\mathbf{r}| \to \infty$ limit of $\Delta\theta(\mathbf{r})$, however in the truly infinite system only analytic arguments hold and exploring this limit is still an open question.

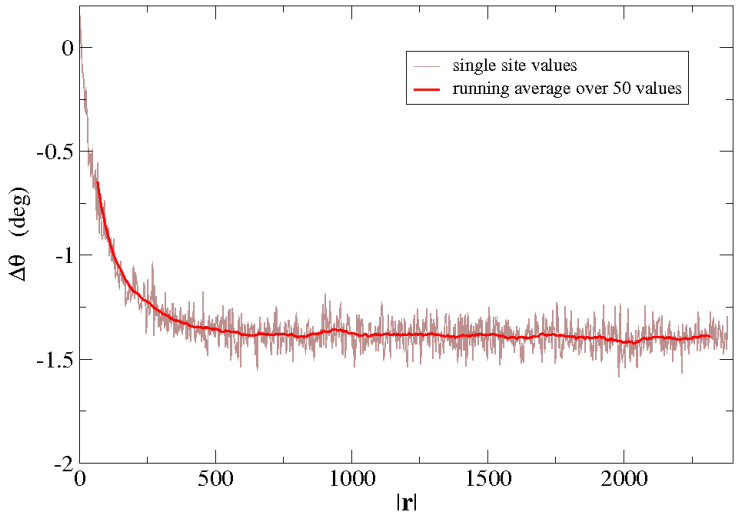

Figure 5.14: Chevron angle $\Delta\theta(\mathbf{r})$ determined by the velocity ratio method as a function of $|\mathbf{r}| = (i^2 + j^2)^{1/2}$ along the the line $j/i = \tan(3\pi/8)$, taken on one site j in each column i, for $M = 2200$ and $\alpha = 0.05$, in a particle system with open boundary conditions subject to alternating parallel update. The light (brown) curve is the average over 2×10^6 time steps after 5000 time steps have been discarded. The dark (red) curve is a running average over 50 points.

The mean-field equations helped us show that the chevron effect is non-linear. They however give no insight on this secondary instability. In the following chapter 6 we will identify a propagation mode compatible with the chevron effect and show that it gives satisfying angle values.

Chapter 6

Effective interactions

In the previous chapter 5 we observed the same pattern formation in the intersection model and in the system of nonlinear mean-field equations (5.4). In periodic boundary conditions diagonal stripes were observed, that were readily accounted for by a linear stability analysis of the equations. In open boundary conditions the striped pattern is still here but the angle of the stripes varies in space, giving rise to the chevron effect. This effect not being found in the linearized equations, and the nonlinear equations being too complicated to be solved, our task is now to find an other way to understand the chevron effect.

We shall first consider only two $\mathcal{E}$ particles, possibly on different rows, placed in a flow of $\mathcal{N}$ particles. We calculate exactly the effective interaction between the $\mathcal{E}$ particles, that is mediated by the flow of $\mathcal{N}$ particles. Apart from being useful for the understanding of the chevron effect, this calculation can also be seen as a contribution to the field of medium mediated effective interactions between colloids or tracers. Indeed, to our knowledge, we provide here the first exact calculation of such an effective interaction in the out-of-equilibrium case.

In a second stage, for the special case of the alternating parallel update we shall show how a stable global mode can be derived for the two-particle construction. This mode presents the characteristics of the chevron effect, and gives a theoretical prediction for the chevron angle.

In section 6.1 we review the literature on effective interactions most relevant to this work. In section 6.2 we define what we will call the 'wake' of a single $\mathcal{E}$ particle in a sea of $\mathcal{N}$ particles, first on a microscopic scale. The wake then gets averaged over the realizations to obtain a fluid mechanics-like density profile. After that we finally show that the other $\mathcal{E}$ particles are attracted by this wake and that this mechanism fixes the chevron angle in section 6.3. In the last section 6.4 a macroscopic mode is deduced from the two-particle interaction in the case of alternating parallel update. These results have been published in Ref. [148].

6.1 Related literature

Medium-mediated interactions are ubiquitous and have been extensively studied in soft matter systems [149]. In seminal works by Asakura and Oosawa [150, 151] it was shown that there is an effective attractive interaction between two macroscopic spheres in a solution, with a direct application to colloids. These depletion interactions are well understood at equilibrium [149], *e.g.* when the surrounding fluid and both spheres are immobile, the effective interaction acting on both spheres as a supplementary force.

In the typical out-of-equilibrium case, either an external force is applied on the colloids or the colloids are held fixed and the fluid is in motion. This case has only be studied quite recently. In Ref. [152] Dzubiella *et al.* compute an effective out-of-equilibrium depletion interaction using the assumption that the perturbations of the density field of the solvent created by the two particles factorize. One of their figures is reproduced in Fig. 6.1 as an illustration. A more general computation was performed by Khair *et al* [153] under the assumption that the interactions between particles of the bath can be neglected. Out-of-equilibrium medium-mediated interactions have also been measured experimentally [154] in the case of a constant force driving of particles confined on a ring.

Lattice gases provide a class of models for fluids, these models having the advantages of being rather simple, easy to simulate and of showing a large variety of phenomena [45]. The behaviour of a tracer particle in these kind of models having been studied in the unbiased [155, 156] as well as in the biased case [157, 158, 159, 160, 161, 162, 163, 164], it seems natural to try to identify some effective interaction effects in these discrete models. Cooperative effects were indeed exhibited in some cases [165, 166]. In a model that will prove the closest to ours, Mejía-Monasterio and Oshanin numerically studied the interaction between two biased particles, the other particles of the medium simply undergoing diffusion [167], see Fig. 6.2. In their paper the focus is on the time average of the correlation function between the positions of the particles. The authors show numerically that there is an attractive force between particles, which is especially pronounced when one particle is in the wake of the other.

In the rest of this section another example of effective interactions relevant for the understanding of the intersection model will be studied. In our case we shall be able to show the localization of one particle in the wake of the other by an exact analytic calculation. We start by examining the wake of a single $\mathcal{E}$ particle in an environment of $\mathcal{N}$ particles.

6.2 Wake of a single particle

6.2.1 Setting up the stage

We start by clearly defining the system and deriving some simple results. We consider an infinite square lattice with a single $\mathcal{E}$ particle called $\mathcal{E}_0$ on it. The other sites may or may not be occupied by $\mathcal{N}$ particles with average probability

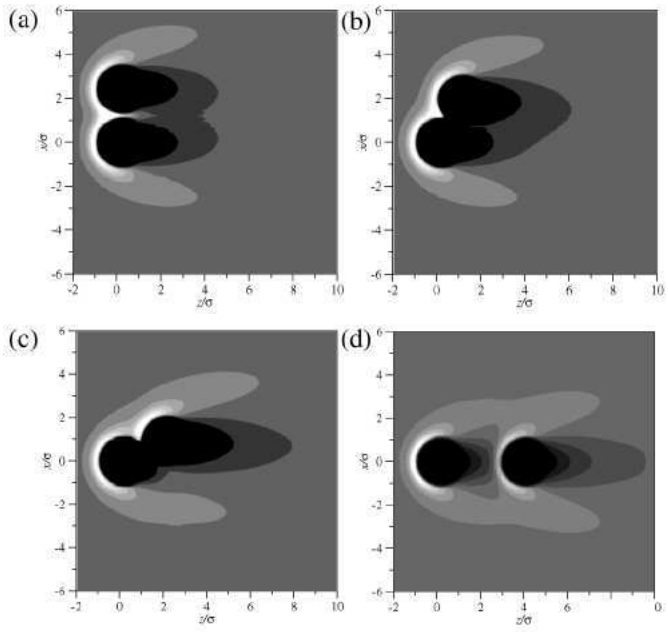

Figure 6.1: Density field of the driven surrounding fluid around two stationary colloidal particles obtained by Dzubiella *et al.* [152].

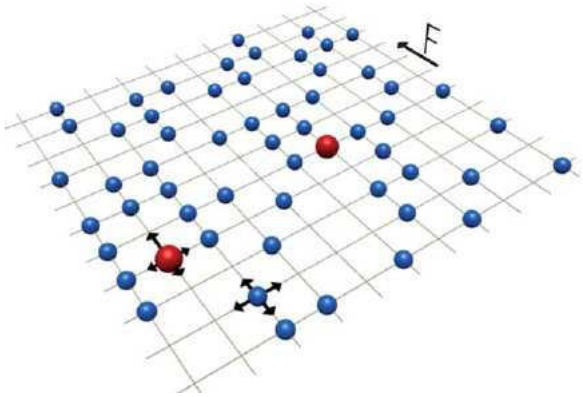

Figure 6.2: Scheme of the model from Ref. [167]. Blue particles of the bath hop symmetrically on a square lattice. The two red particles are subject to an external field and therefore undergo biased motion.

$\overline{\rho}^{\mathcal{N}}$, the correlations between occupations in a column being determined by a fictitious entrance site infinitely far from what we consider, thus depending on the update scheme. We want to study the dynamics of $\mathcal{E}_0$ while averaging over all the irrelevant information. It is also clear that if there were no $\mathcal{E}$ particle the $\mathcal{N}$ particles would all be in free flow phase.

The update schemes considered will still be frozen shuffle update and alternating parallel update, for which the calculations will be done explicitly. Most results will however be stated in the most general possible form to stress the fact that they could be applied to a wider class of updates, thus demonstrating the generality of the exhibited effects. Whereas frozen shuffle update can be seen as a typical member of this wider class of updates, alternating parallel update represents in some sense the limiting case where no fluctuations are present. More precisely we will see that, for two particles on an infinite lattice, alternating parallel update can be seen as a formal limit of frozen shuffle update. For both updates of interest $\mathcal{E}_0$ will then be taken to have a phase equal to 0 for simplicity, whereas the phases of the $\mathcal{N}$ particles in a column are correlated because of the entrance procedure.

6.2.2 Wake for a given realization

In analogy to everyday fluid dynamics $\mathcal{E}_0$ is expected to block some of the $\mathcal{N}$ particles it will encounter, thus creating a *wake* consisting of an empty zone 'behind' the $\mathcal{E}$ particle and of two denser zones on the sides. The empty zone will be called the *shadow*. Here we show that it is possible to construct the ensemble of sites that form the shadow, and that the past motion of $\mathcal{E}_0$ is the only knowledge needed to perform this construction.

For doing so we use the following algorithm.

1. Just before $\mathcal{E}_0$ attempts to hop put a white dot on the site it occupies.

2. After the attempt is performed, successful or not, put a black dot on the site occupied by $\mathcal{E}_0$. The black dot replaces the white dot if $\mathcal{E}_0$ did not move.

3. During the next time step let all the $\mathcal{N}$ particles hop and let all the dots move one site upwards simultaneously. Start again at step 1.

The set of dotted sites constitutes the *shadow*, while the distinction between black and white dots will only become useful later in subsection 6.3.1. The shadow represents the ensemble of sites that will stay empty at all time steps because of the presence of $\mathcal{E}_0$.

An example of construction of the shadow is shown in Fig. 6.3. From this example it can be seen that the shadow can be decomposed into the two different types of row elements shown in Fig. 6.4. In the first case there is a white dotted site with a black dotted site to its right on the row, called row of type D (for 'diagonal'). The second case corresponds to $\mathcal{E}_0$ being blocked at some time in the past, so that there will be only a black dot. It can then be readily

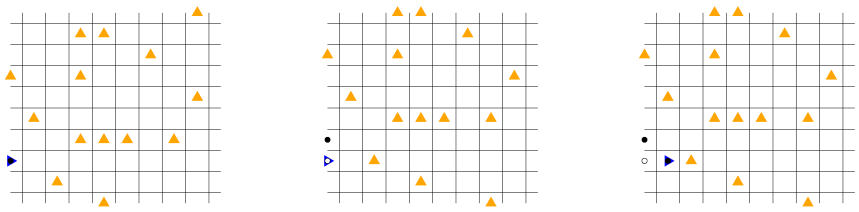

(a) $t = 0^+$ (b) $t = 1^-$ (c) $t = 1^+$

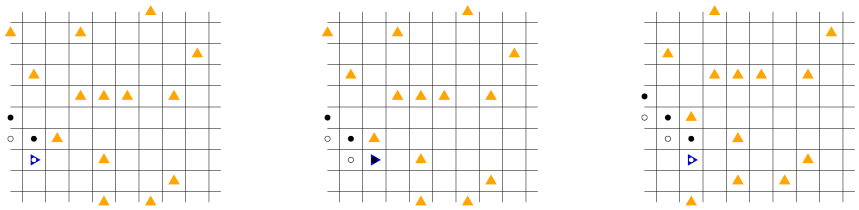

(d) $t = 2^-$ (e) $t = 2^+$ (f) $t = 3^-$

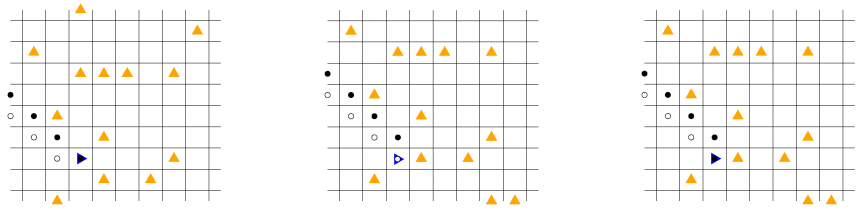

(g) $t = 3^+$ (h) $t = 4^-$ (i) $t = 4^+$

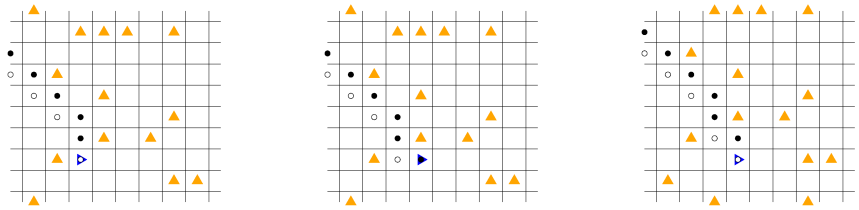

(j) $t = 5^-$ (k) $t = 5^+$ (l) $t = 6^-$

Figure 6.3: First steps of the construction of the shadow of a single $\mathcal{E}$ particle, according to the algorithm of subsection 6.2.2.

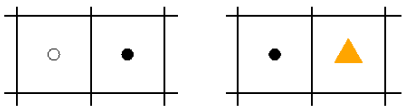

Figure 6.4: Possible types of rows. Type D corresponds to having two dots (a white and a black) in the same row while type K contains only one black dot associated with an $\mathcal{N}$ particle on its right.

seen from the dynamics that the site to the right of the black dot must be occupied by a $\mathcal{N}$ particle, giving a row of type K (for 'kink'), possibly indexed by the value of the phase of the blocking particle in the case of the frozen shuffle update.

Mathematically we encode the dynamics of $\mathcal{E}_0$ by the time it spends on each column. If $\mathcal{E}_0$ has just hopped towards column 0 we associate to each already visited column $p = -1, -2, -3, \ldots$ a number $n_p = 1, 2, 3, \ldots$ corresponding to the number of time steps $\mathcal{E}_0$ spent on the column, the particular moment of time we chose corresponding to $n_0 = 0$. From there we see that the shape of the shadow can be deduced from the values of the sequence $\{n_p\}_{p<0}$, a value n_p on the p^{th} column corresponding to $n_p - 1$ rows of type K followed by a row of type D. Note that in the case of frozen shuffle update the values of the phases of the blocking particles can however not be recovered that way, however their statistical distribution is still known by the fact that we have no *a priori* information about the state of their column.

Having this construction in mind we first perform an ensemble average of the wake. This calculation is independent of the reminder of the chapter and will enable us to study the statistical properties of the system and to test the predictions numerically. It could also be used to compute the effective interactions between two $\mathcal{E}$ particles using a mean-field approximation as in Ref. [152].

6.2.3 Ensemble averaged wake

In this subsection we show how the ensemble averaged density profile of $\mathcal{N}$ particles perturbed by the presence of $\mathcal{E}_0$ can be computed and we apply it to frozen shuffle update. For simplicity, when computing the density profiles we restrict ourselves to the low density case, in which a lot of correlations can be factorized. In principle the calculation can be performed for any density.

We have seen that the shadow could be constructed only from the knowledge of the $\{n_p\}_{p<0}$. In fact it is also true for the statistical properties of the dense zones flanking the shadow. In front of it the surplus of particles is naturally described by the K rows of the shadow. At the back of the shadow one will find the $\mathcal{N}$ particles that have been blocked by $\mathcal{E}_0$, whose statistical properties

clearly stem from the occupation times of $\mathcal{E}_0$ on each column.

It remains to compute the statistics of the occupation times. If there were no $\mathcal{E}$ particle the columns would be uncorrelated. If $\mathcal{E}_0$ is on column 0 its motion is determined solely by the occupation of column 1. Column 1 has however not yet been occupied by $\mathcal{E}_0$, is therefore not correlated with the history of $\mathcal{E}_0$ yet, and the probability of having a certain history factorizes. The system is homogeneous, so that the probability of getting a certain n_p does not depend on p. We define the probability of staying n time steps on a column and denote it by r_n. It is also convenient to introduce the superscripts 'fs' and 'ap' that refer to frozen shuffle and alternating parallel updates.

With alternating parallel update the dynamics does not allow two particles to follow each other without having an empty site between them so that when $\mathcal{E}_0$ arrives in a column it is never blocked more than once and $r_n^{\mathrm{ap}} = 0$ for all $n > 2$. The probability to find a $\mathcal{N}$ particle on the target site of $\mathcal{E}_0$ is then simply the density $\overline{\rho}^{\mathcal{N}}$, so that the probabilities of the occupation times finally read

$$r_n^{\mathrm{ap}} = \begin{cases} 1 - \overline{\rho}^{\mathcal{N},\mathrm{ap}} & n = 1 \\ \overline{\rho}^{\mathcal{N},\mathrm{ap}} & n = 2 \\ 0 & n > 2 \end{cases}, \tag{6.1}$$

for all densities. Note that we keep track of the fact that the expression of the density in terms of the entrance parameter α depends on the update. The case of the frozen shuffle update is a little more complicated and is done in appendix B. Taking carefully the phases of the particles into account leads to

$$r_n^{\mathrm{fs}} = \begin{cases} 1 - \overline{\rho}^{\mathcal{N},\mathrm{fs}} & n = 1 \\ \frac{\overline{\rho}^{\mathcal{N},\mathrm{fs}}}{a} \mathrm{e}^{-a} \displaystyle\sum_{l=n-1}^{\infty} \frac{a^l}{l!} & n = 2, 3, \dots \end{cases}, \tag{6.2}$$

where we still have $\overline{\rho}^{\mathcal{N},\mathrm{fs}} = \frac{a}{1+a}$ and again for all densities.

We now want compute the density field everywhere in the system for a given realization of the n_p. In other words we first average over all the irrelevant information, *i.e.* the $\mathcal{N}$ particles that are not correlated with $\mathcal{E}_0$, and after that we will also average over the $\{n_p\}_{p<0}$ with the weights r_n. For convenience we will compute the density field when $\mathcal{E}_0$ just hopped towards site $(0, 0)$ of the lattice. Obviously the columns $p > 0$ are uncorrelated with $\mathcal{E}_0$ and their density is $\overline{\rho}^{\mathcal{N}}$ everywhere, but the $p \leq 0$ case is more complicated.

We notice that after $\mathcal{E}_0$ leaves a column the density profile in it simply evolves independently of the subsequent motion of $\mathcal{E}_0$ or of the evolution of the other columns; the particle $\mathcal{E}_0$ is the only element that correlates the columns with each other, and this correlation occurs in a very specific way. Indeed, the averaged density profile on a column is determined solely by (i) the number of time steps $\mathcal{E}_0$ has been blocked before arriving in this column and (ii) the number of time steps $\mathcal{E}_0$ stays in the column. The first element indicates how many particles were necessarily present in the column because we know they have blocked $\mathcal{E}_0$ whereas the second one gives us the statistics of the length of the queue of $\mathcal{N}$ particles blocked by $\mathcal{E}_0$. In more precise terms we can label the

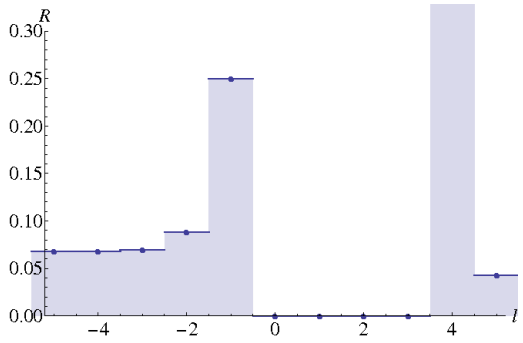

Figure 6.5: Function $R_l^{23}(0)$ for an incoming $\mathcal{N}$ particle density $\overline{\rho}^{\mathcal{N}} = 0.067$. For $l = 5$, the density is smaller than $\overline{\rho}^{\mathcal{N}}$, whereas for $l \geq 6$ it has not been perturbed by $\mathcal{E}_0$. Site 4 is occupied, *i.e.* $R_4^{23}(0) = 1$, because $\mathcal{E}_0$ was blocked once before entering the column. There is an empty region of size $3 + 1 = 4$ for $0 \leq l < 4$ corresponding to $\mathcal{N}$ particles being blocked by $\mathcal{E}_0$. The blocked $\mathcal{N}$ particles then accumulate in the region $l < 0$, where the density gets larger than $\overline{\rho}^{\mathcal{N}}$. The density quickly decreases to its asymptotic value $\overline{\rho}^{\mathcal{N}}$ as l goes towards negative values.

sites of a given column $p < 0$ by their vertical coordinate l and define a function $R_l^{n_{p-1}n_p}(s)$ representing the density profile on this column s time steps after $\mathcal{E}_0$ left it. It should be stressed again that this quantity does not depend explicitly on p but rather on n_{p-1} and n_p.

We first determine $R_l^{n_{p-1}n_p}(0)$. Particle $\mathcal{E}_0$ was blocked $n_{p-1} - 1$ time steps before entering column p due to the presence of $\mathcal{N}$ particles on column p so that when $\mathcal{E}_0$ finally hops towards column p, sites $l = 1$ to $n_{p-1} - 1$ will necessarily be occupied. When $\mathcal{E}_0$ leaves column p these particles will occupy sites $n_p + 1$ to $n_p + n_{p-1} - 1$, leaving a gap between 1 and n_p. Site $n_p + n_{p-1}$ is correlated with these latter, so that the density will get smaller than $\overline{\rho}^{\mathcal{N}}$ there. The particle $\mathcal{E}_0$ has spent n_p time steps on column p and may have blocked $\mathcal{N}$ particles of this column. As a result a queue may have been created on sites $l < 0$, and for low densities the probability to have a queue of length m if $\mathcal{E}_0$ stayed n time steps on a column is a approximately a Poisson distribution of average $\overline{\rho}^{\mathcal{N}} n$. To summarize we have for $p < 0$

$$R_l^{n_{p-1}n_p}(0) \begin{cases} = \overline{\rho}^{\mathcal{N}} & \text{for } l \geq n_{p-1} + n_p + 1 \\ \leq \overline{\rho}^{\mathcal{N}} & \text{for } l = n_{p-1} + n_p \\ = 1 & \text{for } n_p < l < n_{p-1} + n_p \\ = 0 & \text{for } 0 \leq l \leq n_p \\ \geq \overline{\rho}^{\mathcal{N}} & \text{for } -\infty \leq l < 0 \end{cases} \tag{6.3}$$

As we have taken the convention $n_0 = 0$ we also notice that this definition can be generalized to $n_p = 0$. For $n_p = 0$ of course the queue is not formed yet and we have $R_{l<0}^{n_{p-1}n_p}(0) = \overline{\rho}^{\mathcal{N}}$ An example of such function is shown in Fig. 6.5.

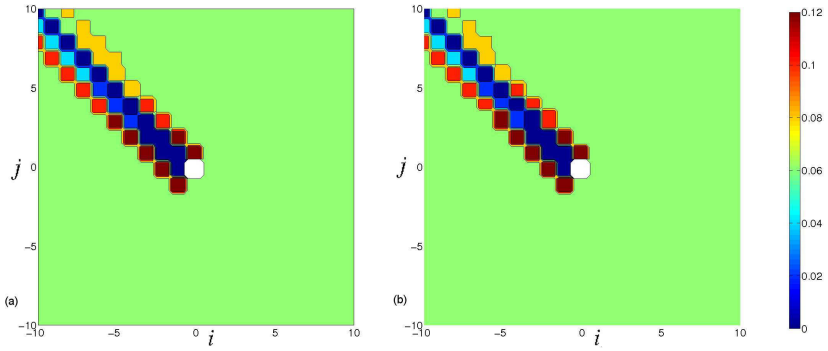

Figure 6.6: Level plot of the density perturbation (wake) created by a single $\mathcal{E}$ particle that just arrived on the $(0,0)$ site (white spot) for $\overline{\rho}^{\mathcal{N}} = 0.068$ using frozen shuffle update. (a) Theoretical wake as calculated in Eq. (6.4). (b) Numerical measurement of the density field immediately after each update of the $\mathcal{E}$ particle, averaged over 5.10^6 time steps.

For $s > 0$ relaxation occurs: the particles that have been blocked by $\mathcal{E}_0$ and compacted may have to wait until there is a hole in front of them in order to move again. The queue of particles, in which initially all the sites are occupied, will however reach a stationary state in which its density reaches the jammed density $\frac{2}{3}$ (see subsection 2.2 for a reminder). Note that there is no relaxation of the n_{p-1} blocking particles, as the fact that they blocked $\mathcal{E}_0$ all in a row proves that they are correctly organized.

The average over the $\{n_p\}_{p<0}$ should now be performed. When $\mathcal{E}_0$ arrives on column 0, column p has been left $\sigma_p \equiv \sum_{k=p+1}^{0} n_k$ time steps ago. Denoting the density on site (i,j) by $\rho^{\mathcal{N}}(i,j)$, taking the average is now straightforward

$$\rho^{\mathcal{N}}(i,j) = \begin{cases} \displaystyle\sum_{n_{i-1}=1}^{\infty} \sum_{n_i=1}^{\infty} \cdots \sum_{n_{-1}=1}^{\infty} r_{n_{i-1}} r_{n_i} \cdots r_{n_{-1}} R_j^{n_{i-1} n_i}(\sigma_i) & i \leq 0 \\ \overline{\rho}^{\mathcal{N}} & i > 0 \end{cases} \tag{6.4}$$

A comparison between the numerically measured shape of the wake and a numerical computation of the expression 6.4 for low density shows that the agreement is very good, as can be seen from Fig. 6.6 in the case of frozen shuffle update.

In a mean-field approximation [152], we could measure the localization of a second $\mathcal{E}$ particle placed in this averaged wake. The second $\mathcal{E}$ particle does however not see the average wake but a given realization of it. We will therefore describe the system at the level of the single realization in order to study the action of the wake of $\mathcal{E}_0$ on another $\mathcal{E}$ particle.

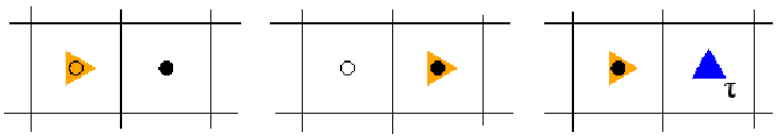

Figure 6.7: Possible states of an $\mathcal{E}$ particle in the shadow of $\mathcal{E}_0$. If the row is of type D the $\mathcal{E}$ particle can be either on a white dot (state D_W) or on a black dot adjacent to a white one (D_B). If the row is of type K the $\mathcal{E}$ particle can only be on the black dot. In the case of the frozen shuffle update there is an extra parameter, the phase τ of the $\mathcal{N}$ particle, hence a continuum of states $K_{\tau\in[0;1)}$.

6.3 Effective interactions

6.3.1 Rate equations and stabilization

We define a particle to be *in the shadow* of $\mathcal{E}_0$ if it occupies one of the dotted sites of subsection 6.2.2 and we consider a second $\mathcal{E}$ particle called $\mathcal{E}_0'$ which is in the shadow of $\mathcal{E}_0$ at initial time and has a phase τ_0 if it is relevant. We want to compute how long $\mathcal{E}_0'$ will stay in the shadow.

We will simply list the possible states of $\mathcal{E}_0'$ and write rate equations for them. From the decomposition of the shadow into the rows of Fig. 6.4 we see that there are three possibilities for the state of $\mathcal{E}_0'$, see Fig. 6.7. Particle $\mathcal{E}_0'$ can be either on the white dotted site of a D row (state D_W), on the black dotted site of a D row (state D_B) or on the black dotted site of a K row (state K_τ, a continuum of states indexed by $\tau \in [0;1)$ in the case of frozen shuffle update or a single state in the case of alternating parallel update).

Determining the dynamics of $\mathcal{E}_0'$ requires the preliminary knowledge of the probability associated to a given shape of the shadow, which is directly deduced from the spatial correlations of the $\mathcal{N}$ particles. From the injection properties of the $\mathcal{N}$ particles we know the correlations between successive sites of a fixed column. From the Markovian character of the injection procedure we can write them in terms of transfer probabilities, that we generically denote by the letter $\mathcal{Q}$. For example for frozen shuffle update we have to define the probabilities $\mathcal{Q}_{\emptyset,\emptyset}$, $\mathcal{Q}_{\tau,\emptyset}$, $\mathcal{Q}_{\emptyset,\tau'}$, $\mathcal{Q}_{\tau,\tau'}$ to find an empty site directly under an empty site, a $\mathcal{N}$ particle with phase τ directly under an empty site, an empty site directly under a $\mathcal{N}$ particle with phase τ' and a particle with phase τ directly under a particle with phase τ', respectively. For alternating parallel update phases do not exist and $\mathcal{Q}$ is a simple 2×2 matrix with entries 'empty site' or 'occupied site' only.

This formulation of the rate equations for the state of $\mathcal{E}_0'$ is exposed in Ref. [148], however it is more complicated and will not be developed here. We simply write the equations for low density frozen shuffle update and alternating parallel update. At lowest order in density a particle is always followed by an empty site and an empty site is followed by a particle with probability $\overline{\rho}^{\mathcal{N}}$.

The first particle $\mathcal{E}_0$ therefore does not encounter more than one $\mathcal{N}$ particle on each column, and the correlations between the phases do not have to be considered. From there we want to calculate the transition rates between the different states of $\mathcal{E}'_0$ that are defined in Fig. 6.7.

• **Frozen shuffle update:**

For frozen shuffle update we define $P_W(t)$ the probability to be in state D_W, the probability $P_B(t)$ to be in state D_B and the probability density $p_\tau(t)$ to be in state K_τ . For low density the continuous family $p_\tau(t)$ can be divided into two probabilities only, defined as

$$P_{<\tau_0}(t) \equiv \int_{\tau=0}^{\tau_0} p_\tau(t)\mathrm{d}\tau, \tag{6.5}$$

and

$$P_{>\tau_0}(t) \equiv \int_{\tau=\tau_0}^{1} p_\tau(t)\mathrm{d}\tau. \tag{6.6}$$

These quantities represent the probability that $\mathcal{E}'_0$ is in state K_τ with τ inferior or superior to τ_0, respectively.

Suppose $\mathcal{E}'_0$ is in the state D_W, *i.e.* occupying a white dotted site. The probability that the row directly under the particle is a D row is $(1-\overline{\rho}^{\mathcal{N},\mathrm{fs}})$. In that case the particle will stay in state D_W at the next time step. The particle can arrive in state $K_{\tau>\tau_0}$ if the row under it is a K row with $\tau > \tau_0$ (probability $\tau_0\overline{\rho}^{\mathcal{N},\mathrm{fs}}$). Similarly it will arrive in state $K_{\tau<\tau_0}$ with probability $(1-\tau_0)\overline{\rho}^{\mathcal{N},\mathrm{fs}}$. This completes the list of possible arrival states for a particle leaving state D_W.

If $\mathcal{E}'_0$ departs from state D_B we have to specify if the site directly to its right is occupied or not. It is empty with probability $(1-\overline{\rho}^{\mathcal{N},\mathrm{fs}})$, in which case the particle can arrive either in state D_B if the row under it is a D row (probability $(1-\overline{\rho}^{\mathcal{N},\mathrm{fs}})$) or get blocked by a $\mathcal{N}$ particle if the row under it is a $K_{\tau<\tau_0}$ row (probability $\tau_0\overline{\rho}^{\mathcal{N},\mathrm{fs}}$), or exit the shadow if the row under it is a $K_{\tau>\tau_0}$ row (probability $(1-\tau_0)\overline{\rho}^{\mathcal{N},\mathrm{fs}}$). If in the initial configuration there is a $\mathcal{N}$ particle on the site to the right of $\mathcal{E}'_0$ particle the next row is necessarily a D row to linear order in $\overline{\rho}^{\mathcal{N}}$. The $\mathcal{E}'_0$ particle will therefore stay in the D_B state if it is not blocked by the $\mathcal{N}$ particle (probability $\tau_0\overline{\rho}^{\mathcal{N},\mathrm{fs}}$) or arrive in the D_W state if it is blocked (probability $(1-\tau_0)\overline{\rho}^{\mathcal{N},\mathrm{fs}}$).

Finally, we notice that $\mathcal{E}'_0$ occupying a state $K_{\tau<\tau_0}$ will necessarily arrive in state D_B at the next time step and that a particle occupying a state $K_{\tau>\tau_0}$ will arrive in D_W. The rate equations to linear order in $\overline{\rho}^{\mathcal{N},\mathrm{fs}}$ then read

$$\begin{cases} P_W^{\mathrm{fs}}(t+1) &= (1-\overline{\rho}^{\mathcal{N},\mathrm{fs}})P_W^{\mathrm{fs}}(t) + \overline{\rho}^{\mathcal{N},\mathrm{fs}}(1-\tau_0)P_B^{\mathrm{fs}}(t) + P_{>\tau_0}^{\mathrm{fs}}(t) \\ P_B^{\mathrm{fs}}(t+1) &= (1-2\overline{\rho}^{\mathcal{N},\mathrm{fs}} + \overline{\rho}^{\mathcal{N},\mathrm{fs}}\tau_0)P_B^{\mathrm{fs}}(t) + P_{<\tau_0}^{\mathrm{fs}}(t) \\ P_{<\tau_0}^{\mathrm{fs}}(t+1) &= \overline{\rho}^{\mathcal{N},\mathrm{fs}}\tau_0 P_W^{\mathrm{fs}}(t) + \overline{\rho}^{\mathcal{N},\mathrm{fs}}\tau_0 P_B^{\mathrm{fs}}(t) \\ P_{>\tau_0}^{\mathrm{fs}}(t+1) &= \overline{\rho}^{\mathcal{N},\mathrm{fs}}(1-\tau_0)P_W^{\mathrm{fs}}(t) \end{cases} \tag{6.7}$$

The quantity of interest is the probability that the particle has stayed in the shadow until time t

$$P_S^{\mathrm{fs}}(t) = P_W^{\mathrm{fs}}(t) + P_B^{\mathrm{fs}}(t) + P_{<\tau_0}^{\mathrm{fs}}(t) + P_{>\tau_0}^{\mathrm{fs}}(t) \tag{6.8}$$

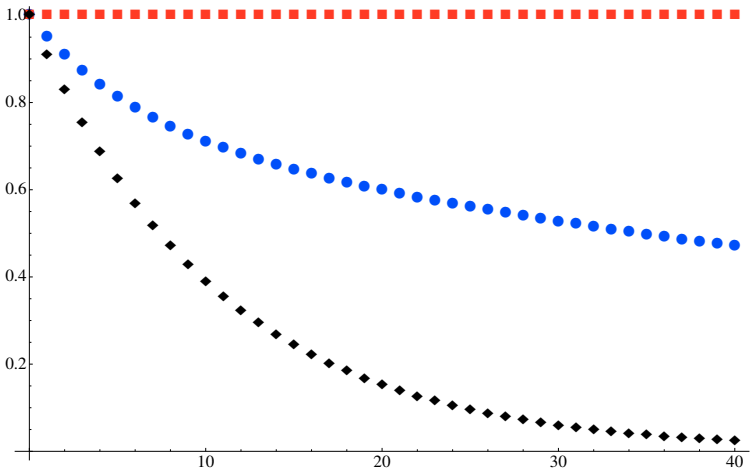

Figure 6.8: Probability that the second particle $\mathcal{E}_0'$ stays in the shadow during the first t time steps for frozen shuffle update (blue disks, Eqs. (6.7)) and alternating parallel update (red squares, Eqs. (6.7) with $\tau_0 = 1$). For comparison, the same quantity has been plotted assuming the two particles are uncorrelated (black diamonds). The density $\overline{\rho}^{\mathcal{N}}$ is 0.1.

and it evolves according to

$$P_S^{\mathrm{fs}}(t+1) = P_S^{\mathrm{fs}}(t) - \overline{\rho}^{\mathcal{N},\mathrm{fs}}(1-\tau_0)P_B^{\mathrm{fs}}(t). \tag{6.9}$$

Equations (6.7) are linear equations that can be solved numerically for a given value of τ_0, here for $\mathcal{E}_0'$ initially in the state D_B. After that an average over the uniform τ_0 distribution is taken, finally giving the value of $P_S^{\mathrm{fs}}(t)$. The probability to stay in the shadow with frozen shuffle update $P_S^{\mathrm{fs}}(t)$ has been plotted in Fig. 6.8 in comparison to a reference curve for which it is supposed that the two particles are not correlated. These results show that the wake of $\mathcal{E}_0$ stabilizes the position of $\mathcal{E}_0'$, as $P_S^{\mathrm{fs}}(t)$ decays like t^{-1} while the reference curve is a decreasing exponential. It can be seen from the equations (6.7), and it will also be true of Eqs. (6.10) for alternating parallel update, that it is impossible for $\mathcal{E}_0'$ to leave the wake from behind, *i.e.* it can only overtake the wake.

In particular, it is impossible to leave the wake directly from state D_W. If the initial state of $\mathcal{E}_0'$ had been D_W the slope of the curves represented in Fig. 6.8 would have vanished at $t = 0$. At large times the decay would however have been the same.

For a fixed value of τ_0 the probability $P_S^{\mathrm{fs}}(t)$ is a sum of exponentials dominated by the largest eigenvalue of the transfer matrix of Eqs. (6.7) in the large time limit. In Fig. 6.9 the longest characteristic escape time is plotted as a function of τ_0. We find that it diverges in $\tau_0 = 0$ and 1 and has a minimum

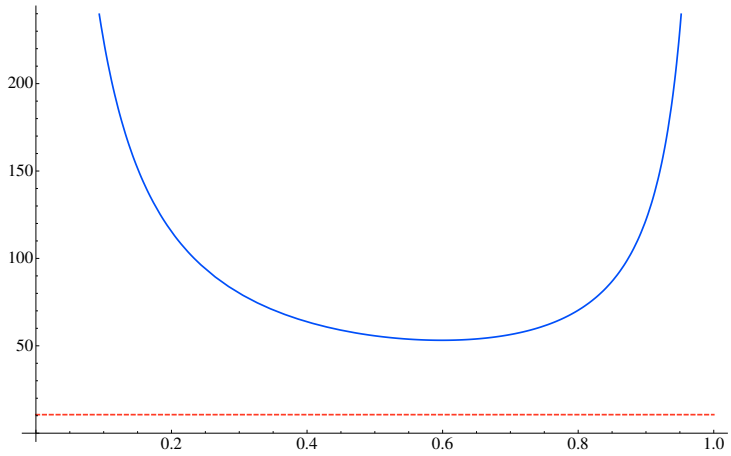

Figure 6.9: Characteristic escape time of a particle $\mathcal{E}'_0$ starting from state D_B in the shadow as a function of its phase τ_0 (blue). The escape time diverges for $\tau_0 = 0$ and 1. The escape time in case of uncorrelated particles has been plotted in red for comparison.

somewhere in-between, while always staying far superior than the reference situation. $P_S^{\text{fs}}(t)$ is then dominated by $\tau_0 = 0$ or 1, and the t^{-1} decay can be recovered from an asymptotic calculation.

• **Alternating parallel update:**

Here we argue that the alternating parallel update can be formally seen as a limit of frozen shuffle update. There are two differences between the updates. Firstly, the hopping order. Particles $\mathcal{E}_0$ and $\mathcal{E}'_0$ hop at the same time in alternating parallel update, which can be simply accounted for by setting $\tau_0 = 0$ or 1 in the frozen shuffle update equations. We take $\tau_0 = 1$. With this choice it is clear that, in frozen shuffle update, all the $\mathcal{N}$ particles hop one after another without any $\mathcal{E}$ particle in-between them. As the $\mathcal{N}$ particles are injected in free flow, they are never blocked and all possible hopping orders are equivalent, so that we may decide that they all hop at half-integer times, following the convention we took for alternating parallel update. In the process of taking all the phases equal we however introduce spurious blockings, that are shown to be unimportant by what follows. The second element is indeed the presence of platoons in frozen shuffle, that do not exist in alternating parallel. To make up for this difference we have to take the low-density limit of the frozen shuffle update, which is already done in equations (6.7). In this limit events where two particles follow each other are negligible and platoons always have only one particle. Finally, the density of $\mathcal{N}$ particles should be replaced with the alternating parallel update expression.

Taking $\tau_0 = 1$ in Eqs. (6.7) gives for alternating parallel update

$$\begin{cases} P_W^{\rm ap}(t+1) & = (1-\overline{\rho}^{\mathcal{N},{\rm ap}})P_W^{\rm ap}(t) \\ P_B^{\rm ap}(t+1) & = (1-\overline{\rho}^{\mathcal{N},{\rm ap}})P_B^{\rm ap}(t) + P_{<\tau_0}^{\rm ap}(t) \\ P_{<\tau_0}^{\rm ap}(t+1) & = \overline{\rho}^{\mathcal{N},{\rm ap}}P_W^{\rm ap}(t) + \overline{\rho}^{\mathcal{N},{\rm ap}}P_B^{\rm ap}(t), \end{cases} \tag{6.10}$$

where $P_{>\tau_0}^{\rm ap}(t) = 0$ does not appear anymore in the system of equations. These equations have been shown to be true for low density, but inspection shows that they are in fact exact for alternating parallel update at all densities. Their most striking property is that $P_S^{\rm ap}(t)$ is conserved: $\mathcal{E}_0'$ cannot exit from the shadow of $\mathcal{E}_0$ at all. More precisely it can be seen that it is impossible for $\mathcal{E}_0'$ to leave a black site for a non-black one. The shadows of both particles are then superimposed. For completeness the constant curve corresponding to alternating parallel update has been reported in Fig. 6.8.

6.3.2 Chevron angle

The occupations of the sites of the lattice have been chosen to be correlated following the injection procedure. These correlations are expected to reproduce the behaviour observed in the intersection. Indeed it has already been argued in section 5.2 that the chevron effect finds its origin in the difference in the organization between the two types of particles, the $\mathcal{N}$ particles being less organized than the $\mathcal{E}$ particles in the lower triangle. The model studied throughout chapter 6 therefore constitutes an approximation of what is expected to happen to a single $\mathcal{E}$ particle in the lower triangle, with more particles being added later. The results depend of course on this postulated organization of the $\mathcal{N}$ particles and would be different if the $\mathcal{N}$ particles were initially organized otherwise, *e.g.* into diagonals.

We have seen that the shadow of $\mathcal{E}_0$ is a favorable zone for $\mathcal{E}_0'$ to stay in. We therefore expect to find important spatial correlations in the direction of the shadow, corresponding to the chevron effect. This direction depends only on the density of $\mathcal{N}$ particles $\overline{\rho}^{\mathcal{N}}$, as a D row is added to the shadow with probability $1-\overline{\rho}^{\mathcal{N}}$ for small densities, with which the shadow makes a diagonal step, and a K row is added with probability $\overline{\rho}^{\mathcal{N}}$, corresponding to a vertical step. The angle of the shadow is therefore given by $\tan\theta_0 = 1-\overline{\rho}^{\mathcal{N}}$, which gives a deviation $\Delta\theta_0 = \theta_0 - \pi/4 \simeq -\frac{\overline{\rho}^{\mathcal{N}}}{2}$rad. This value gives the theoretical curve of Fig. 5.13 and is in good agreement with the alternating parallel case whereas it clearly overestimates the frozen shuffle value.

For frozen shuffle update the escape time is indeed finite, which certainly explains why the chevron effect should be smaller. The escape time however goes to infinity when the two $\mathcal{E}$ particles have very close phases.

In the case of more than two particles we can guess that in the intersection model there will be alignments of particles in a stationary regime where the number of particles joining the shadow will compensate those leaving it, particles in the shadow statistically having their phase close to the one of $\mathcal{E}_0$. It should also be noticed that in the two-particle study we deliberately put aside

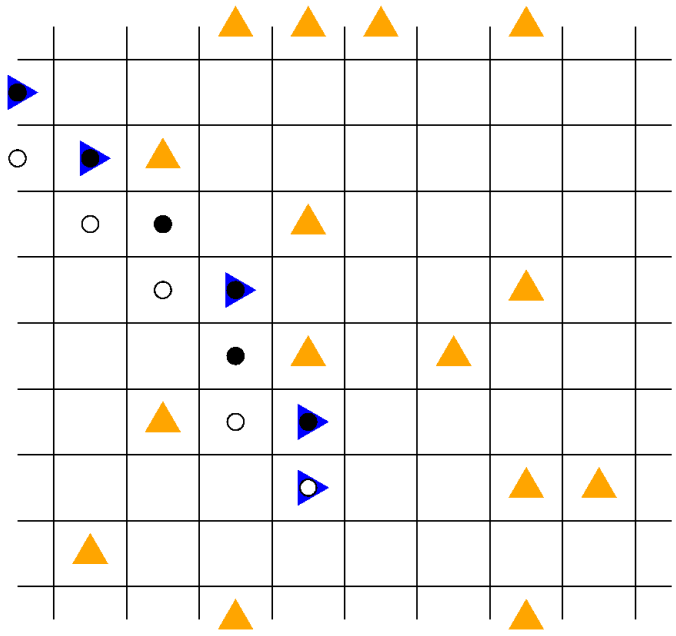

Figure 6.10: Example of macroscopic mode contributing to the chevron effect. In the special case of alternating parallel update this mode is stable, particles can in principle be added on all the black dotted sites.

an important effect: not only particles can exit the shadow but the shadow can itself be destroyed if more $\mathcal{E}$ particles are present. Indeed if there are collisions to the right of the shadow a $\mathcal{N}$ particle may be blocked and then occupy a dotted site.

In the alternating parallel case things are much simpler, and we will see in the next section that a family of macroscopic modes can be constructed exactly from the two-particle case.

6.4 Macroscopic mode

In this section we consider only the case of alternating parallel update.

Using alternating parallel update the set of black sites is stable, and one could put an $\mathcal{E}$ particle on a finite fraction of the black dotted site. Using this procedure a stable macroscopic propagation mode is constructed, a picture of which is shown in Fig. 6.10. The simulations support the preceding arguments, as the aligned structures can indeed be observed in simulations, see Fig. 6.11.

We have seen that simple effective interactions arguments enable one to isolate the main propagation mode accounting for the chevron effect, therefore explaining the value of chevron angle quantitatively for alternating parallel

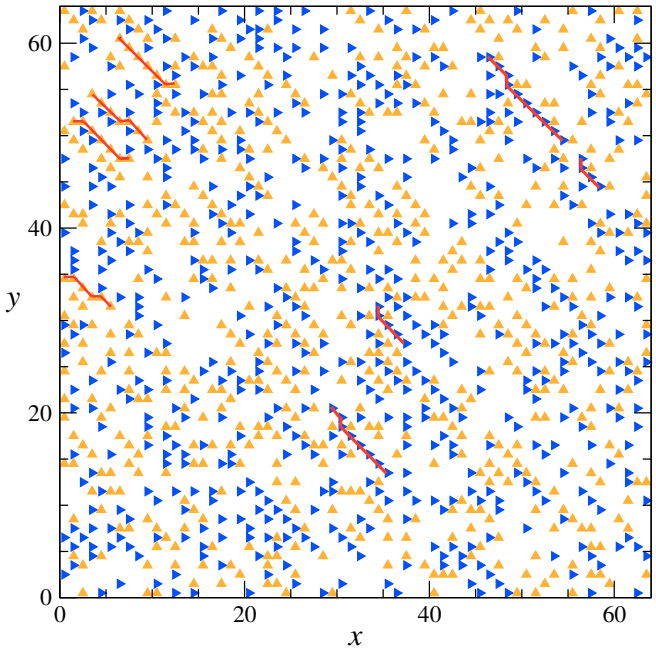

Figure 6.11: Snapshot of the particles in an intersection square of linear dimension $M = 64$ for $\alpha = 0.15$ and alternating parallel update. Red lines identify some instances of the configuration exhibited in Fig. 6.10 where all the black dotted sites are occupied.

update and qualitatively for frozen shuffle update. Alternating parallel update represents the most regular possible case, in which all the information about the system is contained in the occupation variables. This extreme regularity results here in the stability of the set of black sites. The phases introduced in frozen shuffle update act as fluctuations which perturb the stable state, thus giving the escape time a finite value. The construction of the shadow and the arguments leading to the rate equations are expected to work as long as (i) the update scheme is deterministic in the bulk and (ii) the particles hop exactly once per time step. In the case of random shuffle update the velocity of the particles is not exactly equal to 1 in the free flow phase, but it seems reasonable to think that the method used here can be generalized to give similar results for this update. Up to now this has not been done and remains an interesting challenge. For an update scheme with large fluctuations, such as random sequential update, neither the chevron effect nor the diagonals are expected to survive, but it cannot be excluded that small correlations exist.

The findings of this section can be summarized by the rule that was proposed in Ref. [143]:

Rule 1 *At the interface where a disordered species A of density* $\overline{\rho}^A$ *penetrates into a perpendicular traveling and diagonally ordered species B, the speed at which the B diagonals advance is reduced from* 1 *to* $1 - \overline{\rho}^A$*. Moreover, the (acute) angle between the diagonals and the direction of propagation of the disordered species is reduced from* $\frac{\pi}{4}$ *by an amount* $\frac{1}{2}\overline{\rho}^A$*.*

We now turn on to some other mainly numerical studies of this effect in different geometries and with some special choices of parameters.

Chapter 7

Exploring the parameter space of the intersection model

In section 5.2 we restricted the space of parameters quite drastically to keep only the entrance probability per time step α and the size of the intersection M. This strategy proved effective, as having only two parameters has been a convenient way to achieve an understanding of the chevron effect. Here we will see to what extent the phenomena we discovered can be generalized to other parameter regimes. Allowing the intersection to be asymmetric looks like a natural generalization, as most intersecting flows are. Of more relevance to applications is the case where the hopping probability p is smaller than 1, introducing some fluctuations in the system. Too low a value of p is certainly expected to destroy the pattern, since when $p \to 0$ both frozen shuffle and alternating parallel update behave like random sequential update, where no pattern is observed [137, 138]. Finally we study the problem on a cylinder, in which we expect to observe 'half chevrons'. The translational invariance will prove useful to quantitatively test the rule closing chapter 6 and to determine the penetration length, while a subtle transient effect will be accounted for as well. In this whole chapter we still stay in the free flow phase.

The asymmetric intersection is studied in section 7.1, and nondeterministic hops are allowed in section 7.2. The chevron effect on a cylinder with the mean-field equations is finally observed in section 7.3. The work presented in sections 7.1 and 7.2 has not been published, whereas the findings of section 7.3 can be found in Ref. [143].

7.1 Asymmetric intersection

The model we defined in section 4.2 had *a priori* a large number of parameters. With the definition of the TASEP come three intensive parameters governing the entrance, the bulk and the exit dynamics. To these we have to add the length of the system, that must be divided between the length of the entrance lanes and the intersection width in the case of the intersection. Finally we have

two directions in our model, which would give us a total of $(2+3)\times 2 = 10$ independent parameters. In the free flow phase it is however clear that the sizes L_x, L_y do not play any role in the dynamics, while the desire to design a model for pedestrians leads us to take deterministic hopping and exit probabilities, $p = \beta = 1$. We were then left with four parameters, whose number was finally reduced to two by taking a symmetric system.

In the free flow phase only little information propagates in the direction opposite to the flow of particles. In particular, the sites of the bulk are not perturbed too much by the exit boundaries. If we vary the sides M_x and M_y of the intersection, we should therefore expect a given site to have the same properties as long as it stays in the bulk. It therefore seems of little interest to study the case $M_x \neq M_y$ in the free flow phase.

On the contrary the case $\alpha_{\mathcal{E}} \neq \alpha_{\mathcal{N}}$ seems to be an interesting one. Indeed the imposed $\mathcal{E}/\mathcal{N}$ symmetry was a useful but somewhat artificial simplification. Moreover the whole comprehension of the chevron effect is based on the asymmetric organization of the particles, so that adding a supplementary asymmetry could have more dramatic effects.

A level plot of the chevron angle is shown in Fig. 7.1 for asymmetric entrance probabilities per time step $\alpha_{\mathcal{E}} = 0.04 \neq \alpha_{\mathcal{N}} = 0.08$. We observe that the intersection can still roughly be divided in two zones where the chevron angle reaches a plateau value. It has been verified that the plateau values are equal to those expected from section 6.3, *i.e.* $\Delta\theta(\mathbf{r}) \simeq \frac{\overline{\rho}^{\mathcal{E}}}{2}$rad in the upper part and $\Delta\theta(\mathbf{r}) \simeq -\frac{\overline{\rho}^{\mathcal{N}}}{2}$rad in the lower one.

The main surprise comes from the fact that the plateaus are not symmetrical anymore, the separatrix between them having a slope different from 1. This behaviour can however be understood by a simple mean-field argument. Intuitively the species that has undertaken the largest number of collisions is the most organized. At the mean-field level the number of collisions an $\mathcal{E}$ particle has been involved in is simply the distance traveled times the density of $\mathcal{N}$ particles $i\overline{\rho}^{\mathcal{N}}$. The symmetrical argument holds as well and the equation of the separatrix is simply given by

$$i\overline{\rho}^{\mathcal{N}} = j\overline{\rho}^{\mathcal{E}}. \tag{7.1}$$

In the case of Fig. 7.1 we have $\overline{\rho}^{\mathcal{N}} \simeq 1.93\overline{\rho}^{\mathcal{E}}$, which correctly predicts the shape of the plateau zones.

To summarize this subsection, it seems that the intersection with asymmetric entrance probabilities is a direct extension of the symmetric case that can be understood by the arguments of section 6.3 combined with simple modifications.

7.2 Nondeterministic dynamics

In section 4.2 we argued that motion of pedestrians is expected to be quite regular, thus setting the hopping probability p to 1. We also wanted to suppress the effects of possible collisions at the exit of the intersection by choosing the

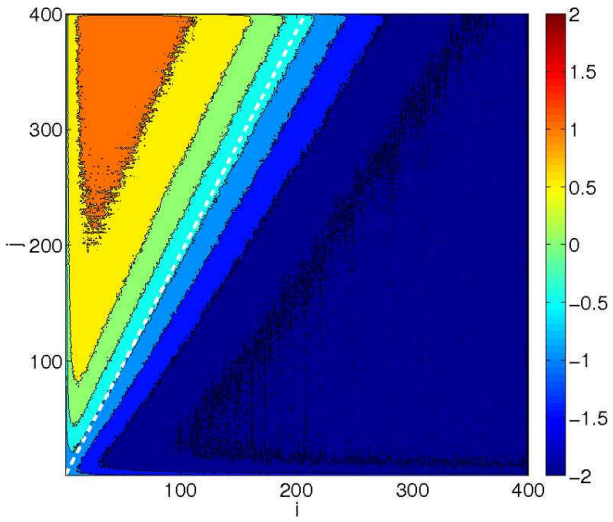

Figure 7.1: Chevron angle $\Delta\theta(\mathbf{r})$ obtained with asymmetric entrance probabilities per time step $\alpha_{\mathcal{E}} = 0.04$ and $\alpha_{\mathcal{N}} = 0.08$, for $M = 400$ with alternating parallel update, and calculated by velocity ratio method. The white dashed line, which separates the two plateaus, is given by Eq. (7.1).

exit probability per time step $\beta = 1$. This allowed us to concentrate on the effects of the interactions inside the crossing. Here we simply give the main observations that characterize the generalization $p < 1$. The results presented in the present section 7.2 give some information about what happens when $p < 1$ but can also be taken as a list of perspectives for future work, as they have not made the object of a systematic study.

Snapshots were taken and the chevron angle was measured by the velocity ratio method for different values of the hopping probability p, all this being shown in Fig. 7.2. The system is observed to get gradually less and less organized as p decreases. First of all the chevron effect gets weaker, the particles however being still organized at an angle closer and closer to 45°. For smaller values of p even the diagonal pattern disappears and the particles seem to be positioned randomly, though it is not excluded that the correlation functions could still exhibit some anisotropy.

Decreasing the value of p decreases the outflow, so that we should expect that the intersection gets blocked for lower and lower α as p increases. It would be interesting to take precise measurements of this transition for $p < 1$, as the diagonal pattern is the one that maximizes the output flow. After the pattern disappears one could therefore expect to see a sharp drop in the critical α value, that would come from the decrease in transport efficiency both of a given lane and of the two-dimensional organization.

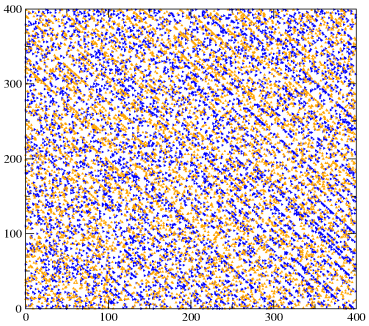

(a) $1 - p = 10^{-3}$

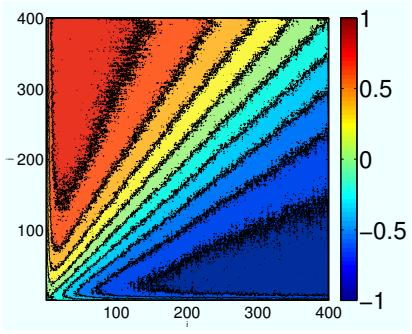

(b) $1 - p = 10^{-3}$

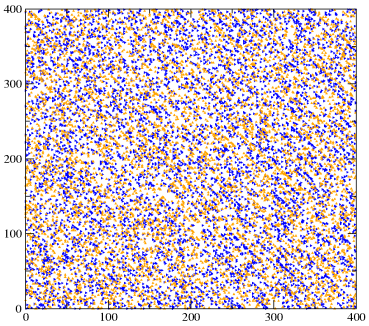

(c) $1 - p = 10^{-2}$

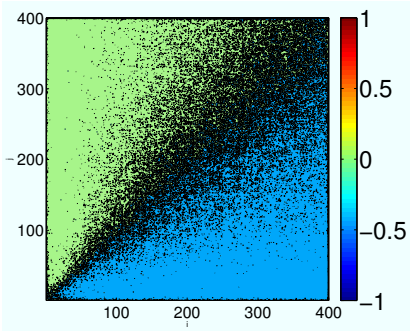

(d) $1 - p = 10^{-2}$

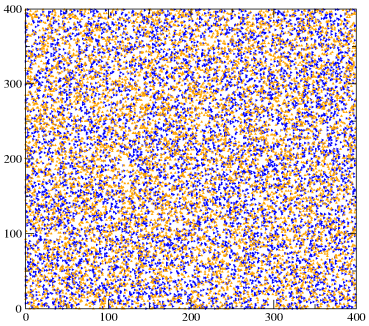

(e) $1 - p = 10^{-1}$

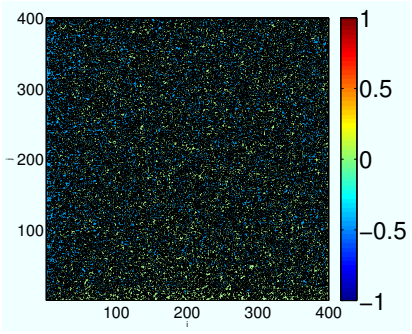

(f) $1 - p = 10^{-1}$

Figure 7.2: Snapshots of intersections (left) and level plots of the chevron angle (right) for intersections with $p < 1$. The parameters are $\alpha = 0.04$, $M = 400$ and the update is alternating parallel. (a)-(b) For p very close to 1 the chevrons are still present. (c)-(d) When $1 - p$ increases the chevrons start to disappear but the diagonals are still visible. (e)-(f) When $1 - p \gtrsim 2\overline{\rho}$ even the diagonals disappear, and the level plot simply fluctuates around 0.

From qualitative arguments it seems that the diagonal pattern should disappear approximately when the probability for a particle not to move because it is blocked is equal to the probability that it does not move because of randomness $1-p \sim \overline{\rho}$. More precisely, equations analogous to the mean-field equations (5.4) can be written for $p<1$,

$$\begin{aligned} \rho^{\mathcal{E}}_{t+1}(\mathbf{r}) &= p[1-\rho^{\mathcal{N}}_t(\mathbf{r})]\rho^{\mathcal{E}}_t(\mathbf{r}-\mathbf{e}_x)+[1-p+p\rho^{\mathcal{N}}_t(\mathbf{r}+\mathbf{e}_x)]\rho^{\mathcal{E}}_t(\mathbf{r}), \quad (7.2)\\ \rho^{\mathcal{N}}_{t+1}(\mathbf{r}) &= p[1-\rho^{\mathcal{E}}_t(\mathbf{r})]\rho^{\mathcal{N}}_t(\mathbf{r}-\mathbf{e}_y)+[1-p+p\rho^{\mathcal{E}}_t(\mathbf{r}+\mathbf{e}_y)]\rho^{\mathcal{N}}_t(\mathbf{r}). \end{aligned}$$

The linear stability analysis of subsection 5.1.5 can be reproduced, showing that the diagonal instability disappears for $1-p>2\overline{\rho}$. We have seen in subsection 5.2.3 that the chevron effect involves only higher-order terms in $\overline{\rho}$, so that we may expect that the chevrons disappear when $1-p\sim\overline{\rho}^2$. These estimates seem to give quite reasonable values, at least in the case of Fig. 7.2, however the decrease of the organization of the two particle types could interfere and modify these estimates. We also note that the observations may depend on the size of the intersection M in a new fashion, as the fact that $p<1$ is expected to give effects on length scales $\gtrsim 1/(1-p)$ only.

In the case of real pedestrians the density is higher than in our simplified model, so that the parameter space domain where the patterns are observed is expected to be larger than in the model for both of them. The diagonal pattern is indeed observed in the experiments, so that we know that for pedestrians the effective hopping probability p is higher than the critical value $1-2\overline{\rho}$. It remains unclear whether chevrons could be observed or not.

In the same direction, one could allow blocking at the exit, *i.e.* $\beta<1$. This case has however not been studied in great detail and is left as a perspective.

7.3 Mean-field equations on a cylinder

7.3.1 Stationary state

In this part we study the mean-field equations on a cylinder. We will see that the chevron effect is still present on the cylinder in agreement with the rule of section 6.3. The translational invariance in the vertical direction enables us to perform averages and the equations have rather low fluctuations. These two factors will enable us to get more precise data concerning for example the penetration length. The cylindrical boundary conditions (CBC) also introduce an asymmetry between the two directions which will be interesting to study.

We take the x direction to be open and the y direction to be periodic. In the intial state the density field $\rho^{\mathcal{E}}_0(\mathbf{r})$ is zero everywhere and the initial $\rho^{\mathcal{N}}_0(\mathbf{r})$ are drawn from a flat distribution between $\frac{1}{2}\overline{\rho}^{\mathcal{N}}$ and $\frac{3}{2}\overline{\rho}^{\mathcal{N}}$, where $\overline{\rho}^{\mathcal{N}}$ is a control parameter. The eastern and western boundary are the same as the first of Eqs. (5.18), respectively, and the control parameter is the average value of the entrance density that we denote $\overline{\eta}^{\mathcal{E}}$.

In Fig. 7.3 a typical configuration of the fields in the stationary state is shown. The stripes still exist and are at an angle less than 45°. Taking benefit

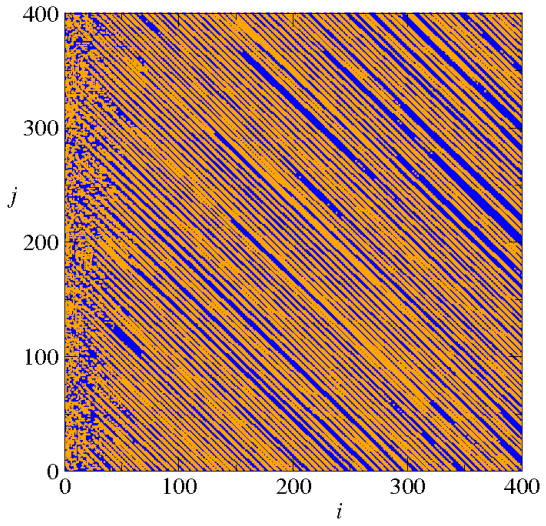

Figure 7.3: Snapshot representing the density fields in the intersection square of size $M = 400$ and subject to cylindrical boundary conditions with control parameters $\overline{\rho}^{\mathcal{N}} = 0.050$ and $\overline{\eta}^{\mathcal{E}} = 0.055$. A site is colored blue or orange depending on which is bigger between $\rho_t^{\mathcal{E}}(\mathbf{r})$ and $\rho_t^{\mathcal{N}}(\mathbf{r})$. A disordered boundary layer along the west entrance is clearly visible. The striped pattern in the bulk has an average slope of $45^\circ - \Delta\theta_0$; for the pattern shown the velocity ratio method gives $\Delta\theta_0 \approx 1.1^\circ$.

from the translational symmetry along the y direction we can plot the chevron angle $\Delta\theta(i)$ as a function of the column index. In Fig. 7.4 the chevron angle is plotted for various values of $\overline{\eta}^{\mathcal{E}}$ for fixed $\overline{\rho}^{\mathcal{N}}$ using the velocity ratio method of section 5.2. One sees that for small i there is a 'boundary plateau' in the value of the chevron angle. There is then a transition zone around $i \simeq 75$, giving a precise meaning to the penetration length ξ independently of the value of $\overline{\eta}^{\mathcal{E}}$. After that the angle reaches a second 'bulk plateau' which seems to be stable.

Although the values of the chevron angle obtained by velocity ratio method do not have any physical interpretation in terms of angle in the penetration zone, the value of the boundary plateau can nevertheless be understood. When both species are uniformly distributed we expect the velocities to have values $v^{\mathcal{E}} = 1 - \overline{\rho}^{\mathcal{N}}$ and $v^{\mathcal{N}} = 1 - \overline{\eta}^{\mathcal{E}}$, which gives after developing Eq. (5.29) for small chevron angles

$$\Delta\theta(1) = \frac{1}{2}\frac{\overline{\rho}^{\mathcal{N}} - \overline{\eta}^{\mathcal{E}}}{1 - \overline{\rho}^{\mathcal{N}}}. \tag{7.3}$$

These values are reported on Fig. 7.4 and are in perfect agreement with the measurements.

Fig. 7.5 shows a set of curves of the chevron angle for constant $\overline{\eta}^{\mathcal{E}}$ and varying $\overline{\rho}^{\mathcal{N}}$. All these curves have roughly the same bulk plateau values $-0.60^\circ < \Delta\theta_0 < -0.50^\circ$. This observation is coherent with rule 1, that pre-

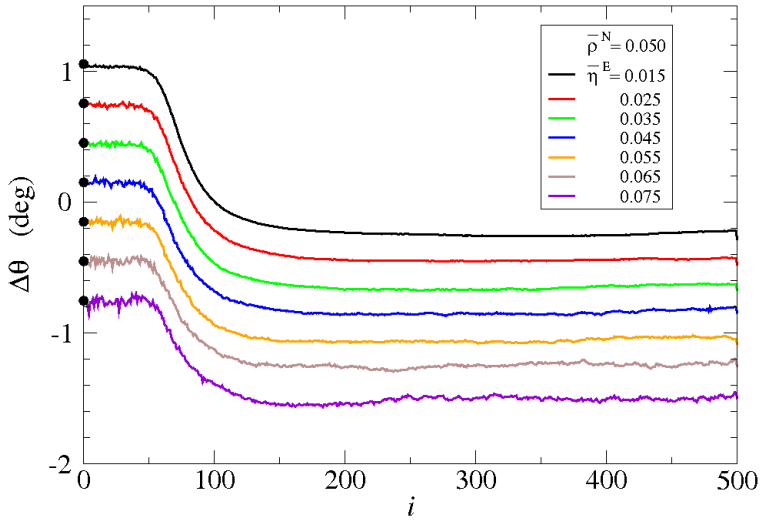

Figure 7.4: Chevron angle $\Delta\theta$ as a function of the column index i, obtained by simulation of the mean field equations 5.4 and measured by means of the velocity ratio method, on a square lattice of linear size $M = 500$ with cylindrical boundary conditions. The northbound particles have a fixed density $\overline{\rho}^{\mathcal{N}} = 0.050$ and the density $\overline{\eta}^{\mathcal{E}}$ of the eastbound particles varies. The dots for $i = 1$ are the boundary values predicted by Eq. (7.3).

dicts that $\Delta\theta_0 = \frac{\overline{\eta}^{\mathcal{E}}}{2}$ independently of $\overline{\rho}^{\mathcal{N}}$. Fig. 7.5 however shows that the bulk value of the angle starts increasing again after reaching its minimum, this drift getting faster as $\overline{\rho}^{\mathcal{N}}$ grows larger. This effect remains largely unexplained for now. Near the boundary Eq. (7.3) works well again. We also notice that, quite intuitively, the boundary layer gets thinner as $\overline{\rho}^{\mathcal{N}}$ grows because of the larger number of collisions. The size of this layer diverges like $1/\overline{\rho}^{\mathcal{N}}$ for small values of $\overline{\rho}^{\mathcal{N}}$.

Of physical interest are also the bulk values. They represent the angle of inclination of the parallel stripes in the bulk, forming one half of the chevrons that are observed in OBC. We have seen in Fig. 7.5 that the bulk value of $\Delta\theta(i)$ seems to increase slightly with i. We choose arbitrarily to define $\Delta\theta_0$ as the average of $\Delta\theta(i)$ for $200 \leq i \leq 300$. A plot of the values of the chevron angle using both the velocity ratio method and the crest method can be found in Fig. 7.6. From Fig. 7.6 it can be seen that both methods are in rather good agreement, though a small systematic discrepancy remains. This ensures that the measurements of $\Delta\theta_0$ make sense.

The angle $\Delta\theta_0$ increases linearly with $\overline{\eta}^{\mathcal{E}}$, which is consistent with what we know of the particle system with OBC. The value of $\Delta\theta_0$ is approximately $\Delta\theta_0 \simeq c'\overline{\eta}^{\mathcal{E}}$ with $c' = 21°$, whereas the prediction of section 6.3 would give $c'_{\text{th}} = \frac{90°}{\pi} \simeq 28.7°$. The fact that the numerical value is smaller may be related

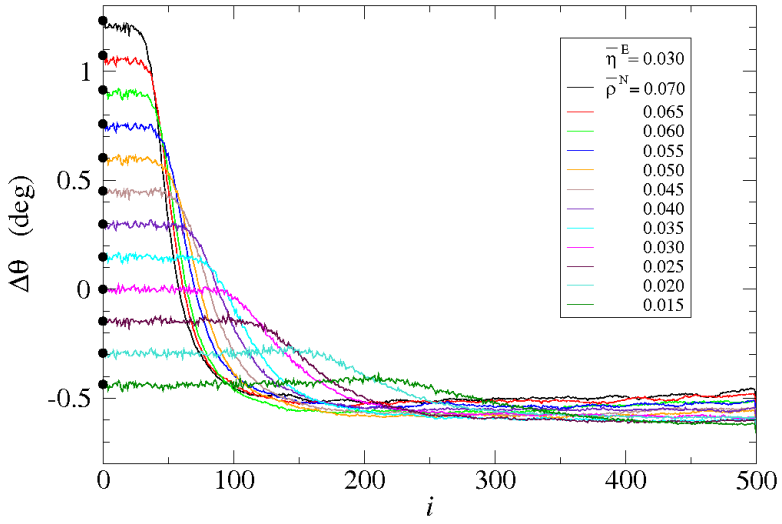

Figure 7.5: Chevron angle $\Delta\theta$ as a function of the column index i measured with the velocity ratio method for $M = 500$ with cylindrical boundary conditions. The eastbound particles have a fixed boundary density $\overline{\eta}^{\mathcal{E}} = 0.030$. Curves for various densities $\overline{\rho}^{\mathcal{N}}$ of the northbound particles show different penetration depths ξ but have closely similar plateau values for $i \gtrsim \xi$. The dots for $i = 1$ are the boundary values predicted by Eq. (7.3).

to the fact that some collisions that occur in the particle system are neglected in the equations.

This study on the cylinder has enabled us to introduce an asymmetry between the two particle species. The same has been done with the particle system and similar results were obtained, in particular concerning the independence of the chevron angle with respect to the $\mathcal{N}$ particle density. All the exhibited measurements are also coherent with the theoretical arguments developed in section 6.3, most notably with the rule at the end. We now put these arguments to an even stronger test, namely we study a transient effect.

7.3.2 A transient effect

Here we consider the same mean-field equations in a cylindrical geometry, that we will however study in a transient regime. We consider a particular initial condition in which $\rho_0^{\mathcal{E}}(\mathbf{r}) = \rho_0^{\mathcal{N}}(\mathbf{r}) = \overline{\rho}_0$ everywhere in the system, which imposes $\overline{\rho}^{\mathcal{N}} = \overline{\rho}_0$, and we choose $\overline{\eta}^{\mathcal{E}} = \overline{\rho}_0$. If no particles entered the system this state would be stationary but here entering $\mathcal{E}$ particles will inject some randomness into it.

Fig. 7.7 shows the state of such a system of size $M = 500$ after $t = 400$ time steps. The fields propagating at maximum velocity 1 the system is obviously in

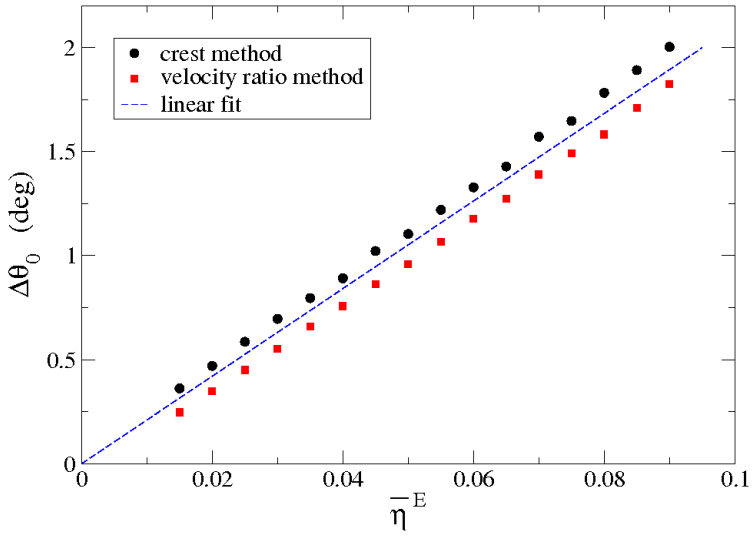

Figure 7.6: Chevron angle $\Delta\theta_0$ as a function of the average density $\overline{\eta}^{\mathcal{E}}$ imposed at the open west boundary and for fixed $\overline{\rho}^{\mathcal{N}} = 0.050$, obtained by simulation of the mean field equations (5.4) and measured by both the crest and the velocity ratio method, on a square lattice of linear size $M = 500$ with cylindrical boundary conditions. The error bars are of the same order as the symbols. The straight line through the origin is the closest fit to both data sets; it has a slope of 21°.

a transient state. The system can be divided in zones which are clearly visible in the $\Delta\theta(i)$ measurements of Fig. 7.8. Let us describe Fig. 7.8 from right to left. Indeed, as the $\mathcal{E}$ field propagates towards east decreasing i at fixed time amounts to describing a certain site in the chronological order.

For $i \geq 400$ the injected $\mathcal{E}$ particles have not invaded the zone yet. The density fields are then simply equal to their initial values $\overline{\rho}_0$. For $325 \lesssim i \leq 400$ the amplitude of the perturbation to the initial state decreases exponentially and no alignments are visible. This zone corresponds to $v > v^*$ in the study of the Green function of the linearized equations, subsection 5.2.3. We now come to zone II where stripes are visible and have the opposite chevron angle value from what is expected in the stationary state. Indeed, when the perturbation of the $\rho_t^{\mathcal{E}}(\mathbf{r})$ field first enters the system $\rho_t^{\mathcal{N}}(\mathbf{r})$ is still equal to its initial value $\overline{\rho}_0$, which is the most disordered state possible. The $\mathcal{E}$ species therefore unexpectedly plays the role of the ordered species and the chevron angle is positive in zone II, for $200 \lesssim i \lesssim 325$. After some time however the $\mathcal{N}$ field becomes organized through collisions and plays the role of the organized species against the freshly entered $\mathcal{E}$ field, and we find ourselves in zone I, $50 \lesssim i \lesssim 175$, and the chevron angle becomes negative as expected. For $i \lesssim 25$ we have the boundary plateau.

The widths of zones I and II increase roughly linearly with time, so that

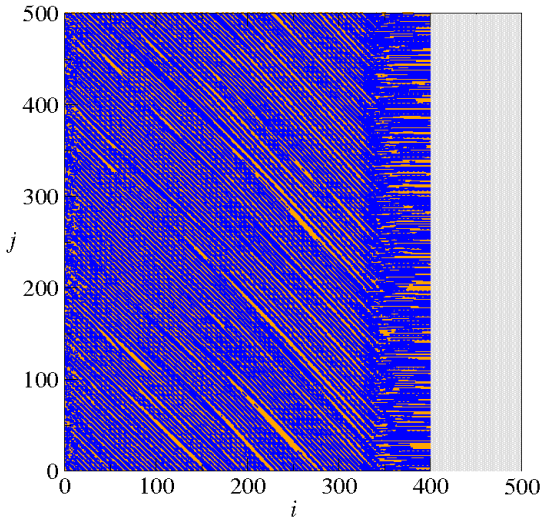

Figure 7.7: Density field showing the transient configuration at time $t = 400$ for size $M = 500$. The west entrance boundary is subject to a random boundary density of average $\overline{\eta}^{\mathcal{E}} = 0.10$. The nonrandom initial condition was $\rho_0^{\mathcal{E},\mathcal{N}}(\mathbf{r}) = 0.10$. In the grey area these initial values still persist at time $t = 400$.

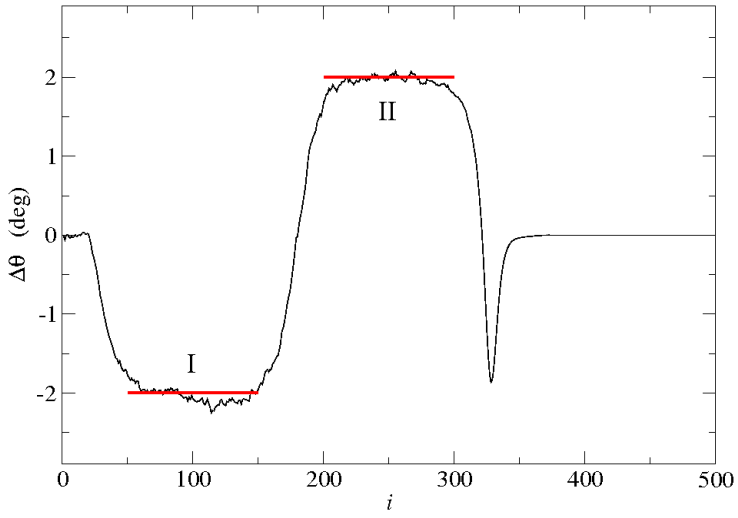

Figure 7.8: Chevron angle $\Delta\theta$ as a function of the column index i, determined by the velocity ratio method in the configuration of Fig. 7.7. The heavy horizontal red lines mark the plateau values $\pm 2°$.

in the stationary state zone I will have invaded the whole system and pushed zone II out of it, recovering a stationary state of the type shown in Fig. 7.3 The fact that we can explain this effect however proves the robustness of the predictions and the validity of rule 1.

Conclusion

In this thesis a model for pedestrians was designed by taking a paradigmatic out-of-equilibrium system from statistical mechanics, the TASEP, and implementing it with a new update scheme, the frozen shuffle update. This update scheme is expected to reproduce the very regular behaviour of pedestrians and the new phase variables associated to the particles may be interpreted as representing the step cycle of pedestrians. These phases already constitute frozen disorder, which allowed us to use the deterministic version of the update scheme. This update scheme was then studied in the simplest geometries, as in the deterministic case many exact calculations can be carried out.

On a one-dimensional periodic lane the density-current relation (or fundamental diagram) has been computed exactly for an infinite system and the leading order finite-size corrections could be obtained as well [91]. This fundamental diagram shows that frozen shuffle update is more efficient at transporting matter than other widely used updates.

With open boundary conditions the phase diagram was derived, showing the transition between free flow and jammed flow common to many variants of TASEP [92]. The values of the density and the current were derived as well. This study also highlighted the notion of platoon, *i.e.* a sequence of particles with ordered phases moving as a whole.

In the case of two one-dimensional open lanes intersecting in one site [93], a pairing mechanism of the platoons was discovered, greatly simplifying the analysis of the model. Thanks to this mechanism the phase diagram could be obtained, showing that each lane can be either in free flow or jammed. The values of the densities and currents could be obtained as well and can even be generalized to more complex geometries.

A useful analytical tool to study jamming transitions in the TASEP is the domain wall theory. Although this theory is very successful when applied to the continuous time TASEP and many of its variants, discrepancies were observed when using updates relevant to traffic applications such as parallel or frozen shuffle update. Indeed, while the spatial correlations are unimportant in the case of continuous time, our calculations show in a very clear way that for a generic updating scheme these correlations cannot be neglected and have a quantitative effect on the dynamics of the wall. Considering the case of parallel update we have shown that the discrepancy can be understood analytically, as a new exact domain wall theory can be built instead. Indeed an exact dynamical

solution of the system is possible in terms of a microscopically-defined domain wall, whose diffusion coefficient is different from what would be given by the usual domain wall theory.

In a second part we model pedestrians at the crossing of streets. Intersecting pedestrian streets is an ubiquitous situation in everyday life, and the presence of the intersection can obviously create jams or even danger in more extreme cases. It has therefore been studied in the pedestrian literature, both experimentally and numerically. In experiments the formation of a striped pattern has been observed, a pattern that numerical codes are required to reproduce as a validation. In this thesis we wanted to provide an explanation to this pattern formation by the means of designing a simple model that would be amenable to analytic methods and studying it. In this process continuous space was replaced by a lattice, pedestrians by hard-core particles, and the complex cognitive procedure each one of us follows to choose his path by an imposed hopping direction for each particle. Here we stress the fact that this model is indeed minimal, as its only ingredients are self-propelled particles with different directions and exclusion, and are clearly both needed to observe pattern formation.

As expected from the studies of part I, in this model a jamming transition occurs, that was studied numerically in Ref. [120]. Here we were more specifically interested in the study of pattern formation, which occurs in the free flow phase, and to test its generality we introduced a second update scheme, namely alternating parallel update. Alternating parallel update is widely used in traffic applications, and also has the advantage of making the calculations simpler. Introducing alternating parallel update also introduced a way to test the robustness of the predictions we made.

The model was first studied on a torus, in which case it becomes very close to the BML model for car traffic in a city [39]. A diagonal pattern similar to the one already observed in pedestrian experiments [10] or simulations [21, 131] was observed. We explained this pattern thanks to a linear instability of some 'mean-field' equations.

With open boundary conditions we found that these stripes are still observed. Their angle however depends on space and is found to be roughly constant above and below the main diagonal, so that the alignments look like chevrons. Two methods were designed and compared in order to measure the chevron angle, showing that it stays roughly constant in two triangles symmetric with respect to the diagonal. Even though it is absent from the linearized equations, the same chevron effect appears in the numerical resolution of the full nonlinear mean-field equations.This is a strong indication of the robustness of the chevron effect, as the effect can now be expected to be seen in all systems that are correctly approximated by the equations, including the particle model with frozen shuffle or alternating parallel update.

The chevron effect can be understood analytically by considering effective

interactions between particles going in the same direction, enabling us to isolate the propagation mode accounting for this deviation. This mode is sustained by collisions, making it an intrinsically nonlinear effect. From a wider perspective, this explanation constitutes a simple instance of effective medium-mediated interactions, as can be found in problems of colloids interacting inside a solution for example. It is even the only out-of-equilibrium case for which exact calculations have been performed, as it requires the description of the interaction at the level of a single realization.

Generalizations of the symmetric open intersection have been briefly studied as well. Asymmetric entrance rates result in an asymmetry in the triangle shapes and in the values of the angles, that can however be understood by straightforward extensions of the arguments for the symmetric case. Studying a nondeterministic variant of the intersection shows that the ordered structure is destroyed by the fluctuations in our model. Fluctuations are of course present as well in real pedestrian systems, but we have to keep in mind that the diagonal pattern is indeed observed in reality, putting a theoretical upper bound on the noise. Finally, in a cylindrical geometry some more involved transient effects can be explained as well.

It is not clear whether the chevron effect could be observed in pedestrian experiments, but here we will give some arguments in favor of this possibility. At first one could think that looking for the chevron effect is hopeless. In the model, the deviation from 45° is of order $\overline{\rho}$ and therefore quite small, and can be measured only for large intersections. Real pedestrians also are clearly more noisy than our ideal particles [89, 13], which could destroy the effect. Actually, it has been argued in section 4.2 that the relevant parameter to quantify the intensity of the chevrons is the number of collisions a particle undertakes when it goes through the crossing. In experiments the average density $\overline{\rho}$ is much larger than in our simulations, which allows the diagonal stripes to manifest themselves in much smaller intersections. Moreover pedestrians are larger than the particles with respect to the size of the intersection, which may amplify the chevron effect. As a result, the total number of collisions undertaken by a particle in our simulations, which scales like $\overline{\rho}M$, becomes comparable to typical experimental values. We may add that, even if the motion of real pedestrians is not completely regular, the diagonal striped pattern is still observed, putting a theoretical upper bound on the noise. Up to now, the measurements that would allow one to characterize precisely the diagonal pattern in experiments have not been performed yet, and there is of course no proof that the chevron effect exists.

In chapter 2 a new update for pedestrians has also been designed, that could potentially be applied to many standard situations of pedestrian modeling. Evacuation models constitute a wide class of pedestrian models, being either simple lattice models as the one studied in my thesis [60, 84, 61, 19, 35] or more sophisticated ones for precise applications [168, 85, 86].

In a collaboration between C. Appert-Rolland, C. Arita and myself frozen shuffle update is used in a standard room evacuation model, where particles, still representing pedestrians, are directed towards the exit of a room. In evacuation models a very popular 'faster-is-slower effect' was discovered, in which the total exit time of the room is larger when people are more strongly directed towards the exit. In the cellular automaton model with parallel update of Ref. [84] the effect is rather expectable, as the authors introduce a 'friction' that render the output flow less effective when more pedestrians are present, the underlying idea being that the pedestrians may impede each other. We will show that this effect can be reproduced without friction by appropriately choosing the update scheme in future work.

We have spent some time attempting to assess the generality of the chevron effect, which basically requires that the hopping rates are deterministic and that every particle hops exactly once per time step. This problem can be recast in the more general framework of cellular automata. Wolfram extensively studied one dimensional deterministic cellular automata [169, 170]. He ended up classifying them in 'universality classes' depending on the type of pattern observed in the stationary state [170], this classification being partly extended to two dimensions [171]. In our case we have to deal with stochastic cellular automata, and the mean-field equations presented in this thesis seem to act like a classifying device in the sense that we expect all the cellular automata that are described by these mean-field equations to share some properties, *e.g.* the chevron effect.

Generalizations of the model are possible and have not been studied. Lane changes could for example be allowed, and their effect on the patterns would probably depend on the precise implementation. This modification does however not seem that relevant to pedestrians, as it seems much harder to overtake in a dense crowd composed of large pedestrians than in our enormous crossings with small diluted particles, and we know anyway that the diagonal pattern is indeed observed in the experiments. Allowing the particles to change their direction could provide a model for *e.g.* turning cars but also, depending on the dynamical rules, a discrete version of the Vicsek model for active matter [172].

Although the main features of the diagonal pattern have been explained analytically, there are still a lot of perspectives in this direction. For example, we stress the fact that no analytical prediction exists for the jamming transition. This indeed seems a pretty hard problem, as there seems to exist long-lived metastable states, the jamming transition possibly being controlled by rare events that are *a priori* not simple to isolate at all. Whereas the mean-field equations were rather successful, more analytical predictions could perhaps be derived from a possible space-continuous version of these equations, for example for the envelope of the instability.

Finally, the $M \to \infty$ limit is certainly not relevant to pedestrians but is a fundamental property of the model from a statistical physics point of view.

While numerical results on the particle system with OBC seem to indicate that the chevron pattern is stable in an infinite intersection, the results from the equations in CBC suggest the contrary. In any case only an analytic proof holds for an infinite intersection, which seems hard to obtain by arguments similar to those of chapter 6.

To summarize, the topic studied in this thesis is intermediate between pedestrian modeling and statistical mechanics. The inspiration to propose frozen shuffle update and the intersection model came from pedestrian issues and a lot of attention has been given to the pedestrian literature. The methods used to model this intersection however come directly from statistical mechanics, the model ending up being very simple and the dimension of the parameter space reduced to 2 for most of this thesis. This work therefore addresses issues relevant to out-of-equilibrium statistical mechanics as well, such as the importance of the update scheme or the development of approximate coarse-grained theories such as the domain wall theory. It is also clear that with simplicity comes generality, and that neither the one-dimensional models nor the intersection model are very specific to pedestrians. This is for example shown by the quite unexpected link between the effective interactions treatment from section 6.3 and fluid mechanics problems of colloidal solutions.

Bibliography

[1] C. Castellano, S. Fortunato, and V. Loreto, "Statistical physics of social dynamics," *Rev. Mod. Phys.*, vol. 81, pp. 591–646, 2009.

[2] V. Yakovenko, "Econophysics, statistical mechanics approach to," in *Encyclopedia of Complexity and System Science* (R. A. Meyers, ed.), Springer, 2009.

[3] R. A. Blythe and A. J. McKane, "Stochastic models of evolution in genetics, ecology and linguistics," *J. Stat. Mech.: Theor. Exp.*, p. P07018, 2007.

[4] T. Gueudré, A. Dobrinevski, and J.-P. Bouchaud, "Explore or exploit? a generic model and an exactly solvable case," *Phys. Rev. Lett.*, vol. 112, p. 050602, 2014.

[5] T. Chou, K. Mallick, and R. K. P. Zia, "Non-equilibrium statistical mechanics: from a paradigmatic model to biological transport," *Reports on progress in physics*, vol. 74, p. 116601, 2011.

[6] D. Helbing, A. Johansson, and H. Z. Al-Abideen, "The dynamics of crowd disasters: An empirical study," *Phys, Rev. E*, vol. 75, p. 046109, 2007.

[7] X. Zhang, W. Weng, H. Yuan, and J. Chen, "Empirical study of a unidirectional dense crowd during a real mass event," *Physica A-Stat. Mech. and its Applic.*, vol. 392, pp. 2781–2791, 2013.

[8] U. Weidmann, U. Kirsch, and M. Schreckenberg, eds., *Pedestrian and Evacuation Dynamics 2012*. Springer, 2014.

[9] M. Boltes, M. Chraibi, A. Schadschneider, and A. Seyfried, eds., *Traffic and Granular Flows 2013*. Springer, 2014.

[10] S. P. Hoogendoorn and W. Daamen, "Self-organization in walker experiments," in *Traffic and Granular Flow '03* (S. Hoogendoorn, S. Luding, P. Bovy, and et al., eds.), pp. 121–132, Springer, 2005.

[11] U. Chattaraj, A. Seyfried, and P. Chakroborty, "Comparison of pedestrian fondamental diagram across cultures," *Advances in Complex Systems*, vol. 12, pp. 393–405, 2009.

[12] C. Appert-Rolland, A. Jelić, P. Degond, J. Fehrenbach, J. Hua, A. Crétual, R. Kulpa, A. Marin, A.-H. Olivier, S. Lemercier, and J. Pettré, "Experimental study of the following dynamics of pedestrians," in *Pedestrian and Evacuation Dynamics 2012* (ed.:, ed.), Berlin, Springer, 2012.

[13] A. Jelić, C. Appert-Rolland, S. Lemercier, and J. Pettré, "Properties of pedestrians walking in line – fundamental diagrams," *Phys. Rev. E*, vol. 85, p. 036111, 2012.

[14] A. Jelić, S. Lemercier, C. Appert-Rolland, and J. Pettré, "Properties of pedestrians walking in line: Stepping behavior," *Phys. Rev. E*, vol. 86, p. 046111, 2012.

[15] M. Moussaïd, E. Guillot, M. Moreau, J. Fehrenbach, O. Chabiron, S. Lemercier, J. Pettré, C. Appert-Rolland, P. Degond, and G. Theraulaz, "Traffic instabilities in self-organized pedestrian crowds," *PLoS Computational Biology*, vol. 8, p. 1002442, 2012.

[16] W. Daamen and S. P. Hoogendoorn, "Experimental research of pedestrian walking behavior," *Transportation Research Record*, vol. 1828, pp. 20–30, 2003.

[17] E. Cepolina and N. Tyler, "Understanding capacity drop for designing pedestrian environments," in *Proceedings of the 6th international Walk21 conference*, 2005.

[18] T. Kretz, A. Grünebohm, and M. Schreckenberg, "Experimental study of pedestrian flow through a bottleneck," *J. Stat. Mech.*, p. P10014, 2006.

[19] D. Yanagisawa, A. Kimura, A. Tomoeda, R. Nishi, Y. Suma, K. Ohtsuka, and K. Nishinari, "Introduction of frictional and turning function for pedestrian outflow with an obstacle," *Phys. Rev. E*, vol. 80, p. 036110, 2009.

[20] D. Helbing, "Traffic and related self-driven many-particle systems," *Rev. Mod. Phys.*, vol. 73, pp. 1067–1141, 2001.

[21] S. Hoogendoorn and P. H. L. Bovy, "Simulation of pedestrian flows by optimal control and differential games," *Optim. Control Appl. Meth.*, vol. 24, pp. 153–172, 2003.

[22] J. Ondrej, J. Pettré, A.-H. Olivier, and S. Donikian, "A synthetic-vision based steering approach for crowd simulation," in *SIGGRAPH '10: ACM SIGGRAPH 2010 Papers*, 2010.

[23] S. Paris, J. Pettré, and S. Donikian, "Pedestrian reactive navigation for crowd simulation: a predictive approach," *Computer Graphics Forum - Eurographics*, vol. 26, no. 3, pp. 665–674, 2007.

[24] J. Pettré, J. Ondřej, A.-H. Olivier, A. Cretual, and S. Donikian, "Experiment-based modeling, simulation and validation of interactions between virtual walkers," in *SCA '09: Proceedings of the 2009 ACM SIGGRAPH/Eurographics Symposium on Computer Animation*, pp. 189–198, The Eurographics Association, 2009.

[25] S. Guy, S. Curtis, M. Lin, and D. Manocha, "Least-effort trajectories lead to emergent crowd behaviors," *Phys. Rev. E*, vol. 85, p. 016110, 2012.

[26] S. Lemercier, A. Jelić, R. Kulpa, J. Hua, J. Fehrenbach, P. Degond, C. Appert-Rolland, S. Donikian, and J. Pettré, "Realistic following behaviors for crowd simulation," in *Eurographics 2012* (T. P. Cignoni, ed.), vol. 31, 2012.

[27] P. Degond, C. Appert-Rolland, M. Moussaid, J. Pettré, and G. Theraulaz, "A hierarchy of heuristic-based models of crowd dynamics," *J. Stat. Phys.*, vol. 152, pp. 1033–1068, 2013.

[28] P. Degond, C. Appert-Rolland, J. Pettré, and G. Theraulaz, "Vision-based macroscopic pedestrian models," *Kinetic and Related Models*, vol. 6, pp. 809–839, 2013.

[29] A. Keßel, H. Klüpfel, and M. Schreckenberg, "Microscopic simulation of pedestrian crowd motion," in *Pedestrian and Evacuation Dynamics* (M. Schreckenberg and S. Sharma, eds.), pp. 193–202, Springer, 2002.

[30] A. Schadschneider, A. Kirchner, and K. Nishinari, "From ant trails to pedestrian dynamics," in *Pedestrian and Evacuation Dynamics* (M. Schreckenberg and S. S. (Eds.), eds.), Springer, 2002.

[31] A. Schadschneider, "Modelling of transport and traffic problems," *Lecture Notes in Computer Science*, vol. 5191, pp. 22–31, 2008.

[32] R. L. Hughes, "A continuum theory for the flow of pedestrians," *Transportation Research Part B*, vol. 36, pp. 507–535, 2002.

[33] C. Appert-Rolland, P. Degond, and S. Motsch, "Two-way multi-lane traffic model for pedestrians in corridors," *Networks and Heterogeneous Media*, vol. 6, pp. 351–381, 2011.

[34] A. Schadschneider, "Cellular automaton approach to pedestrian dynamics - theory," in *Pedestrian and Evacuation Dynamics* (M. Schreckenberg and S. S. (Eds.), eds.), pp. 75–85, Springer, 2002.

[35] J. Tanimoto, A. Hagishima, and Y. Tanaka, "Study of bottleneck effect at an emergency evacuation exit using cellular automata model, mean field approximation analysis, and game theory," *Physica A*, vol. 389, pp. 5611–5618, 2011.

[36] S. Wolfram, *A new kind of science*. Wolfram media, 2002.

[37] T. Naka, "Mechanism of cross passenger flow," *Transactions of the Architectural Institute of Japan*, vol. 258, pp. 93–102, 1977.

[38] K. Ando, H. Ota, and T. Oki, "Forecasting the flow of people," *Railway Research Review*, vol. 45, pp. 8–14, 1988.

[39] O. Biham, A. Middleton, and D. Levine, "Self-organization and a dynamic transition in traffic-flow models," *Phys. Rev. A*, vol. 46, pp. R6124–R6127, 1992.

[40] C. T. MacDonald, J. H. Gibbs, and A. C. Pipkin, "Kinetics of biopolymerization on nucleic acid templates," *Biopolymers*, vol. 6, pp. 1–25, 1968.

[41] F. Spitzer, "Interaction of markov processes," *Advances in Mathematics*, vol. 5, pp. 246–290, 1970.

[42] T. Liggett, *Interacting Particle Systems*. Springer, 1985.

[43] T. Liggett, *Stochastic Interacting Systems: Contact, Voter and Exclusion Processes*. Springer, 1999.

[44] S. Katz, J. L. Lebowitz, and H. Spohn, "Nonequilibrium steady states of stochastic lattice gas models of fast ionic conductors," *J. Stat. Phys.*, vol. 34, pp. 497–537, 1984.

[45] B. Schmittmann and R. Zia, *Statistical Mechanics of driven diffusive systems*, vol. 17 of *Phase Transitions and Critical Phenomena*. Academic Press, New York, 1995.

[46] M. R. Evans and T. Hanney, "Nonequilibrium statistical mechanics of the zero-range process and related models," *J. Phys. A: Math. Gen.*, vol. 38, pp. R195–R239, 2005.

[47] M.Kardar, G.Parisi, and Y.-C. Zhang, "Dynamic scaling of growing interfaces," *Phys. Rev. Lett.*, vol. 56, pp. 889–892, 1986.

[48] T. Kriecherbauer and J. Krug, "A pedestrians view on interacting particle systems, KPZ universality, and random matrices," *J. Phys. A.*, vol. 43, p. 403001, 2010.

[49] B. Derrida and J. Lebowitz, "Exact large deviation function in the asymmetric exclusion process," *Phys. Rev. Lett.*, vol. 80, pp. 209–213, 1998.

[50] B. Derrida, "An exactly soluble non-equilibrium system: the asymmetric simple exclusion process," *Physics Reports*, vol. 301, pp. 65–83, 1998.

[51] B. Derrida, J. L. Lebowitz, and E. R. Speer, "Free energy functional for nonequilibrium systems: An exactly solvable case," *Phys. Rev. Lett.*, vol. 87, p. 150601, 2001.

[52] R. Glauber, "Time-dependent statistics of the ising model," *J. Math. Phys.*, vol. 4, pp. 294–307, 1963.

[53] D. T. Gillespie, "Exact stochastic simulation of coupled chemical reactions," *J. Chem. Phys.*, vol. 281, pp. 2340–2361, 1977.

[54] M. Wölki, A. Schadschneider, and M. Schreckenberg, "Asymmetric exclusion processes with shuffled dynamics," *J. Phys. A: Math. Gen.*, vol. 39, pp. 33–44, 2006.

[55] D. A. Smith and R. E. Wilson, "Dynamical pair approximation for cellular automata with shuffle update," *J. Phys. A: Math. Theor.*, vol. 40, no. 11, pp. 2651–2664, 2007.

[56] K. Nagel and M. Schreckenberg, "A cellular automaton model for freeway traffic," *J. Physique I*, vol. 2, pp. 2221–2229, 1992.

[57] D. Chowdhury and A. Schadschneider, "Self-organization of traffic jams in cities: Effects of stochastic dynamics and signal periods," *Phys. Rev. E*, vol. 59, pp. R1311–R1314, 1999.

[58] D. Chowdhury, L. Santen, and A. Schadschneider, "Statistical physics of vehicular traffic and some related systems," *Physics Reports*, vol. 329, pp. 199–329, 2000.

[59] K. Nagel, "Particle hopping models and traffic flow theory," *Phys. Rev. E*, vol. 53, pp. 4655–4672, 1996.

[60] C. Burstedde, K. Klauck, A. Schadschneider, and J. Zittartz, "Simulation of pedestrian dynamics using a 2-dimensional cellular automaton," *Physica A*, vol. 295, p. 507525, 2001.

[61] A. Kirchner, K. Nishinari, and A. Schadschneider, "Friction effects and clogging in a cellular automaton model for pedestrian dynamics," *Phys. Rev. E*, vol. 67, pp. 1–10, 2003.

[62] J. Krug, "Boundary-induced phase transitions in driven diffusive systems," *Phys. Rev. Lett.*, vol. 67, p. 1882, 1991.

[63] B. Derrida, E. Domany, and D. Mukamel, "An exact solution of a one-dimensional asymmetric exclusion model with open boundaries," *J. Stat. Phys.*, vol. 69, p. 667, 1992.

[64] B. Derrida, M. R. Evans, V. Hakim, and V. Pasquier, "Exact solution of a 1d asymmetric exclusion model using a matrix formulation," *J. Phys. A: Math. Gen.*, vol. 26, pp. 1493–1517, 1993.

[65] G. Schütz and E. Domany, "Phase transitions in an exactly soluble one-dimensional exclusion process," *J. Stat. Phys.*, vol. 72, pp. 277–296, 1993.

[66] N. Rajewsky, L. Santen, A. Schadschneider, and M. Schreckenberg, "The asymmetric exclusion process: Comparison of update procedures," *J. Stat. Phys.*, vol. 92, pp. 151–194, 1998.

[67] G. Schütz, "Exact solution of the master equation for the asymmetric exclusion process," *J. Stat. Phys.*, vol. 88, pp. 427–445, 1997.

[68] T. Sasamoto, "Fluctuations of the one-dimensional asymmetric exclusion process using random matrix techniques," *J. Stat. Mech.*, p. P07007, 2007.

[69] K. Johansson, "Shape fluctuations and random matrices," *Commun. Math. Phys.*, vol. 209, pp. 437–476, 2000.

[70] M. R. Evans, N. Rajewsky, and E. R. Speer, "Exact solution of a cellular automaton for traffic," *J. Stat. Phys.*, vol. 95, pp. 45–96, 1999.

[71] B. Derrida, J. L. Lebowitz, and E. R. Speer, "Exact large deviation functional of a stationary open driven diffusive system," *Phys. Rev. Lett.*, vol. 89, pp. 1–4, 2002.

[72] B. Derrida, J. L. Lebowitz, and E. R. Speer, "Exact large deviation functional of a stationary open driven diffusive system: The asymmetric exclusion process," *J. Stat. Phys.*, vol. 110, pp. 775–810, 2003.

[73] D. Chowdhury, A. Schadschneider, and K. Nishinari, "Physics of transport and traffic phenomena in biology: from molecular motors and cells to organisms," *Physics of life reviews*, vol. 2, p. 318, 2005.

[74] A. Parmeggiani, T. Franosch, and E. Frey, "Phase coexistence in driven one dimensional transport," *Phys. Rev. Lett.*, vol. 90, p. 086601, 2003.

[75] A. Parmeggiani, T. Franosch, and E. Frey, "Totally asymmetric simple exclusion process with Langmuir kinetics," *Phys. Rev. E*, vol. 70, p. 046101, 2004.

[76] L. Ciandrini, M. C. Romano, and A. Parmeggiani, "Stepping and crowding: statistical kinetics from an exclusion process perspective," *arXiv:1312.1911*.

[77] R. J. Concannon and R. A. Blythe, "Spatiotemporally complete condensation in a non-poissonian exclusion process," *Phys. Rev. Lett.*, vol. 112, p. 050603, 2014.

[78] C. Schiffmann, C. Appert-Rolland, and L.Santen, "Shock dynamics of two-lane driven lattice gases," *J. Stat. Mech.*, p. P06002, 2010.

[79] T. Reichenbach, T. Franosch, and E. Frey, "Exclusion processes with internal states," *Phys. Rev. Lett.*, vol. 97, p. 050603, 2006.

[80] E. Pronina and A. B. Kolomeisky, "Asymmetric coupling in two-channel exclusion processes," *Physica A*, vol. 372, pp. 12–21, 2006.

[81] I. Neri, N. Kern, and A. Parmeggiani, "Modelling cytoskeletal traffic: an interplay between passive diffusion and active transport," *Phys. Rev. Lett.*, vol. 110, p. 098102, 2013.

[82] I. Neri, N. Kern, and A. Parmeggiani, "Exclusion processes on networks as models for cytoskeletal transport," *New J. Phys.*, vol. 15, p. 085005, 2013.

[83] M. E. Foulaadvand, Z. Sadjadi, and M. R. Shaebani, "Optimized traffic flow at a single intersection: traffic responsive signalization," *J. Phys. A: Math. Gen.*, vol. 37, pp. 561–576, 2004.

[84] A. Kirchner, H. Klüpfel, K. Nishinari, A. Schadschneider, and M. Schreckenberg, "Simulation of competitive egress behavior: comparison with aircraft evacuation data," *Physica A*, vol. 324, pp. 689–697, 2003.

[85] S. Heliövaara, H. Ehtamo, D. Helbing, and T. Korhonen, "Patient and impatient pedestrians in a spatial game for egress congestion," *Phys. Rev. E*, vol. 87, p. 012802, 2013.

[86] S. Bouzat and M. N. Kuperman, "Game theory in models of pedestrian room evacuation," *Phys. Rev. E*, vol. 87, p. 022802, 2013.

[87] K. Nishinari, K. Sugawara, T. Kazama, A. Schadschneider, and D. Chowdhury, "Modelling of self-driven particles: Foraging ants and pedestrians," *Physica A*, vol. 372, pp. 132–141, 2006.

[88] J. Zhang, W. Mehner, S. Holl, M. Boltes, E. Andresen, A. Schadschneider, and A. Seyfried, "Universal flow-density relation of single-file bicycle, pedestrian and car motion," *arXiv:1312.2735v1*, 2014.

[89] A. Schadschneider and A. Seyfried, "Empirical results for pedestrian dynamics and their implications for modeling," *Networks and Heterogeneous Media*, vol. 6, pp. 545–560, 2011.

[90] H. Klüpfel, "The simulation of crowds at very large events," in *Traffic and Granular Flow ' 05* (A. Schadschneider, T. Poschel, R. Kuhne, M. Schreckenberg, and D. Wolf, eds.), pp. 341–346, 2007.

[91] C. Appert-Rolland, J. Cividini, and H. J. Hilhorst, "Frozen shuffle update for an asymmetric exclusion process on a ring," *J. Stat. Mech.*, p. P07009, 2011.

[92] C. Appert-Rolland, J. Cividini, and H. J. Hilhorst, "Frozen shuffle update for an asymmetric exclusion process with open boundary conditions," *J. Stat. Mech.*, p. P10013, 2011.

[93] C. Appert-Rolland, J. Cividini, and H. J. Hilhorst, "Intersection of two TASEP traffic lanes with frozen shuffle update," *J. Stat. Mech.*, p. P10014, 2011.

[94] J. Cividini, C. Appert-Rolland, and H. J. Hilhorst, "Frozen shuffle update in simple geometries : a first step to simulate pedestrians," in *Proceedings of the 6th International Conference on Pedestrian and Evacuation Dynamics*, Springer, 2014.

[95] J. Cividini, H. J. Hilhorst, and C. Appert-Rolland, "Exact domain wall theory for deterministic tasep with parallel update," *J. Phys. A: Math. Theor.*, vol. 47, p. 222001, 2014.

[96] A. J. Bray, "Theory of phase ordering kinetics," *Advances in Physics*, vol. 43, pp. 357–459, 1994.

[97] T. Vachaspati, *Kinks and Domain Walls An Introduction to Classical and Quantum Solitons*. Cambridge, 2010.

[98] A. Vilenkin, "Cosmic strings and domain walls," *Physics reports*, vol. 121, pp. 263–315, 1985.

[99] A. B. Kolomeisky, G. M. Schütz, E. B. Kolomeisky, and J. P. Straley, "Phase diagram of one-dimensional driven lattice gases with open boundaries," *J. Phys. A*, vol. 31, pp. 6911–6919, 1998.

[100] M. Dudzinski and G. M. Schütz, "Relaxation spectrum of the asymmetric exclusion process with open boundaries," *J. Phys. A*, vol. 33, p. 8351, 2000.

[101] Z. Nagy, C. Appert, and L. Santen, "Relaxation times in the ASEP model using a DMRG method," *J. Stat. Phys.*, vol. 109, pp. 623–639, 2002.

[102] P. Pierobon, A. Parmeggiani, F. von Oppen, and E. Frey, "Dynamic correlation functions and Boltzmann-Langevin approach for driven one-dimensional lattice gas," *Phys. Rev. E*, vol. 72, p. 036123, 2005.

[103] R. Juhasz and L. Santen, "Dynamics of an exclusion process with creation and annihilation," *J. Phys. A: Math. Gen.*, vol. 37, pp. 3933–3944, 2004.

[104] T. Reichenbach, T. Franosch, and E. Frey, "Domain wall delocalization, dynamics and fluctuations in an exclusion process with two internal states," *The European Physical Journal E: Soft Matter and Biological Physics*, vol. 27, pp. 47–56, 2008.

[105] C. Arita and A. Schadschneider, "Dynamical analysis of the exclusive queuing process.," *Phys. Rev. E*, vol. 83, p. 051128, 2011.

[106] E. Pronina and A. B. Kolomeisky, "Theoretical investigation of totally asymmetric exclusion processes on lattices with junctions," *J. Stat. Mech.*, p. P07010, 2005.

[107] Y.-M. Yuan, R. Jiang, R. Wang, Q.-S. Wu, and J.-Q. Zhang, "Spontaneous symmetry breaking in totally asymmetric simple exclusion processes on two intersected lattices," *J. Phys. A: Math. Theor.*, vol. 41, p. 035003, 2008.

[108] V. Popkov and G. M. Schütz, "Steady-state selection in driven diffusive systems with open boundaries," *Europhys. Lett.*, vol. 48, pp. 257–263, 1999.

[109] J. de Gier and F. H. L. Essler, "Bethe ansatz solution of the asymmetric exclusion process with open boundaries," *Phys. Rev. Lett.*, vol. 95, p. 240601, 2005.

[110] J. de Gier and F. H. L. Essler, "Exact spectral gaps of the asymmetric exclusion process with open boundaries," *J. Stat. Mech.: Theor. Exp.*, p. P12011, 2006.

[111] A. Proeme, R. A. Blythe, and M. R. Evans, "Dynamical transition in the open-boundary totally asymmetric exclusion process," *J. Phys. A: Math. Theor.*, vol. 44, p. 035003, 2011.

[112] C. Pigorsch and G. M. Schütz, "Shocks in the asymmetric simple exclusion process in a discrete-time update," *J. Phys. A: Math. Gen.*, vol. 33, pp. 7919–7933, 2000.

[113] L. J. Cook and R. K. P. Zia, "Feedback and fluctuations in a totally asymmetric simple exclusion process with finite resources," *J. Stat. Mech.*, p. P02012, 2009.

[114] V. Belitsky and G. M. Schütz, "Cellular automaton model for molecular traffic jams," *J. Stat. Mech.*, p. P07007, 2011.

[115] V. Belitsky and G. M. Schütz, "Microscopic position and structure of a shock in CA 184," *J. Phys. A: Math. Theor.*, vol. 44, p. 445003, 2011.

[116] J. D. Gier and B. Nienhuis, "Exact stationary state for an asymmetric exclusion process with fully parallel dynamics," *Phys. Rev. E*, vol. 59, pp. 4899–4911, 1999.

[117] L. G. Tilstra and M. H. Ernst, "Synchronous asymmetric exclusion processes," *J. Phys. A: Math. Gen.*, vol. 31, pp. 5033–5063, 1998.

[118] B. Derrida, S. A. Janowsky, J. L. Lebowitz, and E. R. Speer, "Exact solution of the totally asymmetric simple exclusion process: Shock profiles," *J. Stat. Phys.*, vol. 73, pp. 813–842, 1993.

[119] T. Kretz, "Crowd research at school: Crossing flows." Talk at the TGF'13 conference, 2013.

[120] H. J. Hilhorst and C. Appert-Rolland, "A multi-lane TASEP model for crossing pedestrian traffic flows," *J. Stat. Mech.*, p. P06009, 2012.

[121] W. Daamen and S. Hoogendoorn, "Qualitative results from pedestrian laboratory experiments," in *Pedestrian and Evacuation Dynamics* (E. Galea, ed.), pp. 121–132, 2003.

[122] J. Dzubiella, G. P. Hoffmann, and H. Löwen, "Lane formation in colloidal mixtures driven by an external field," *Phys. Rev. E*, vol. 65, p. 021402, 2002.

[123] A. Jelić, C. Appert-Rolland, and L. Santen, "A bottleneck model for bidirectional transport controlled by fluctuations," *Europhys. Lett.*, vol. 98, 2012.

[124] D. Helbing, I. Farkas, and T. Vicsek, "Simulating dynamical features of escape panic," *Nature*, vol. 407, pp. 487–490, 2000.

[125] D. Helbing and A. Johansson, "Pedestrian, crowd, and evacuation dynamics," *Encyclopedia of Complexity and Systems Science*, vol. 16, pp. 6476–6495, 20013.

[126] S. Soria, R. Josens, and D. Parisi, "Experimental evidence of the "faster is slower" effect in the evacuation of ants," *Safety Science*, vol. 50, pp. 1584–1588, 2012.

[127] D. Helbing, L. Buzna, A. Johansson, and T. Werner, "Self-organized pedestrian crowd dynamics: Experiments, simulations, and design solutions," *Transportation Science*, vol. 39, pp. 1–24, 2005.

[128] J. D'Alessandro, D. Chen, A. C. de Verdière, A. Gabeur, T. Giovachini, B. Teinturier, and E. Tham, "Quelques problèmes d'optimisation de flux de personnes dans le métro." Project report of students of the Ecole Polytechnique, 2010.

[129] M. Plaue, "On measuring pedestrian density and flowfields in dense as well as sparse crowds." Talk at the PED2012 conference, 2012.

[130] Y. Chiffaudel, "Modélisation sur réseau d'interactions entre flux piétonniers." Internship report, 2013.

[131] K. Yamamoto and M. Okada, "Continuum model of crossing pedestrian flows and swarm control based on temporal/spatial frequency," in *2011 IEEE International Conference on Robotics and Automation*, pp. 3352–3357, 2011.

[132] S.-I. Tadaki and M. Kikuchi, "Jam phases in a two-dimensional cellular-automaton model of traffic flow," *Phys. Rev. E*, vol. 50, pp. 4564–4570, 1994.

[133] J. M. Molera, F. C. Martinez, J. A. Cuesta, and R. Brito, "Theoretical approach to two-dimensional trafiic how models," *Phys. Rev. E*, vol. 51, pp. 175–187, 1995.

[134] F. C. Martinez, J. A. Cuesta, J. M. Molera, and R. Brito, "Random versus deterministic two-dimensional traffic flow models," *Phys. Rev. E*, vol. 51, pp. R835–R838, 1995.

[135] S.-I. Tadaki, "Two-dimensional cellular automaton model of traffic flow with open boundaries," *Phys. Rev. E*, vol. 54, pp. 2409–2413, 1996.

[136] R. M. D'Souza, "Coexisting phases and lattice dependence of a cellular automaton model for traffic flow," *Phys. Rev. E*, vol. 71, p. 066112, 2005.

[137] Z.-J. Ding, R. J., and B.-H. Wang, "Traffic flow in the Biham-Middleton-Levine model with random update rule," *Phys. Rev. E*, vol. 83, p. 047101, 2011.

[138] Z.-J. Ding, R. Jiang, W. Huang, and B.-H. Wang, "Effect of randomization in the Biham-Middleton-Levine traffic flow model," *J. Stat. Mech.*, p. P06017, 2011.

[139] Z.-J. Ding, R. Jiang, M. Li, Q.-L. Li, and B.-H. Wang, "Effect of violating the traffic light rule in the Biham-Middleton-Levine traffic flow model," *Europhys. Lett.*, vol. 99, p. 68002, 2012.

[140] F. Peruani, T. Klauss, A. Deutsch, and A. Voss-Boehme, "Traffic jams, gliders, and bands in the quest for collective motion of self-propelled particles," *Phys. Rev. Lett.*, vol. 106, p. 128101, 2011.

[141] H. J. Hilhorst, J. Cividini, and C. Appert-Rolland, "Continuous and first-order jamming transition in crossing pedestrian traffic flows," in *Perspectives and Challenges in Statistical Physics and Complex Systems for the Next Decade*, World Scientific, 2014.

[142] J. Cividini, C. Appert-Rolland, and H. J. Hilhorst, "Diagonal patterns and chevron effect in intersecting traffic flows," *Europhys. Lett.*, vol. 102, p. 20002, 2013.

[143] J. Cividini, H. J. Hilhorst, and C. Appert-Rolland, "Crossing pedestrian traffic flows,diagonal stripe pattern, and chevron effect," *J. Phys. A: Math. Theor.*, vol. 46, p. 345002, 2013.

[144] J. Cividini and H. J. Hilhorst *In preparation.*

[145] J. Cividini, "Pattern formation in 2d traffic flows," *DCDS-S*, vol. 7, pp. 395–409, 2014.

[146] J. Cividini in *Proceeding of the TGF'13 conference*, preprint.

[147] C. Barré, "Trafic piétonnier." Internship report, 2012.

[148] J. Cividini and C. Appert-Rolland, "Wake-mediated interaction between driven particles crossing a perpendicular flow," *J. Stat. Mech.*, p. P07015, 2013.

[149] C. Likos, "Effective interactions in soft condensed matter physics," *Physics Reports*, vol. 348, pp. 267–439, 2001.

[150] S. Asakura and F.Oosawa, "On interaction between two bodies immersed in a solution of macromolecules," *J. Chem Phys*, vol. 22, p. 1255, 1954.

[151] S. Asakura and F.Oosawa, "Interactions between particles suspended in solutions of macromolecules.," *Journal of polymer science*, vol. 33, pp. 183–192, 1958.

[152] J. Dzubiella, H. Löwen, and C. N. Likos, "Depletion forces in nonequilibrium," *Phys. Rev. Lett.*, vol. 91, pp. 1–4, 2003.

[153] A. S. Khair and J. F. Brady, "On the motion of two particles translating with equal velocities through a colloidal dispersion," *Proc. R. Soc. A*, vol. 463, pp. 223–240, 2007.

[154] Y. Sokolov, D. Frydel, D. Grier, H. Diamant, and Y. Roichman, "Hydrodynamic pair attractions between driven colloidal particles," *Phys. Rev. Lett.*, vol. 107, p. 158302, 2011.

[155] R. Arratia, "The motion of a tagged particle in the simple symmetric exclusion system on Z," *Ann. Probab.*, vol. 11, pp. 227–456, 1983.

[156] M. J. A. M. Brummelhuis and H. J. Hilhorst, "Tracer particle motion in a two-dimensional lattice gas with low vacancy density," *Physica A*, vol. 156, no. 2, pp. 575–598, 1989.

[157] S. F. Burlatsky, G. Oshanin, M. Moreau, and W. P. Reinhardt, "Motion of a driven tracer particle in a one-dimensional symmetric lattice gas," *Phys. Rev. E*, vol. 54, p. 3165, 1996.

[158] C. Landim, S. Olla, and S. B. Volchan, "Driven tracer particle in one dimensional symmetric simple exclusion," *Commun. Math. Phys.*, vol. 192, pp. 287–307, 1998.

[159] J. D. Coninck, G. Oshanin, and M. Moreau, "Dynamics of a driven probe molecule in a liquid monolayer," *Europhys. Lett.*, vol. 38, p. 527, 1997.

[160] O. Bénichou, A. M. Cazabat, J. D. Coninck, M. Moreau, and G. Oshanin, "Directed random walk in adsorbed monolayer," *Physica A*, vol. 272, p. 56, 1999.

[161] O. Bénichou, A. Cazabat, J. D. Coninck, M. Moreau, and G. Oshanin, "Stokes formula and density perturbances for driven tracer diffusion in an adsorbed monolayer," *Phys. Rev. Lett.*, vol. 84, p. 511, 2000.

[162] O. Bénichou, J. Klafter, M. Moreau, and G. Oshanin, "Generalized model for dynamic percolation," *Phys. Rev. E*, vol. 62, p. 3327, 2000.

[163] O. Bénichou, A. M. Cazabat, J. D. Coninck, M. Moreau, and G. Oshanin, "Force-velocity relation and density profiles for biased diffusion in an adsorbed monolayer," *Phys. Rev. B*, vol. 63, p. 235413, 2001.

[164] O. Bénichou, P. Illien, C. Mejía-Monasterio, and G. Oshanin, "A biased intruder in a dense quiescent medium: looking beyond the force-velocity relation," *J. Stat. Mech.*, p. P05008, 2013.

[165] I. M. Jánosi, T. Tèl, D. E. Wolf, and J. A. C. Gallas, "Chaotic particle dynamics in viscous flows: The three-particle stokeslet problem," *Phys. Rev. E*, vol. 56, pp. 2858–2868, 1997.

[166] F. Pacheco-Vázquez and J. Ruiz-Suárez, "Cooperative dynamics in the penetration of a group of intruders in a granular medium," *Nat. Communs.*, vol. 1, p. 123, 2010.

[167] C. Mejía-Monasterio and G. Oshanin, "Bias- and bath-mediated pairing of particles driven through a quiescent medium," *Soft Matter*, vol. 7, pp. 993–1000, 2011.

[168] H. Klüpfel, T. Meyer-König, J. Wahle, and M. Schreckenberg, "Microscopic simulation of evacuation processes on passenger ships," in *Theory and Practical Issues on Cellular Automata* (T. W. S. Bandini, ed.), pp. 63–71, Springer London, 2001.

[169] S. Wolfram, "Statistical mechanics of cellular automata," *Rev. Mod. Phys.*, vol. 55, pp. 601–644, 1983.

[170] S. Wolfram, "Universality and complexity in cellular automata.," *Physica D*, vol. 10, pp. 1–35, 1984.

[171] N. Packard and S. Wolfram, "Two-dimensional cellular automata.," *J. Stat. Phys.*, vol. 38, pp. 901–946, 1985.

[172] T. Vicsek, A. Czirk, E. Ben-Jacob, I. Cohen, and O. Shochet, "Novel type of phase transition in a system of self-driven particles," *Phys. Rev. Lett.*, vol. 75, pp. 1226–1229, 1995.

Appendix A

Linear equations in OBC

In this appendix we present the intermediate steps of the calculation of the Green function of the linear equations (5.19)-(5.20) outlined in subsection 5.2.3.

We define $\delta\rho_t^{\mathcal{E}}$ as the M^2-component vector that contains al the $\delta\rho_t^{\mathcal{E}}(\mathbf{r})$, similarly for $\delta\rho_t^{\mathcal{N}}$, and we group these two vectors into $\delta\rho_t \equiv (\delta\rho_t^{\mathcal{E}}\,\delta\rho_t^{\mathcal{N}})^T$. Writing $\mathbf{I}$ for the $M \times M$ identity matrix and defining two other $M \times M$ matrices $\mathbf{A}$ and $\mathbf{B}$ by $\mathbf{A}_{i;i'} \equiv (1-\rho)\delta_{i;i'+1} + \rho\delta_{i;i'}$ and $\mathbf{B}_{i;i'} \equiv -\rho\delta_{i;i'} + \rho\delta_{i;i'-1}$, the equations can be rewritten in the form (5.21), with the matrix $\mathbf{M}$ given by

$$\mathbf{M} \equiv \begin{pmatrix} \mathbf{A}\otimes\mathbf{I} & \mathbf{B}\otimes\mathbf{I} \\ \mathbf{I}\otimes\mathbf{B} & \mathbf{I}\otimes\mathbf{A} \end{pmatrix}. \tag{A.1}$$

In the tensor products the first matrix acts on the rows and the second one acts on the columns, *e.g.* $[\mathbf{A}\otimes\mathbf{I}]_{i,j;i',j'} = \mathbf{A}_{i,i'}\mathbf{I}_{j,j'}$.

We now define the generating function of any quantity X_t as $\hat{X}(z) \equiv \sum_{t=0}^{\infty} X_t z^t$ where z is such that the series converge. This transformation may be inverted by integrating in the complex plane $X_t = (2\pi\mathrm{i})^{-1}\oint_{\Gamma_0}\frac{dz}{z^{t+1}}\hat{X}(z)$, where Γ_0 runs counterclockwise around the origin. Applied to Eq. (5.21) this gives

$$z^{-1}\hat{\delta\rho}(z) = \mathbf{M}\hat{\delta\rho}(z) + (1-\overline{\eta})\hat{\eta}(z). \tag{A.2}$$

Eqs. A.2 can be inverted in the z space to give a formal expression of the Green functions defined in Eq. 5.22,

$$\begin{aligned} G^{\mathcal{E}\mathcal{E}}_{i,j;j'}(t-t') &= \frac{1-\overline{\eta}}{2\pi\mathrm{i}}\oint_{\Gamma_0}\frac{\mathrm{d}z}{z^{t-t'}}\left[(\mathbf{I}\otimes\mathbf{I}-\mathbf{F}\otimes\mathbf{F})^{-1}(\mathbf{E}\otimes\mathbf{I})\right]_{i,j;1,j'}, \\ G^{\mathcal{E}\mathcal{N}}_{i,j;i'}(t-t') &= \frac{1-\overline{\eta}}{2\pi\mathrm{i}}\oint_{\Gamma_0}\frac{\mathrm{d}z}{z^{t-t'}}\left[(\mathbf{I}\otimes\mathbf{I}-\mathbf{F}\otimes\mathbf{F})^{-1}(\mathbf{F}\otimes\mathbf{E})\right]_{i,j;i',1}, \end{aligned} \tag{A.3}$$

where the $M \times M$ matrices $\mathbf{E}$ and $\mathbf{F}$ are defined by $\mathbf{E}(z) \equiv (\mathbf{I}-z\mathbf{A})^{-1}$ and $\mathbf{F}(z) \equiv (\mathbf{I}-z\mathbf{A})^{-1}z\mathbf{B}$.

The explicit expression of $\mathbf{E}$ reads

$$\begin{aligned}\mathbf{E}_{i;i'} &= \sum_{p=0}^{\infty} z^p [\mathbf{A}^p]_{i;i'} \\ &= \Theta(i \geq i') \frac{1}{1-z\overline{\eta}} \zeta^{i-i'} \end{aligned} \tag{A.4}$$

with $\zeta(z) \equiv \frac{(1-\overline{\eta})z}{1-\overline{\eta}z}$ and $\Theta(a) = 1$ if assertion a is true and 0 otherwise. To compute $(\mathbf{I}\otimes\mathbf{I} - \mathbf{F}\otimes\mathbf{F})^{-1}$ we need to diagonalize $\mathbf{F}$. Its explicit expression reads

$$\begin{aligned}\mathbf{F}_{i;i'} &= [\mathbf{E}z\mathbf{B}]_{i;i'} \\ &= (\zeta\Theta(2 \leq i' \leq i+1) - \Theta(1 \leq i' \leq i)) \frac{z\overline{\eta}}{1-z\overline{\eta}} \zeta^{i-i'}, \end{aligned} \tag{A.5}$$

The eigenvalues λ and the right and left eigenvectors ψ^λ and ϕ^λ of $\mathbf{F}$ can now be determined. We define the auxiliary quantity $a_q \equiv \cos q + \mathrm{i}(\zeta^{-1} - \cos^2 q)^{1/2}$. The equations $\mathbf{F}\psi^\lambda = \lambda\psi^\lambda$ and $\phi^\lambda\mathbf{F} = \lambda\phi^\lambda$ then give, in components

$$\begin{aligned}\lambda &= \frac{\zeta^2 a_q^2}{c^2}, \\ \psi_k^\lambda &= \mathrm{i}\zeta^k a_q^k (e^{\mathrm{i}kq} - e^{-\mathrm{i}kq}), \\ \phi_k^\lambda &= \frac{-\mathrm{i}}{N_q \zeta^k a_q^k} \Big[\big(1 - a_q^{-1} e^{-\mathrm{i}q}\big) e^{-\mathrm{i}kq} - \big(1 - a_q^{-1} e^{\mathrm{i}q}\big) e^{\mathrm{i}kq} \Big], \end{aligned} \tag{A.6}$$

for $q = \frac{\pi\kappa}{M+1}$, $\kappa = 1, \ldots, M$, with $c \equiv \sqrt{\frac{1-\overline{\eta}}{\overline{\eta}}}$ and where $N_q = (M+1)\frac{2\mathrm{i}(\zeta^{-1} - \cos^2 q)^{1/2}}{a_q}$ ensures that $\phi^\lambda \cdot \psi^\lambda = 1$. Writing

$$\big[(\mathbf{I}\otimes\mathbf{I} - \mathbf{F}\otimes\mathbf{F})^{-1}(\mathbf{E}\otimes\mathbf{I})\big]_{i,j;i',j'} = \sum_{\lambda,\mu} \frac{\psi_i^\lambda \psi_j^\mu \phi_{j'}^\mu}{1-\lambda\mu} \sum_{i''=1}^{M} \phi_{i''}^\lambda \mathbf{E}_{i'';i'}, \tag{A.7}$$

and

$$\big[(\mathbf{I}\otimes\mathbf{I} - \mathbf{F}\otimes\mathbf{F})^{-1}(\mathbf{F}\otimes\mathbf{E})\big]_{i,j;i',j'} = \sum_{\lambda,\mu} \lambda \frac{\psi_i^\lambda \psi_j^\mu \phi_{i'}^\lambda}{1-\lambda\mu} \sum_{j''=1}^{M} \phi_{j''}^\mu \mathbf{E}_{j'';j'}, \tag{A.8}$$

injecting the explicit expressions (A.4) and (A.6), and taking the $M \to \infty$ limit we finally get the explicit expressions (5.23).

We now perform the asymptotic analysis of (5.23) in the limit $t \to \infty$ with $i = vt + u\sqrt{t}$ and $j = vt - u\sqrt{t}$. We also define more convenient integration variables $R \equiv c\frac{\cos q + \cos p}{2}$ and $S \equiv c\sqrt{t}\frac{\cos q - \cos p}{2}$. The strategy is the following. Despite the square roots appearing in (5.24) it can be shown that the contributions of the cuts vanish after integrating over q and p. We therefore perform the integral over z by isolating the dominant pole and then the integrals over R and S will be evaluated by a saddle point calculation.

We first determine the poles in the z plane. Since we are in the limit $t \to \infty$ and that $i-j$ is subdominant in this limit we can perform the calculation in the case $i=j$ and expand it for small $i-j$. In the case $i=j$ we suppose that the dominant saddle point will be found for $S=0$, which is necessarily a saddle point by symmetry. The function $g_{i,j;j'}(\zeta;q,q)$ has a high order pole at $z=1/\overline{\eta}$ that we choose to ignore. The other poles are roots of $a_q^2\zeta^2 = \epsilon c^2$ for $\epsilon = \pm 1$, which can be shown to imply

$$Y^4 - 2(1+2\epsilon R^2)Y^2 + 8R^2 Y + (1-4\epsilon R^2) = 0, \quad \epsilon = \pm 1, \tag{A.9}$$

for the variable $Y \equiv c^2\zeta^{-1}$. The solutions of (A.9) that are indeed poles of $g_{i,j;j'}(\zeta;q,q)$ are given by $Y_{\epsilon\eta} \equiv -\epsilon + 2\eta\epsilon^{1/2}R$. Using the residue theorem we may finally write, in the general case $u \neq 0$,

$$\frac{1}{2\pi \mathrm{i}} \oint_{\Gamma_0} \frac{\mathrm{d}z}{z^t}\, g_{i,j;j'}(z;q,p) = \sum_{\alpha,\beta=\pm 1} \sum_{\epsilon,\eta=\pm 1} \alpha\beta\, A_{\epsilon\eta}(R,S) \mathrm{e}^{t\mathcal{G}_{\epsilon\eta,\alpha\beta}(R,S;v,u)}, \tag{A.10}$$

where the indices α and β come from the decomposition of sines into exponentials. In the exponential we have

$$\begin{aligned} \mathcal{G}_{\epsilon\eta,\alpha\beta}(R,S;v,u) \quad \equiv \quad & -t\log z_{\epsilon\eta} + vt\log(\zeta_{\epsilon\eta}^2 a_{q\epsilon\eta} a_{p\epsilon\eta}) + u\sqrt{t}\log(a_{q\epsilon\eta}/a_{p\epsilon\eta}) \\ & + \mathrm{i}\alpha(vt+u\sqrt{t})q + \mathrm{i}\beta(vt-u\sqrt{t})p, \end{aligned} \tag{A.11}$$

where $\zeta_{\epsilon\eta}$ and $a_{q\epsilon\eta}$ stand for ζ and a_q evaluated at $z_{\epsilon\eta}$. It turns out that the only pole for which a saddle point appears in the R plane is $z_{-1,-1} = \frac{1}{2\overline{\eta}\left(1-\mathrm{i}R-\frac{\mathrm{i}RS^2}{2(1-\mathrm{i}R)^2 t}\right)} + O(t^{-2})$, and that this saddle point appears only for $\alpha = \beta = -1$. All the other contributions are expected to self-average to zero, therefore we only keep the $\epsilon=\eta=\alpha=\beta=-1$ contribution, and we write $\mathcal{G}(R,S;v,u) \equiv \mathcal{G}_{-1-1,-1-1}(R,S;v,u)$. To find the expression for $\mathcal{G}$ we expand the various quantities appearing in (A.11) in the vicinity of $S=0$. In particular we have $\zeta_{-1-1}a_{q-1-1} = \mathrm{i}c + \frac{cS}{(1-\mathrm{i}R)\sqrt{t}} + O(t^{-1})$. We get

$$\begin{aligned} \mathcal{G}(R,S;v,u) \quad = \quad & \log 2 - \log(1+c^2) + 2v\log c + \mathrm{i}v\pi - 2\mathrm{i}v \arccos\left(\frac{R}{c}\right) \\ & + \log(1-\mathrm{i}R) + 2\mathrm{i}\frac{Su}{t}\left(\frac{1}{\sqrt{c^2-R^2}} - \frac{1}{1-\mathrm{i}R}\right) \\ & - \mathrm{i}\frac{RS^2}{t}\left(\frac{1}{2(1-\mathrm{i}R)^3} - \frac{v}{(c^2-R^2)^{3/2}}\right) + O(t^{-2}). \end{aligned} \tag{A.12}$$

Defining $\mathcal{R}_\theta(v) \equiv \frac{4\mathrm{i}v^2 + \theta(c^2 - (1+c^2)4v^2)^{1/2}}{1-4v^2}$, the saddle points $\theta = \pm 1$ are found at

$$R_\theta^{\mathrm{s}}(v,u) \quad = \quad \mathcal{R}_\theta(v) + O(t^{-1}) \tag{A.13}$$

$$S_\theta^{\mathrm{s}}(v,u) \quad = \quad \frac{-4uv}{1+2v}\frac{[1-\mathrm{i}\mathcal{R}_\theta(v)]^2}{\mathcal{R}_\theta(v)} + O(t^{-1}). \tag{A.14}$$

Here we see that for $v < v^* \equiv \frac{\sqrt{1-\overline{\eta}}}{2}$ the $R^{\rm s}_\theta$ are pure imaginary, $\mathcal{G}$ is real and the Green function is just an exponential. We are more interested in the case $v > v^*$, for which the $R^{\rm s}_\theta$ are complex and the Green function shows oscillations.

We write $\mathcal{G}^s_\theta(v,u) \equiv \mathcal{G}(R^{\rm s}_\theta, S^{\rm s}_\theta, v, u)$. On the diagonal $u = 0$, $S^{\rm s}_\theta = 0$ we have

$$\begin{aligned}
\Re\mathcal{G}^s_\pm(v,0) &= \log 2 - \frac{1}{2}\log(1+c^2) - \frac{1}{2}(1-2v)\log(1-2v) \\
&\quad -\frac{1}{2}(1+2v)\log(1+2v) + 2v\log c, \qquad \text{(A.15)} \\
\Im\mathcal{G}^s_\pm(v,0) &= \mp\Big[\arctan[(c^2-(1+c^2)4v^2)^{1/2}] \\
&\quad -2v\arctan[(c^2-(1+c^2)4v^2)^{1/2}/2v]\Big].
\end{aligned}$$

The $\mathcal{G}^s_\theta$ are complex conjugate, so that the Green function oscillates. The first of Eqs. (A.15) is the same as (5.27). The maximal amplitude occurs where $\Re\mathcal{G}^s_\pm$ is maximal, namely for $v = v_g \equiv 1/2 - \overline{\eta}$. The pulsation and wavevector of the oscillations are obtained by identifying $t\Im\mathcal{G}^s_\pm = \mp(\omega t - ik)$ and give Eq. (5.28).

Appendix B

The coefficients $r_n^{\rm fs}$

In this appendix we compute the $r_n^{\rm fs}$ defined in subsection 6.2.3 for the frozen shuffle update.

Consider an $\mathcal{E}$ particle with phase 0 (without loss of generality) in a flow of $\mathcal{N}$ particles, trying to hop towards site $(0,0)$ at time 0. This site is either empty, with probability $1-\overline{\rho}^{\mathcal{N},\rm fs}=r_1^{\rm fs}$, or it is occupied with probability $\overline{\rho}^{\mathcal{N},\rm fs}dx$ by a $\mathcal{N}$ particle that we call $\mathcal{N}_1$, with phase between $1-x$ and $(1-x)+dx$. In the second case, and using continous time, we define T_2 as the interval separating the departure of particle $\mathcal{N}_1$ from site $(0,0)$ from the arrival of its direct follower $\mathcal{N}_2$ on the same site. From there we see that the $\mathcal{E}$ particle will attempt to hop towards $(0,0)$ again at time 1, whereas particle $\mathcal{N}_2$ will try at time $1-x+T_2$. The $\mathcal{E}$ particle will therefore hop before $\mathcal{N}_2$ if $T_2>x$. For a fixed x we get an infinitesimal contibution to $r_2^{\rm fs}$: $dr_2^{\rm fs}(x)=\overline{\rho}^{\mathcal{N},\rm fs}{\rm Prob}[T_2>x]dx$.

If the $\mathcal{E}$ particle is blocked again by particle $\mathcal{N}_2$, we have to consider a third particle $\mathcal{N}_3$ coming in site $(0,0)$ after $\mathcal{N}_2$ after an interval T_3. Applying the same argument as in the previous paragraph, we see that for fixed x, $dr_3^{\rm fs}(x)=\overline{\rho}^{\mathcal{N},\rm fs}{\rm Prob}[(T_2+T_3>x)\,\text{and}\,(T_2<x)]dx$. We can finally generalize to higher numbers of blockings : $dr_n^{\rm fs}(x)=\overline{\rho}^{\mathcal{N},\rm fs}{\rm Prob}[(T_2+\ldots+T_n>x)\,\text{and}\,(T_2+\ldots+T_{n-1}<x)]dx$.

We have assumed that the incoming $\mathcal{N}$ particles were moving in free flow with velocity 1. Thus, the distribution of arrival times of the $\mathcal{N}$ particles in a given site is the same as the distribution of injection times. The probability density distribution of the T_i is given by the entrance kernel (2.1). One finally computes, for $n\geq 1$

$$\begin{aligned} dr_n^{\rm fs}(x) &= \overline{\rho}^{\mathcal{N},\rm fs}\int_{T_2=0}^{x}\cdots\int_{T_{n-1}=0}^{x-\sum_{i=2}^{n-2}T_i}\int_{T_n=x-\sum_{i=2}^{n-1}T_i}^{\infty}\prod_{i=2}^{n}K(T_i)dT_i \\ &= \overline{\rho}^{\mathcal{N},\rm fs}\tfrac{(ax)^{n-2}}{(n-2)!}{\rm e}^{-ax} \end{aligned} \tag{B.1}$$

By averaging uniformly over x we obtain Eq.(6.2).